ATTENTION: The Singapore Copyright Act applies to the use of this document. Nanyang Technological University Library

a365165

Growth and Characterization of Carbon Doped GaAs- and InP- Based Heterojunction Bipolar Transistors

Zhang Rong

School of Electrical & Electronic Engineering

A thesis submitted to the Nanyang Technological University
in fulfillment of the requirement for the degree of
Doctor of Philosophy

2005

TK
7871.96
.B55
Z63
2005

ATTENTION: The Singapore Copyright Act applies to the use of this document. Nanyang Technological University Library

Dedicated to the memory of my father…

…For his countless love and encouragement

ATTENTION: The Singapore Copyright Act applies to the use of this document. Nanyang Technological University Library

Abstract

The results described in this work demonstrate the comprehensive characterization of C-doped GaAs and $In_{0.53}Ga_{0.47}As$ materials and C-doped GaAs-based and InP-based HBT devices grown by SSMBE system using CBr_4 as p-type dopant precursor. The characteristics of C-doped GaAs materials, such as the hole concentration, mobility, lattice mismatch, surface morphology, and optical properties, have been comprehensively investigated using various techniques, which help to gain the insight and understanding of the material properties. Especially, the compensation effects of dicaron defects have been studied. The optimization of the growth conditions has been carried out and discussed, which benefits the development of C-doped GaAs as base layer of GaInP/GaAs HBT devices. Preliminary results of C-doped GaInP/GaAs HBT devices demonstrated poor characteristics due to trap-related recombination. With better control of growth process, improved performances of GaInP/GaAs HBTs have been obtained. Elevated temperature properties revealed good material quality of these devices. C-doped InP/InGaAs SHBTs and composite collector DHBTs have been grown and studied, and the promising device performance demonstrate the potential for commercial wireless communication applications. The complex breakdown characteristics of composite collector DHBTs have been investigated.

ATTENTION: The Singapore Copyright Act applies to the use of this document. Nanyang Technological University Library

Acknowledgements

First of all, I would like to express my deepest appreciation to my supervisor, Professor Yoon Soon Fatt, for his patient guidance, continuous support, understanding and encouragement throughout the three years of my study in NTU. Without his wisdom and guidance, this work would not have been successful.

Special thanks to Mr. Tan Kian Hua, Dr. Sun Zhongzhe and Dr. Huang Qingfeng for the MBE material growth work. The fruitful and enjoyable collaboration and assistances from them are gratefully acknowledged.

I am also very thankful for having the opportunity to learn from Dr. Lew Kim Luong, who gives me much assistance in device processing and many valuable discussions in device physics. Dr. Wang Shanzhong is specially acknowledged for the valuable discussions about the materials. I am very grateful for the help and equipment training from Dr. Loke Wan Khai, and Mr. Ng Tien Khee. The friendship and assistance from the other members of the MBE group in NTU, Mr. Yew Kuok Chuin, Mr. Xie Shiyong, and Mr. Satrio Wicaksono are appreciated.

I also wish to express my sincere gratitude to Assistant Professor Wang Hong for his generous assistance and suggestions. The efforts of the MMIC group in NTU are appreciated, without the constant assistance from them, the experiments would have taken considerably longer. In particular, the friendship and help from Ms.Yang Hong, Ms.Bu Jing, Dr.Yuan Kaihua, Dr.Tian Yuan, Ms.Liu Yuwei, Mr.Cheong Wai Chye, Mr.Tan Chee Leong, Mr.Neo Wah Peng, and Mr.Loo Chih Chien Martin, are greatly appreciated.

The friendship and support from Dr.Yang Zhiwei, Dr.Zhang Guohai, Dr.Wang Sigen, Mr.Yang Dajiang, Mr.Sun Lu, Mr.Yang Lieyong, Mr.Kumta Amit Sudhakar,

ATTENTION: The Singapore Copyright Act applies to the use of this document. Nanyang Technological University Library

and Dr.Katri are greatly appreciated.

I would like to thank our Cleanroom and Characterization Lab technical staffs, Mr. Foo Tai Ho, Mr. Muhd Fauzi bin Abdullah, and Mr. Loo Kok Chuan, for their help during my study.

Also, I would like to express my appreciation to my mother and my brother, for their consistent support, enduring patience, care and endless love. Finally, and most importantly, I thank my husband, Chongyang, for his love, humor, intelligence, understanding, encouragement and companionship.

ATTENTION: The Singapore Copyright Act applies to the use of this document. Nanyang Technological University Library

Summary

Carbon is a superior p-type dopant to beryllium or zinc in GaAs and InGaAs primarily because of its lower diffusion coefficient and higher electrical activity. The usage of carbon in the base of heterojunction bipolar transistors (HBTs) increases the device reliability. Carbon tetrabromide (CBr_4) has become a popular choice for carbon doping precursors because of its high doping efficiency and relative insensitivity to growth conditions. Solid-source molecular beam epitaxy (SSMBE) offers the advantage of a hydrogen-free environment for the growth of carbon-doped III-V semiconductor layers, eliminating the passivation of carbon acceptors by hydrogen that is commonly observed in carbon doped GaAs (or InGaAs) layers grown by techniques with hydrogen rich environment.

In the work presented in this thesis, the carbon doped (C-doped) GaAs materials grown by SSMBE using CBr_4 as p-type dopant precursor have been systematically characterized using various techniques, which help to obtain the insight and understanding of the material properties. Especially, the compensation effects of dicarbon defects have been studied. The optimization of the growth conditions has been carried out and discussed, which benefits the development of C-doped GaAs as base layer of GaInP/GaAs HBT devices. C-doped GaInP/GaAs HBTs have been grown and fabricated successfully. The current transport mechanism studies have been carried out through the elevated temperature characteristics investigation. This provides an indirect way to assess the material quality. C-doped InP/InGaAs single heterojunction bipolar transistors (SHBTs) and composite collector double heterojunction Bipolar Transistors (DHBTs) have been grown and studied. The promising device performance demonstrates the potential for commercial wireless

ATTENTION: The Singapore Copyright Act applies to the use of this document. Nanyang Technological University Library

communication applications. The following summarizes the major investigation carried out in this thesis.

C-doped GaAs materials have been successfully grown by SSMBE using CBr_4 as p-type dopant precursor, and the materials have been comprehensively characterized. Sustainable and stable CBr_4 flux with variation lower than 2.5% has been obtained. For the doping level commonly used for HBTs (~ 5×10^{19} cm^{-3}), the memory effect is negligible. Full activation of carbon atoms incorporated into GaAs has been achieved at CBr_4 flux level below 2.6×10^{-7} torr. PL linewidth broadening and narrow bandgap have been observed from heavily C-doped GaAs. Reasonably good C pulsed doping profile has been achieved and verified by SIMS measurement on samples grown without the use of growth interruption.

When the CBr_4 flux exceeds 2.6×10^{-7} torr, further increase in the C atomic concentration causes the formation and rapid increase in dicarbon defects. The compensating effects of the dicarbon defects induce the decrease in hole concentration, drop in mobility, and increase in lattice parameter. Unlike the samples grown at CBr_4 flux below 2.6×10^{-7} torr, the lattice mismatch data of the compensated samples, which were grown at high CBr_4 flux exceeding 2.6×10^{-7} torr, deviate from Vegard's Law. The structure of the dicarbon defects formed at high CBr_4 flux needs further investigation. The atomic force microscopy (AFM) images of surface morphology show signs of growth mode transformation from 2D to 3D island formation following increase in CBr_4 flux. The results suggest a possible relationship between increase in surface roughness and formation of dicarbon defects in C-doped GaAs.

The effect of substrate temperature, growth rate, and V/III ratio on C-doped GaAs grown by SSMBE was investigated. Within the range of experimental conditions in our MBE system, substrate temperature between 560 ºC -590 ºC, growth

ATTENTION: The Singapore Copyright Act applies to the use of this document. Nanyang Technological University Library

rate of 1 μm/h or 0.5 μm/h and V/III ratio between 18 and 25 are the optimum parameters for C-doped GaAs growth for HBT applications.

C-doped GaInP/GaAs HBTs have been grown by SSMBE and fabricated using conventional photolithography and wet chemical etching. The preliminary results of the devices showed poor I-V characteristics. The temperature dependent I-V characteristics suggest that trap-related recombination played a significant role in the poor device DC characteristics. The reverse leakage current of the base-collector junction suggests that the dominant mechanism could be related to the SRH generation-recombination process. On the other hand, the reverse leakage current of the base-emitter junction could be dominated by carrier tunneling effects.

With better control of the growth process, improved characteristics of GaInP/GaAs HBTs with base doping concentration of 4×10^{19} cm^{-3} have been obtained. From the temperature dependent Gummel plot, the activation energies of collector current and base current were obtained. For the collector current, the activation energy is 1.4 eV, which is close to the bandgap of the GaAs base, indicates that the collector current is determined by drift-diffusion process. For the base current, the activation energy is also 1.4 eV, indicating that band-to-band recombination plays a dominant role in determining the base current. No trap-related recombination is observed for the base and collector currents, which further indicates the good base material quality for the HBT structures. Properties of current gain versus collector current at different temperatures were also investigated and analyzed. High-performance C-doped GaInP/GaAs HBTs with base doping concentration of 2×10^{19} cm^{-3} grown by SSMBE using CBr_4 as p-type precursor has also been obtained, which indicate the stability of the C-doping growth technique in our group.

C-doped InP/InGaAs SHBTs and composite collector DHBTs have been

ATTENTION: The Singapore Copyright Act applies to the use of this document. Nanyang Technological University Library

grown by SSMBE using CBr_4 as p-type dopant precursor. The hole mobilities in C-doped $In_{0.53}Ga_{0.47}As$ layers grown by our SSMBE system are comparable to those grown by GSMBE, MOCVD, and other groups with SSMBE data. The near unity ideality factors of the base and collector currents of both SHBT and DHBT indicate good junction qualities for both device types. The InP/InGaAs composite collector DHBT exhibits lower output conductance and higher breakdown voltage of 10 V, compared to 6 V in the SHBT. The common base characteristics show that the current blocking effect was reduced due to the composite collector design. The maximum current gain of the InP/InGaAs composite collector DHBT (current gain: 40) is comparable to that of the SHBT (current gain: 45). The temperature-dependent breakdown characteristic of the base-collector junction demonstrates the complex breakdown mechanisms in the composite collector DHBT.

ATTENTION: The Singapore Copyright Act applies to the use of this document. Nanyang Technological University Library

Table of Contents

Acknowledgement.. **I**

Summary.. **III**

Table of Contents.. **VII**

List of Figures.. **XI**

List of Tables.. **XVI**

Chapter 1 Introduction.. **1**

1.1 Motivation.. 1

1.1.1 P-type doping issue in GaAs.. 2

1.1.2 Modern epitaxial growth techniques (MOCVD, SSMBE, GSMBE, MOMBE & CBE).. 5

1.1.3 Current status of SSMBE carbon doping research and device applications.. 7

1.2 Objectives.. 8

1.3 Major contributions of the thesis.. 8

1.4 Organization of the thesis.. 9

Chapter 2 Background.. **11**

2.1 Heterojunction Bipolar Transistor (HBT) operation theory.......... 11

2.2 The development of carbon sources for MBE........................ 14

2.2.1 Graphite filament.. 14

2.2.2 CCl_4 and CBr_4.. 15

2.3 A brief review of carbon behavior in GaAs and InGaAs............ 16

2.4 Material systems investigated.. 18

ATTENTION: The Singapore Copyright Act applies to the use of this document. Nanyang Technological University Library

2.4.1 GaInP/GaAs.. 19
2.4.2 InP/InGaAs.. 20
2.5 Summary.. 21

Chapter 3 Experimental techniques.. 22

3.1 Introduction to SSMBE.. 22
3.1.1 The basic MBE process.. 23
3.1.2 The SSMBE apparatus.. 24
3.2 Material characterization techniques.. 27
3.2.1 X-Ray Diffraction (XRD).. 27
3.2.2 Photoluminescence (PL).. 30
3.2.3 Atomic Force Microscopy (AFM).. 32
3.2.4 Hall measurement.. 34
3.2.5 Secondary Ion Mass Spectrometry (SIMS).. 34
3.3 Summary.. 35

Chapter 4 Growth and characterization of C-doped GaAs.. 36

4.1 Introduction.. 36
4.1.1 Brief review of C-doped GaAs grown by various techniques.. 36
4.1.2 Heavy doping issue in C-doped GaAs.. 37
4.2 CBr_4 source installation and flux calibration.. 38
4.2.1 CBr_4 gas handling system.. 38
4.2.2 CBr_4 flux control.. 39
4.2.3 Investigation of memory effect.. 41
4.3 Growth and characterization of C-doped GaAs.. 41
4.3.1 Hall results of C-doped GaAs.. 42
4.3.2 XRD results of C-doped GaAs.. 45
4.3.3 AFM results of C-doped GaAs.. 49
4.3.4 PL results of C-doped GaAs.. 52
4.3.5 SIMS results of C-doped GaAs.. 54

ATTENTION: The Singapore Copyright Act applies to the use of this document. Nanyang Technological University Library

4.4 C-doped GaAs PN junction 56
4.4.1 Epitaxial structure & schematic of the PN junction.......... 56
4.4.2 Electrical properties of the PN junction........................ 57
4.5 Summary.. 61

Chapter 5 Optimization of growth conditions for C-doped GaAs......... 63

5.1 Sample growth... 63
5.2 Effect of substrate temperature.. 64
5.3 Effect of growth rate... 66
5.4 Effect of V/III ratio... 67
5.5 Summary.. 69

Chapter 6 Results of C-doped GaInP/GaAs HBTs.......................... 70

6.1 Brief review of GaInP/GaAs HBTs...................................... 70
6.2 SSMBE growth of C-doped GaInP/GaAs HBTs......................... 71
6.3 Fabrication of C-doped GaInP/GaAs HBTs.............................. 72
6.3.1 Mesa formation.. 73
6.3.2 Formation of ohmic contacts.................................... 74
6.4 DC characteristics of C-doped GaInP/GaAs HBTs.................... 76
6.5 Investigation on root cause for poor characteristics of GaInP/ GaAs HBT.. 83
6.6 Summary.. 83

Chapter 7 Improved characteristics of C-doped GaInP/GaAs HBTs...... 84

7.1 Growth and fabrication of C-doped GaInP/GaAs HBT with improved performance.. 84
7.2 Improved DC characteristics of C-doped GaInP/GaAs HBT with base doping concentration of $4\times10^{19}cm^{-3}$............................ 88
7.3 C-doped GaInP/GaAs HBT with base doping concentration of $2\times10^{19}cm^{-3}$.. 95

ATTENTION: The Singapore Copyright Act applies to the use of this document. Nanyang Technological University Library

7.4 Summary........ 97

Chapter 8 C-doped InGaAs and InP/InGaAs HBTs........ 99

8.1 Introduction........ 99

8.1.1 Applications of InP-based HBT technology........ 99

8.1.2 State-of-the art of C-doped $In_{0.53}Ga_{0.47}As$ and InP-based HBTs........ 100

8.1.3 InP/InGaAs SHBT and DHBT........ 101

8.2 Growth and characterization of C-doped $In_{0.53}Ga_{0.47}As$........ 102

8.3 Growth and fabrication of C-doped InP/InGaAs SHBTs and DHBTs........ 105

8.4 Study of DC characteristics of InP/InGaAs SHBTs and DHBTs........ 108

8.4.1 Energy bandgap analysis of InP/InGaAs composite collector DHBTs........ 108

8.4.2 DC characteristics of C-doped InP/InGaAs SHBTs and DHBTs........ 108

8.4.3 Temperature-dependence of breakdown characteristics of InP/InGaAs composite collector DHBT........ 114

8.5 Summary........ 116

Chapter 9 Conclusions and future work........ 117

9.1 Conclusions........ 117

9.2 Recommendations for further work........ 121

Author's publications........ 123

Bibliography........ 125

ATTENTION: The Singapore Copyright Act applies to the use of this document. Nanyang Technological University Library

List of Figures

Fig.1.1 Gummel plot of a typical fast-degrading HBT under bias stress at 200 ºC 3

Fig.1.2 Gummel plot of a typical slow-degrading HBT under bias stress at 240 ºC 4

Fig.2.1 Schematic band diagram of an abrupt *n-p-n* HBT under typical operation conditions.. 12

Fig.2.2 Relative incorporation efficiency of carbon in GaAs from various halomethane doping sources as a function of the average carbon nucleus-ligand bond strength of the precursor [27]...................... 15

Fig.2.3 Metal-C bond energy for commonly used group III and V elements [34]... 17

Fig.2.4 In molar fraction dependence of carrier concentration in C-doped $In_xGa_{1-x}As$ grown on (100) InP substrates [36]......................... 17

Fig.2.5 Energy bandgap *vs.* lattice constant of some commonly used semiconductor materials.. 18

Fig.2.6 Energy band alignment between $Al_{0.30}Ga_{0.70}As$/GaAs, $In_{0.49}Ga_{0.51}P$/GaAs, and InP/$In_{0.53}Ga_{0.47}As$.............................. 19

Fig.2.7 Equilibrium carrier velocity *vs.* electric field of various semiconductors.. 21

Fig.3.1 Schematic diagram of SSMBE growth chamber......................... 25

Fig.3.2 The diagram showing the path difference of the incident and

ATTENTION: The Singapore Copyright Act applies to the use of this document. Nanyang Technological University Library

diffracted X-ray beams.. 28

Fig.3.3 The schematic diagram of the PL experimental apparatus........... 32

Fig.3.4 Schematic diagram of AFM.. 33

Fig.4.1 Schematic illustration of the CBr_4 gas handling system.............. 38

Fig.4.2 CBr_4 relative flux vs. leak valve open position with CBr_4 source keeping at a given temperature.. 39

Fig.4.3 Plot of CBr_4 flux vs. leak valve opening position at different cylinder temperature... 40

Fig.4.4 Doping concentration vs. CBr_4 flux. A comparison between Hall effect and SIMS measurement... 43

Fig.4.5 Mobility vs. hole concentration at 300K. The mobility data of the Be-doped samples are from ref. [68].................................. 45

Fig.4.6 Plot of lattice-mismatch *vs*. CBr_4 flux................................... 46

Fig.4.7 Plot of lattice-mismatch *vs*. hole concentration........................ 46

Fig.4.8 Experimental X-Ray Bragg Diffraction patterns (004 reflection) of the C-doped GaAs grown at CBr_4 flux of 2.5×10^{-7} torr.............. 49

Fig.4.9 AFM micrographs of C-doped GaAs surface grown at CBr_4 flux of: a) 5×10^{-8} torr, b) 2×10^{-7} torr, and c) 4.8×10^{-7} torr................. 51

Fig.4.10 Normalized PL spectra of C-doped GaAs samples for various doping levels.. 53

ATTENTION: The Singapore Copyright Act applies to the use of this document. Nanyang Technological University Library

Fig.4.11 Normalized PL spectra for various temperatures of a C-doped GaAs sample with hole concentration of $1.02\times10^{19}cm^{-3}$............. 54

Fig.4.12 Pulsed C-doping profile of a GaAs sample measured by SIMS...... 55

Fig.4.13 Schematic of the PN junction... 57

Fig.4.14 I-V and breakdown characteristic of the PN junction................... 58

Fig.4.15 Reverse leakage current at different temperatures...................... 59

Fig.4.16 Ideality factor of the PN junction at medium current.................. 60

Fig.4.17 Ideality factor of the PN junction at low current...................... 60

Fig.5.1 Plot of hole concentration *vs*. substrate temperature.................. 65

Fig.5.2 Plot of rms surface roughness (with error bars) *vs*. substrate temperature.. 66

Fig.5.3 Plot of hole concentration and hole mobility *vs*. V/III ratio.......... 67

Fig.5.4 Plot of rms surface roughness (with error bars) *vs*. V/III ratio....... 68

Fig.5.5 Plot of ideality factor of PN junctions *vs*. V/III ratio................. 68

Fig.6.1 SEM image of C-doped GaInP/GaAs HBT grown by SSMBE...... 75

Fig.6.2 Plot of total resistance as a function of TLM pad gap size for GaInP/GaAs HBT base layer.. 76

Fig.6.3 Common-emitter I-V characteristics of GaInP/GaAs HBT.......... 78

ATTENTION: The Singapore Copyright Act applies to the use of this document. Nanyang Technological University Library

Fig.6.4 Plot of current gain *vs.* collector current characteristics at different temperatures.. 79

Fig.6.5 Gummel plot of GaInP/GaAs HBT at different temperatures......... 80

Fig.6.6 Temperature dependence of: a) base-collector junction, b) base-emitter junction characteristics.................................... 82

Fig.7.1 SIMS profiles of C, Si, P, and Br concentration in the GaInP/GaAs HBT structure with abrupt emitter-base junction and base doping concentration of 4×10^{19} cm^{-3}... 86

Fig.7.2 Schematic cross section of the GaInP/GaAs HBT.................... 87

Fig.7.3 Gummel plot of GaInP/GaAs HBT before and after HF passivation.. 88

Fig.7.4 Plot of GaInP/GaAs HBT common-emitter I-V characteristics at 300K and 380K... 89

Fig.7.5 Temperature dependent characteristics of: a) base-emitter junction, and b) base-collector junction.. 90

Fig.7.6 Gummel plot of GaInP/GaAs HBT at different temperature......... 91

Fig.7.7 Activation energy plots for collector and base currents extrapolated to V_{BE}=0V.. 92

Fig.7.8 Plot of current gain *vs.* collector current characteristics at different temperature.. 93

Fig.7.9 Gummel plots of C-doped GaInP/GaAs HBTs with base doping concentration of $2\times10^{19}cm^{-3}$ and $4\times10^{19}cm^{-3}$.......................... 96

ATTENTION: The Singapore Copyright Act applies to the use of this document. Nanyang Technological University Library

Fig.7.10 Current gain vs. collector current for C-doped GaInP/GaAs HBTs with base doping concentration of 2×10^{19} cm^{-3} and 4×10^{19} cm^{-3}..... 96

Fig.8.1 Room temperature hole mobility *vs.* hole concentration in C-doped InGaAs.......... 103

Fig.8.2 4K PL spectra of C-doped InGaAs grown at different V/III ratios... 104

Fig.8.3 Schematic cross section of InP/InGaAs: a) SHBT, b) composite collector DHBT.......... 107

Fig.8.4 Schematic diagram of conduction band at base-collector junction of the InGaAs/InP DHBT: a) without composite collector; b) with undoped InGaAs layer; c) with an additional n^+-InP layer........... 109

Fig.8.5 Gummel plots of InP/InGaAs SHBT and composite collector DHBT.......... 110

Fig.8.6 Common-emitter I-V characteristics of: a) InP/InGaAs SHBT; b) InP/InGaAs composite collector DHBT.......... 111

Fig.8.7 Common-base I-V characteristics of InP/InGaAs composite collector DHBT.......... 112

Fig.8.8 Common-emitter current gain *vs.* collector current characteristics of InP/InGaAs SHBT and composite collector DHBT.......... 113

Fig.8.9 Base-collector junction I-V characteristics at different temperatures: a) InP/InGaAs composite collector DHBT; b) InP/ InGaAs SHBT.......... 115

ATTENTION: The Singapore Copyright Act applies to the use of this document. Nanyang Technological University Library

List of Tables

Table 1.1 Comparison of degradation of GaAs/AlGaAs HBTs with carbon ($p=7\times10^{19}cm^{-3}$) or beryllium ($p=4\times10^{19}cm^{-3}$) doped base layers..... 4

Table 1.2 Comparison of basic principles and of main components of modern epitaxial techniques... 6

Table 4.1 Development of C-doped GaAs grown by various techniques.. 37

Table 4.2 Investigation of memory effect.. 41

Table 4.3 Size comparison of C atom, As atom and the C-C pairs on different crystal orientation... 48

Table 4.4 Epitaxial structure of the PN junction................................... 56

Table 6.1 Layer structure of GaInP/GaAs HBT.................................. 72

Table 7.1 Layer structure of GaInP/GaAs HBT with improved performance.. 85

Table 8.1 State-of-the art of C-doped $In_{0.53}Ga_{0.47}As$.............................. 100

Table 8.2 State-of-the art of InP/InGaAs DHBTs................................. 102

Table 8.3 Epitaxial layer structure of: a) InP/InGaAs SHBT; b) composite collector DHBT... 105

ATTENTION: The Singapore Copyright Act applies to the use of this document. Nanyang Technological University Library

Chapter 1

Introduction

In this chapter, the background and motivation as well as objectives of the present work are firstly introduced. It is followed by the general layout of the thesis.

Heterojunction Bipolar Transistors (HBTs) have become practical for many high-speed applications due to advantages in performance and cost over other device technologies. High gain and power efficiency in addition to excellent high frequency chanracteristics make HBTs attractive for a variety of applications while relaxed lithography requirements and smaller circuit sizes result in a manufacturable and commercially viable device technology. Specific applications for which HBTs are well suited include linear amplifiers, lower-power electronics, analog-to-digital converters, and optoelectronic integrated circuits (OEIC). High performance HBT-based integrated circuits are becoming commercially available.

1.1 Motivation

Soon after the first demonstration of the transistor in 1947 by Bardeen and Brattain at Bell Labs, William Shockley described the concept of a heterojunction bipolar transistor (HBT) in a U.S. patent filed in 1948 [1]. In 1957, Kroemer published the first theoretical treatment of HBT operation [2]. They envisioned that using a wider energy bandgap material in the emitter than in the base could result in significant improvement in transistor performance. However, practical development of this HBT idea was not realized until a breakthrough in semiconductor epitaxy technology took place in the 1970s, particularly Molecular Beam Epitaxy (MBE) and

ATTENTION: The Singapore Copyright Act applies to the use of this document. Nanyang Technological University Library

Metal Organic Chemical Vapor Deposition (MOCVD). These advanced epitaxy techniques provide exceptional control of doping concentration and layer thickness. As a result, interface free of impurities and structural defects between dissimilar semiconductor materials could be obtained, which still presents the technical challenge for the development of heterostructure devices.

For *n-p-n* HBTs, the doping of the base layer during epitaxy is very important for the performance of the device. In current art, the most commonly used p-type dopants in the base layer of the HBT structures are different for various growth systems: carbon (C) for MOCVD system; beryllium (Be) or zinc (Zn) for conventional MBE system. However, carbon is a superior dopant to beryllium and zinc due to its lower diffusion coefficient in GaAs [3,4,5]. The Solid Source MBE (SSMBE) system has its unique advantage in terms of safety. Therefore, material growth using SSMBE with carbon as p-type dopant is a promising project. The above motivation will be explained in detail in the following part.

1.1.1 P-type doping issue in GaAs

Beryllium exhibits significant diffusion [3] and surface segregation in GaAs, which are detrimental to the performance of devices. The diffusion coefficient for Be in GaAs rises rapidly for doping levels above 5×10^{19} cm^{-3}, a diffusion coefficient as high as 2×10^{-12} cm^2/s was observed at 600 °C [6]. This leads to an increase in base transit time in a HBT structure and more carrier recombination in the emitter layer. It has been reported that HBTs containing beryllium show a current-induced degradation of their direct current (DC) characteristics during operation of the devices [4]. The Gummel plot of a typical fast-degrading HBT (Be-doped) before and after stress under bias at 200 °C is shown in Fig.1.1 [5]. The Gummel plot of a typical

ATTENTION: The Singapore Copyright Act applies to the use of this document. Nanyang Technological University Library

slow-degrading HBT (Be-doped) at 240 °C is shown in Fig.1.2. It can be seen that after some time of stress the current gain decreased and the ideal factors degraded greatly. Similar problems occur when Zn is used as the acceptor dopant in HBT structures.

Research on carbon doping in GaAs [7,8] has demonstrated that, in addition to having a higher level of electrical activity, carbon also has a much lower diffusion coefficient of below 6×10^{-15} cm^2s^{-1} at 800 °C, which is more than two orders of magnitude smaller than that of both Be and Zn. As shown in Table 1.1 [4], the use of carbon as p-type dopant in the base of HBTs increases the device reliability by minimizing dopant diffusion into the emitter during epitaxy growth and reducing the current-induced degradation of device DC gain during operation. Recent report in 1999 on the reliability comparison between Be-doped and C-doped AlGaAs/GaAs HBTs also shows that the degradation induced by RTP for Be-doped HBT is due to the outdiffusion of Be from the highly doped base [9].

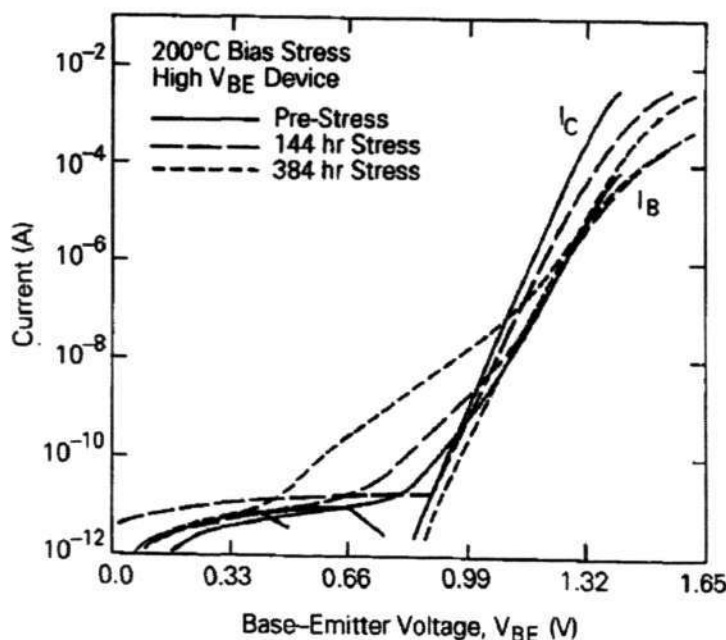

Fig.1.1 Gummel plot of a typical fast-degrading HBT under bias stress at 200 °C [5].

ATTENTION: The Singapore Copyright Act applies to the use of this document. Nanyang Technological University Library

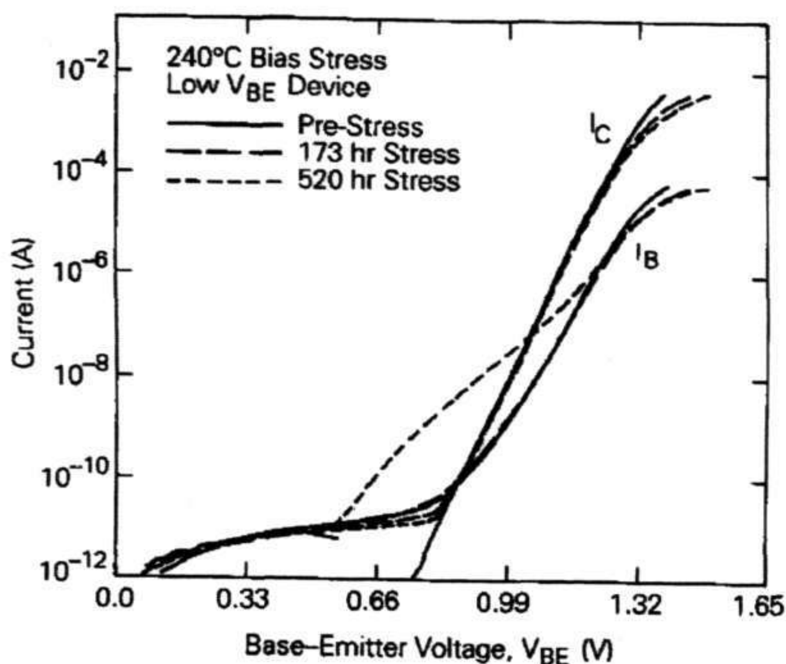

Fig.1.2 Gummel plot of a typical slow-degrading HBT under bias stress at 240 °C [5].

Table 1.1 Comparison of degradation of GaAs/AlGaAs HBTs with carbon ($p = 7\times10^{19}$ cm^{-3}) or beryllium ($p = 4\times10^{19}$ cm^{-3}) doped base layers. The device size was 2×10 μm^2, the operating temperature 200 °C and the collector current density 2.5×10^4 A/cm^3 for both types of material. We show current gains and junction ideality factors *n* before and after device operation at 200°C for various periods [4].

	Be doped		C doped	
	Initial	After 2 hours	Initial	After 12 hours
Current gain	16	1.5	17	16
Ideality factor of base-emitter junction	1.3	2.4	1.4	1.4
Ideality factor of base-collector junction	2.0	4.5	1.3	1.3

ATTENTION: The Singapore Copyright Act applies to the use of this document. Nanyang Technological University Library

1.1.2 Modern epitaxial growth techniques (MOCVD, SSMBE, GSMBE, MOMBE & CBE)

The most important epitaxial techniques for the growth of HBT devices are MOCVD and MBE. Conventional MBE usually refers to the solid source MBE (SSMBE). There exists other vacuum growth techniques similar to the SSMBE where the precursors are supplied in different ways: gas source MBE (GSMBE), and metalorganic MBE (MOMBE), and chemical beam epitaxy (CBE). In the SSMBE system, both group III and group V sources are solid sources; compared with SSMBE, in the GSMBE system group V solid source is replaced with gas source; in the MOMBE system the group III solid source is replaced with gas source; in the CBE system both group III and V precursors are replaced by gas sources (hydrides or metalorganics--MO).

The basic principles of MBE and MOCVD differ from the nature of sources used as precursors of layer constituents and from the growth reactor pressure [10,11,12,13]. The MBE growth is performed from the evaporation of elemental sources under low pressure (<10^{-4} torr) so that the mean-free path of species is longer than the source to substrate distance and that gas phase interactions are avoided. In the MOCVD process, the sources are gaseous and arrive as a premixed gas flow into the reactor at atmospheric or slightly reduced pressure for decomposition and reaction at the substrate surface. The key points for all these epitaxial techniques are: (i) accurate and reproducible flow or pressure control; (ii) high growth uniformity by beam tailoring or source premixing; (iii) efficient source switching by shutter or valve operation. The relationship between these techniques and their differences concerning the basic components of growth equipments are summarized in Table 1.2 [10].

ATTENTION: The Singapore Copyright Act applies to the use of this document. Nanyang Technological University Library

Table 1.2 Comparison of basic principles and of main components of modern epitaxial techniques [10].

	SSMBE	CBE	MOCVD
Pressure	$<10^{-4}$ torr		> 100 torr
III source	Solid	Gaseous (MO)	
V source	Solid	Gaseous (hyd./MO)	
Pumping	Primary +secondary static	Primary +secondary dynamic	Primary
Growth reactor	Metal	Metal	Metal, quartz
Source injection	Evaporation cell + cracker cell	Cracker cell + gas cell	Gas manifold
Source control	Temperature	Flow, pressure	Flow
Source switching	Shutter	Valve	Valve

Compared with MOCVD, SSMBE has the following advantages [14]:

- No flow pattern problem encountered in multiwafer scale-up;
- Beam nature produces very abrupt heterointerfaces and ultrathin layers conveniently;
- Because MBE operates within an ultrahigh vacuum (UHV) environment, a wide range of analysis instruments can be used in situ to monitor the chemical and structural properties of the epitaxial layers, e.g., reflection high energy electron diffraction (RHEED);
- MBE is compatible with other high vacuum thin film processing methods, e.g., metal evaporation, ion beam milling and ion implantation;

ATTENTION: The Singapore Copyright Act applies to the use of this document. Nanyang Technological University Library

- SSMBE offers the advantage of a hydrogen-free environment for the growth of carbon-doped III-V semiconductor layers, eliminating the passivation of carbon acceptors by hydrogen that is commonly observed in carbon doped GaAs (or InGaAs) layers grown by techniques with hydrogen rich environment, such as MOCVD and GSMBE;
- Most important of all, SSMBE has a unique advantage over MOCVD and CBE: safety. There is no toxic gas to handle, and the standard pumping facilities (cryopumping, ionic pumping) do not have any exhaust. Therefore, the growth can proceed in a strictly tight chamber: no gas inlet, no pumping outlet.

Due to above advantages, SSMBE with carbon as p-type dopant is a promising project in both material growth and the device application.

1.1.3 Current status of SSMBE carbon doping research and device applications

The first carbon doped (C-doped) GaAs grown by SSMBE using carbon tetrabromide (CBr_4) as p-type dopant precursor was reported in 1993 [15]. After that, the memory effect [16], substrate orientation dependence [17], iodine incorporation [18], and low temperature growth performance [19] of the C-doped materials have been reported. However, although there are reports on the realization of C-doped AlGaAs/GaAs HBTs [20] and InAlAs/InGaAs HBTs [21] grown by SSMBE using CBr_4, the detailed characteristics of these devices and the current transport mechanism studies are still lacking.

ATTENTION: The Singapore Copyright Act applies to the use of this document. Nanyang Technological University Library

1.2 Objectives

Due to the advantages of both the carbon as p-type dopant and SSMBE system, the objective of this study is to grow C-doped GaAs and InGaAs by SSMBE system using CBr_4 as p-type dopant precursor and incorporate the materials into GaAs- and InP- based HBT devices for applications. The research work will focus on two aspects: 1) growth, characterization and optimization of C-doped GaAs and InGaAs materials; 2) understanding of C-doped GaAs-based and InP-based HBTs' characteristics and transport mechanisms.

1.3 Major contributions of the thesis

In this work, C-doped GaAs and InGaAs materials, C-doped GaInP/GaAs HBTs and InP/InGaAs HBTs grown by SSMBE using CBr_4 as p-type dopant precursor have been systematically characterized. The most important contributions of this thesis are summarized as follows:

1) C-doped GaAs and InGaAs materials have been successfully grown by SSMBE using CBr_4 as p-type dopant precursor. The electrical and structural properties, and doping mechanism of C-doped GaAs materials grown by SSMBE have been comprehensively investigated. Especially, compensation effects due to the formation of dicarbon defects at high CBr_4 flux have been described.

2) The effect of different growth conditions, such as substrate temperature, growth rate and V/III ratio on the properties of C-doped GaAs grown by SSMBE have been systematically investigated and optimum growth conditions have been obtained.

ATTENTION: The Singapore Copyright Act applies to the use of this document. Nanyang Technological University Library

3) C-doped GaInP/GaAs HBTs have been grown and fabricated successfully. Detailed DC characteristics have been investigated. The current transport mechanism studies have been carried out through the elevated temperature characteristics investigation. This provides an indirect way to assess the material quality.

4) C-doped InP/InGaAs SHBTs and composite collector DHBTs have been successfully grown by SSMBE and fabricated. DC characteristics of C-doped InP/InGaAs SHBTs and composite collector DHBTs have been compared. Both devices have shown promising DC characteristics. The complex breakdown behavior and mechanisms involved in the composite collector DHBTs have been elucidated.

1.4 Organization of the thesis

The thesis was organized in the following manner: Chapter 1 provides the motivation of this investigation. Chapter 2 briefly summarizes the principles of HBT devices. A brief review of carbon behavior in GaAs and InGaAs is presented. The material systems investigated are also introduced in this chapter. In Chapter 3, experimental techniques involved in this work including SSMBE, and the material characterization methods, such as X-ray Diffraction (XRD), photoluminescence (PL), atomic force microscopy (AFM), Hall measurement and secondary ion mass spectroscopy (SIMS) are described. In Chapter 4, the installation of CBr_4 source and calibration of CBr_4 flux are presented. The memory effect has been investigated. Chapter 4 also reports the growth and characterization of C-doped GaAs layers. Detailed characteristics of the layers, such as hole concentration, mobility, lattice mismatch, surface morphology, and optical properties have been discussed. Then, the C-doped GaAs PN homojunction grown by SSMBE has been successfully fabricated.

ATTENTION: The Singapore Copyright Act applies to the use of this document. Nanyang Technological University Library

In Chapter 5, the effects of growth conditions on the properties of C-doped GaAs have been investigated and optimum growth conditions have been obtained. Chapter 6 explores the application of C-doped GaAs as the base layer for HBT devices. The preliminary results of C-doped base-line GaInP/GaAs HBT grown by SSMBE are demonstrated and analyzed. In Chapter 7, improved DC characteristics of GaInP/GaAs HBTs have been analyzed and elevated temperature characteristics have been studied. Chapter 8 describes the growth and properties of C-doped InGaAs layers. C-doped InP/InGaAs SHBTs and composite collector DHBTs have been grown and fabricated. Breakdown characteristics of the composite collector DHBT have been investigated. Finally in Chapter 9, conclusions of this work are made and some recommendations for the future work are given.

ATTENTION: The Singapore Copyright Act applies to the use of this document. Nanyang Technological University Library

Chapter 2
Background

In this chapter, a brief account of heterojunction bipolar transistor (HBT) operation theory is presented. The development of carbon sources for SSMBE is described. A brief review of carbon doping behavior in GaAs and InGaAs is presented in the third part of this chapter. And the material systems investigated in the thesis are introduced.

2.1 Heterojunction Bipolar Transistor (HBT) operation theory

In a typical HBT, the emitter is made of a material which has a wider bandgap than the material used for the base and collector. Due to the different bandgap energy of the emitter and base materials, band offsets (discontinuities) exist in the conduction band and valence band at the emitter-base interface, as shown in Fig.2.1. For the abrupt HBT shown in Fig.2.1, the hole barrier (for the backward-injection current from base to emitter) is larger than the electron barrier (for the forward-injection current from emitter to base) by a magnitude of ΔE_v (since $V_{12} = V_{34}$). The forces acting on the electrons and holes are different, favoring the electron injection from the emitter into the base to the hole back-injection from the base into the emitter. The maximum common-emitter current gain (with the "secondary" current components neglected), β_{max}, for a wider-bandgap emitter HBT is given by, [22,23]

$$\beta_{max} \cong \frac{D_{nB} N_E L_{pE}}{D_{pE} N_B W_B} \exp\left(\frac{\Delta E_v}{kT}\right) \qquad \text{(for abrupt HBT)} \qquad (2.1)$$

ATTENTION: The Singapore Copyright Act applies to the use of this document. Nanyang Technological University Library

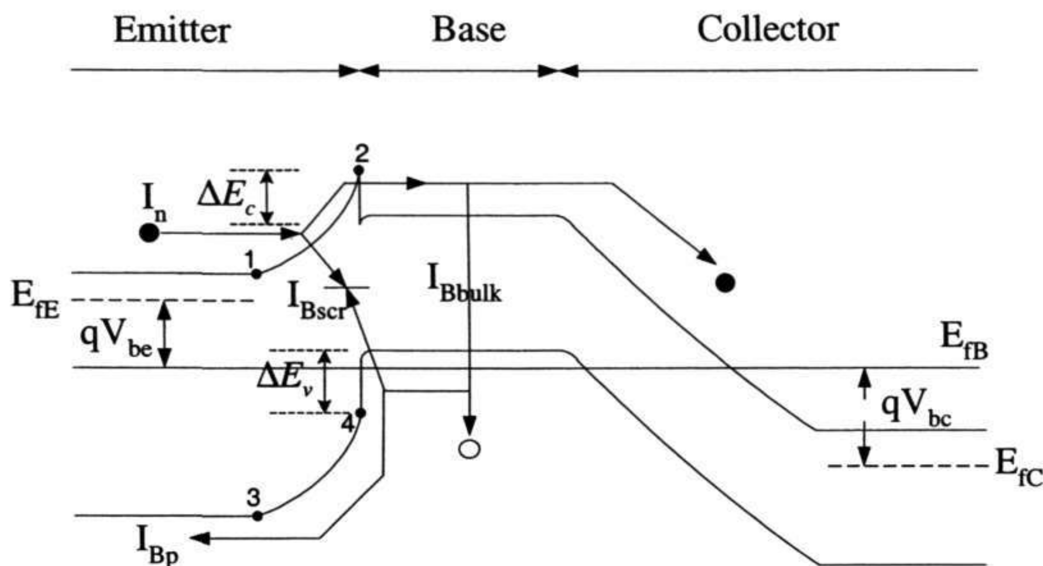

Fig.2.1 Schematic band diagram of an abrupt *n-p-n* HBT under typical operation conditions.

where D_{nB} is the minority hole diffusion coefficient, D_{pE} is the minority electron diffusion coefficient, N_E is the emitter doping level, N_B is the base doping level, L_{pE} is the hole diffusion length in the emitter region, and W_B is the base thickness. As Eq. (2.1) shows, even a relatively small valence band offset (ΔE_v) at the emitter-base junction can drastically increase the maximum current gain due to the exponential proportionality of $\beta_{\max}$ to ΔE_v. On the other hand, by inspection of Eq. (2.1), which does not require a huge ΔE_v though, a reasonably high common-emitter current gain can still be obtained even if the ratio of N_E and N_B is small. A lower doping of the emitter region (N_E) leads to a smaller emitter-base capacitance, which in turn improves the cut-off frequency (f_t). A higher base doping (N_B) reduces the

ATTENTION: The Singapore Copyright Act applies to the use of this document. Nanyang Technological University Library

base resistance, which in turn improves the maximum oscillation frequency (f_{max}). The higher doped base also allows narrower base thickness to be used without sacrificing the base resistance. This in turn gives rise to lower base transit time thus higher f_t. Both higher f_t and f_{max} values are desirable for high-speed application. Furthermore, much higher Early voltage is possible due to higher base doping.

For a real HBT, the parasitic currents must be taken into consideration. The base current can be classified into four components, namely, a) current of holes injected from base into the emitter region (I_{Bp}); b) surface recombination current in the exposed extrinsic base region (I_{Bsurf}); c) space charge region recombination current (I_{Bscr}); d) neutral bulk base region recombination current (I_{Bbulk}) [24].

The three terminal currents of a real HBT (I_e, I_b and I_c) are given [22] as follows:

$$I_e = I_n + I_{Bp} + I_{Bsurf} \tag{2.2}$$

$$I_b = I_{Bp} + I_{Bsurf} + I_{Bscr} + I_{Bbulk} \tag{2.3}$$

$$I_c = I_n - I_{Bscr} - I_{Bbulk} \tag{2.4}$$

where I_n is the current of electrons injected from emitter to the base.

The common-emitter current gain (β) of an HBT is given by:

$$\beta = \frac{I_c}{I_b} = \frac{I_n - I_{Bscr} - I_{Bbulk}}{I_{Bp} + I_{Bsurf} + I_{Bscr} + I_{Bbulk}} \tag{2.5}$$

At low current level, the surface recombination current I_{Bsurf} and space charge region recombination current I_{Bscr} may be the most important component dominating the base current. At high current level, neutral base recombination current I_{Bbulk} dominates the base current. The current gain is limited by the minority carrier lifetime.

ATTENTION: The Singapore Copyright Act applies to the use of this document. Nanyang Technological University Library

Optimization of the material growth and device fabrication process to reduce the parasitic components is particularly important to fabricate HBT devices with good DC characteristics.

2.2 The development of carbon sources for MBE

2.2.1 Graphite filament

Previously, C-doped HBTs have been grown in MBE using resistively heated graphite filament sources [25, 26]. While high doping (5×10^{19} cm^{-3}) can be obtained with a filament source, no high quality HBTs have been reported (current gain is below 10 when the base doping concentration is at 1×10^{19} cm^{-3}, and even lower when the base doping concentration increases), presumably because of the extremely short minority carrier lifetimes observed in those materials. At the higher doping levels required for HBT structures, the material quality degraded resulting in reduced HBT current gain. The low gain is due to the incorporation of additional nonradiative recombination centers during growth. Ito *et al.* [25] explained that the incorporation of nonradiative recombination centers into the GaAs base is related to chemical reactions of C atoms on the substrate surface during growth, such as compensation, pair formation, interstitial formation, and defect formation associated with carbon atoms. Although the C diffusion coefficient in the bulk GaAs is low enough to suppress the reactions between C atoms, this may not be the case on the surface. Pair formation may be much easier in the case of MBE, because thermally evaporated C atoms on the substrate surface can be very active, which is different from the case of C atoms dissociated from methyl or C-Cl bonds.

ATTENTION: The Singapore Copyright Act applies to the use of this document. Nanyang Technological University Library

2.2.2 CCl_4 and CBr_4

The halomethanes tetrachloride (CCl_4) and tetrabromide (CBr_4) have become the favored carbon doping precursors because they are efficient sources of carbon acceptors and also because carbon incorporation from them is relatively insensitive to growth conditions. Both CCl_4 and CBr_4 have been used in GSMBE [27,28,29] and MOCVD [30,31,32] with good doping and device results and without degradation of material quality associated with the presence of halogens in the growth system. However, in addition to the negative environmental impact of Cl-containing compounds, the relatively strong dependence of growth rate on doping level and the incorporation of chlorine into the layer are the main drawbacks of CCl_4 [33].

For CBr_4, the lower reactivity of bromine allows for better environmental compatibility. Furthermore, CBr_4 is a more efficient doping source. Fig.2.2 [27]

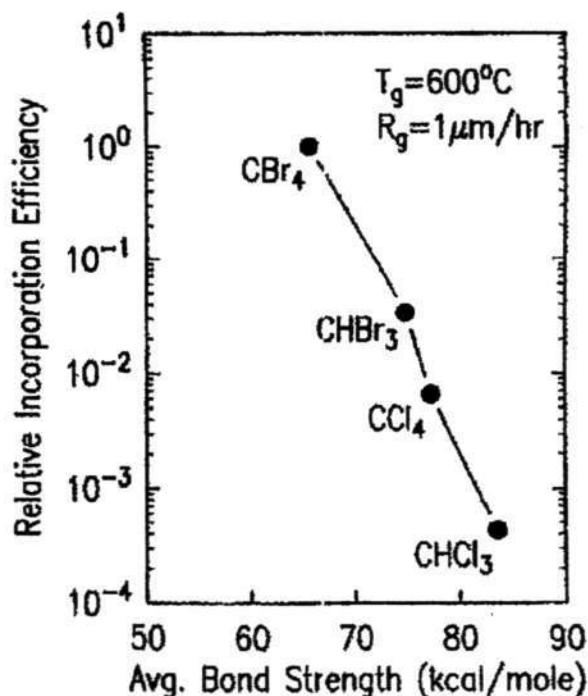

Fig.2.2 Relative incorporation efficiency of carbon in GaAs from various halomethane doping sources as a function of the average carbon nucleus-ligand bond strength of the precursor [27].

ATTENTION: The Singapore Copyright Act applies to the use of this document. Nanyang Technological University Library

shows the relative incorporation efficiency of carbon in GaAs from various halomethane doping sources as a function of the average carbon nucleus-ligand bond strength of the precursor. CBr_4 has 150 times higher doping efficiency than that of CCl_4. The higher efficiency of CBr_4 is due to the bond strength between C and Br (66 kcal/mole) being weaker than that between C and Cl (78 kcal/mole). Also, it has 750 times higher doping efficiency than that of trimethyl gallium (TMGa), which is used as a source of both C and Ga for MOCVD system. Furthermore, CBr_4 has a vapor pressure of about 400 times lower than that of TMGa. These data suggest that CBr_4 has the potential of reducing the gas pumping load at high doping levels. Therefore, this source is a very attractive candidate for carbon doping in MBE. We choose CBr_4 from Morton Int. as carbon source in our experiment.

2.3 A brief review of carbon behavior in GaAs and InGaAs

Carbon is of amphoteric nature. Depending on whether carbon occupies the group III site or the group V site, it behaves as donor or acceptor, respectively. Fig.2.3 shows the metal-carbon bond energy of group III and V elements commonly used in MBE [34]. According to Ito *et al.* [35], carbon tends to occupy sites which have weaker metal-carbon bond energy. This explains why it is easier to realize p-type doping in C-doped GaAs than in C-doped InGaAs. As shown in Fig.2.3, the bond energy for Ga-C is higher than that of As-C. Therefore, carbon is in favor of occupying the group V site (As) and behaves as an acceptor. However, the bond energy of As-C is higher than that of In-C, resulting in the substitution of carbon in the group III site and donor-like behavior. Therefore, carbon doping of InAs always results in n-type rather than p-type. In the case of $In_xGa_{1-x}As$, the behavior of carbon

ATTENTION: The Singapore Copyright Act applies to the use of this document. Nanyang Technological University Library

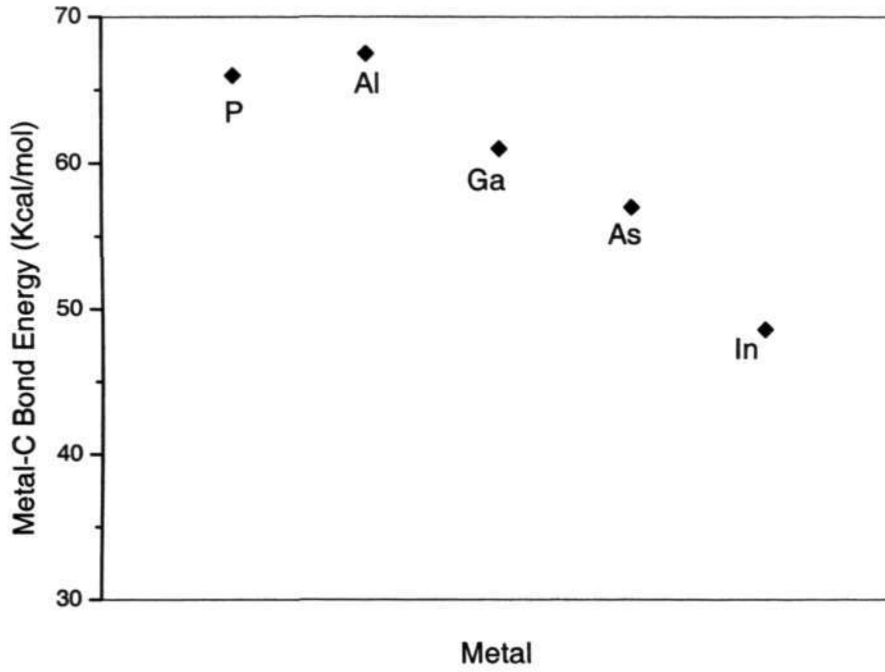

Fig.2.3 Metal-C bond energy for commonly used group III and V elements [34].

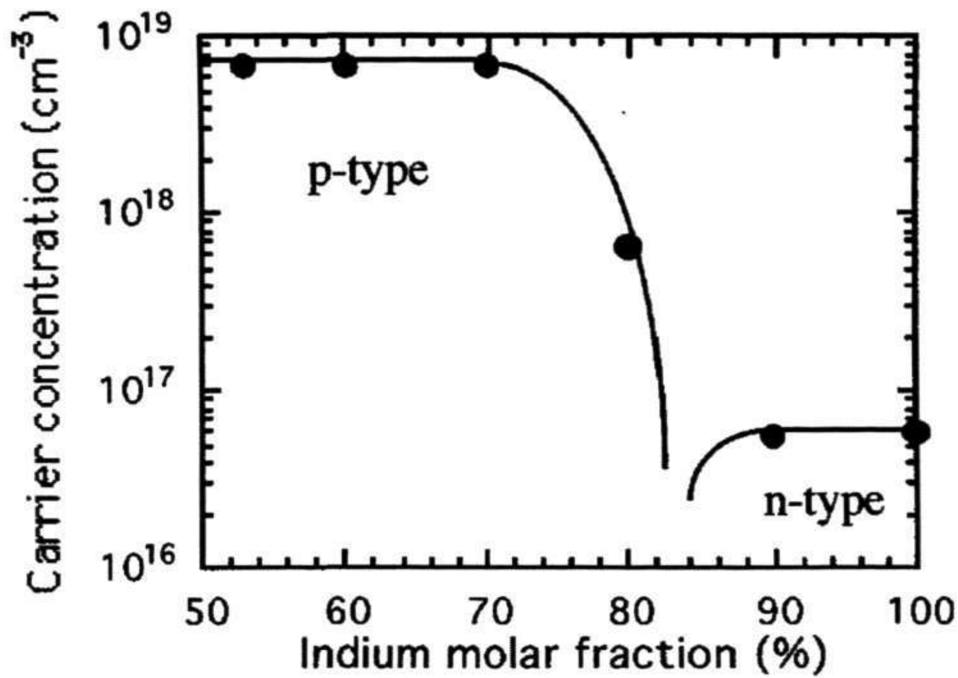

Fig.2.4 In molar fraction dependence of carrier concentration in C-doped $In_xGa_{1-x}As$ grown on (100) InP substrates [36].

ATTENTION: The Singapore Copyright Act applies to the use of this document. Nanyang Technological University Library

depends on the composition x of In. Experimental results show that for C-doped $In_xGa_{1-x}As$ grown by SSMBE using CBr_4 as p-type dopant precursor, carbon can be used as effective p-type dopant with In molar fraction up to $x = 0.7 - 0.8$. Fig.2.4 shows the dependence of carrier concentration in $In_xGa_{1-x}As$ layers as a function of In molar fraction [36].

2.4 Material systems investigated

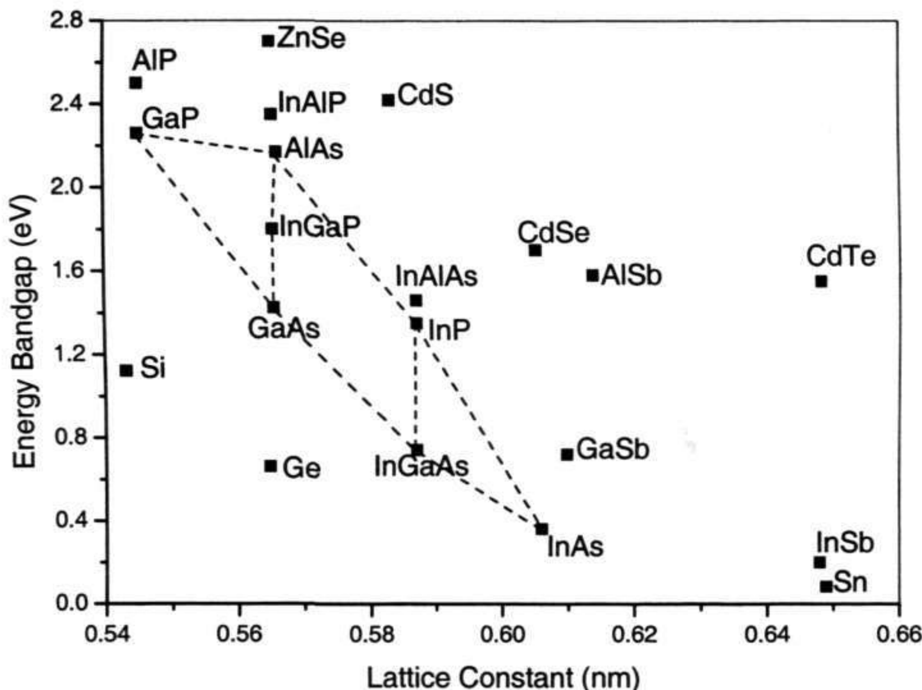

Fig.2.5 Energy bandgap *vs*. lattice constant of some commonly used semiconductor materials.

Figure 2.5 shows the energy bandgap *vs*. lattice constant of some commonly used semiconductor materials [37]. Two main families of III-V semiconductors, GaAs and InP, exist based on their substrate lattice constants. The lattice matched AlGaAs/GaAs system has been the most common material systems for HBT

ATTENTION: The Singapore Copyright Act applies to the use of this document. Nanyang Technological University Library

applications for wireless and optical communication systems. In recent years, GaInP/GaAs HBTs have become the focus of intense activity as alternatives to AlGaAs/GaAs HBTs due to their attractive features. In addition, compound semconductors lattice matched to InP have been developed for their high speed characteristics. The characteristics of the material systems investigated in this dissertation, GaInP/GaAs, InP/InGaAs, are briefly discussed in next section.

2.4.1 GaInP/GaAs

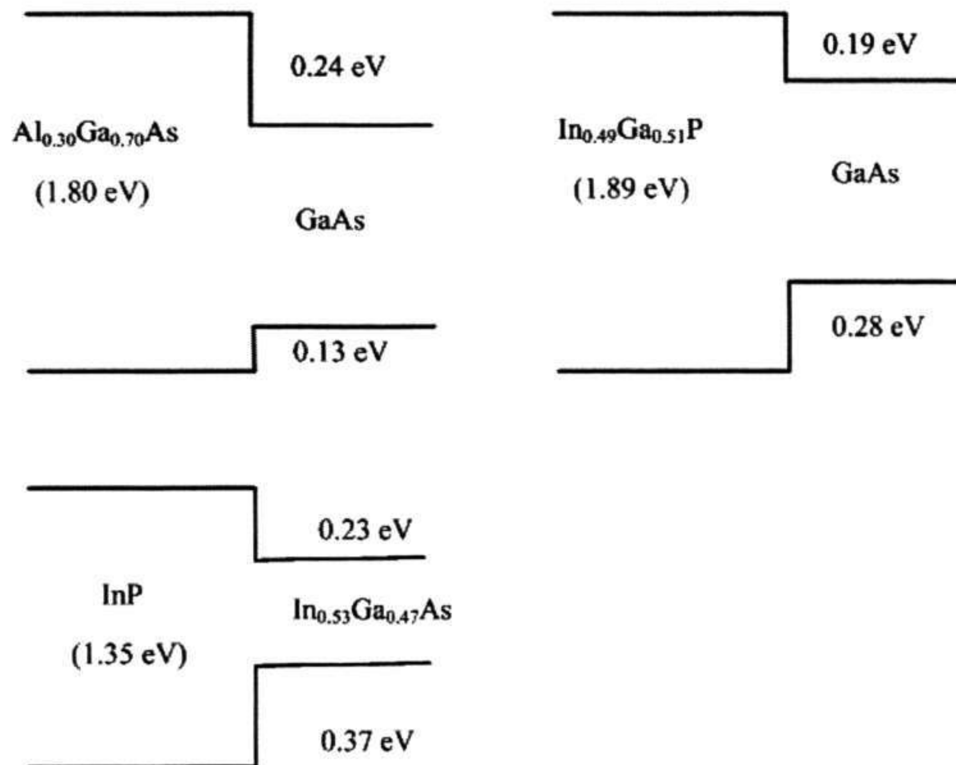

Fig.2.6 Energy band alignment between $Al_{0.30}Ga_{0.70}As$/GaAs, $In_{0.49}Ga_{0.51}P$/GaAs, and InP/$In_{0.53}Ga_{0.47}As$.

The ternary GaInP lattice matched to GaAs has gained increased acceptance as an alternative to AlGaAs as an emitter material [38]. The first advantage offered by $Ga_{0.51}In_{0.49}P$/GaAs devices is related to their emitter-base heterojunction which has a

ATTENTION: The Singapore Copyright Act applies to the use of this document. Nanyang Technological University Library

larger valence band offset (ΔE_v) and smaller conduction band offset (ΔE_c) as shown in Fig.2.6 a) and b). This provides the possibility of better injection efficiency compared with $Al_{0.30}Ga_{0.70}As$/GaAs HBTs. The second advantage of GaInP/GaAs over AlGaAs/GaAs is the extremely high etching selectivity between GaInP and GaAs, which enhances the process yield. Moreover, AlGaAs is easily oxidized when exposed to air because of the acute reactivity of aluminum. This impacts the device lifetime (reliability) and is a primary cause of noise. In contrast, the base-emitter space-charge region recombination in GaInP/GaAs HBTs is low enough to produce a base current ideality factor close to 1 and nearly-ideal current-voltage (I-V) characteristics with constant current gain.

2.4.2 InP/InGaAs

In recent years, InP-based HBTs have attracted great attention because InP and InGaAs lattice matched to InP ($In_{0.53}Ga_{0.47}As$) have unique material properties which enable better device performances than GaAs-based HBTs [39]. Because of the lower bandgap of $In_{0.53}Ga_{0.47}As$ (E_g ~ 0.75eV) than that of GaAs (E_g ~ 1.42eV) or Si (E_g ~ 1.12eV), it is suitable as an ohmic-contact layer and as the base layer of HBTs with a lower turn-on voltage. $In_{0.53}Ga_{0.47}As$ has a much higher electron mobility of 13,000 cm^2/Vs at room temperature which is 1.6 and 9 times higher than that of GaAs (8,000 cm^2/Vs) and Si (1,450 cm^2/Vs), respectively. This results in a short base transit time and a low concomitant diffusion capacitance. Figure 2.7 shows the velocity-field characteristics of InP and $In_{0.53}Ga_{0.47}As$ compared to GaAs and Si [40]. The extent of transient electron velocity overshoot is higher in $In_{0.53}Ga_{0.47}As$ than that in GaAs due to the separation between the gamma conduction band minimum and the satellite valleys ($\Delta E(\Gamma\text{-}L)$ = 0.55eV, $\Delta E(\Gamma\text{-}X)$ = 1.00eV) being considerably higher than that in

ATTENTION: The Singapore Copyright Act applies to the use of this document. Nanyang Technological University Library

GaAs (ΔE(Γ-L) = 0.30eV, ΔE(Γ-X) = 0.48eV). So $In_{0.53}Ga_{0.47}As$/InP material system is excellent for high-speed HBT implementation. Furthermore, a lower surface recombination velocity in $In_{0.53}Ga_{0.47}As$ allows easier scaling down of device dimensions with negligible surface recombination current. The higher thermal conductivity of InP substrate also improves the heat dissipation capability.

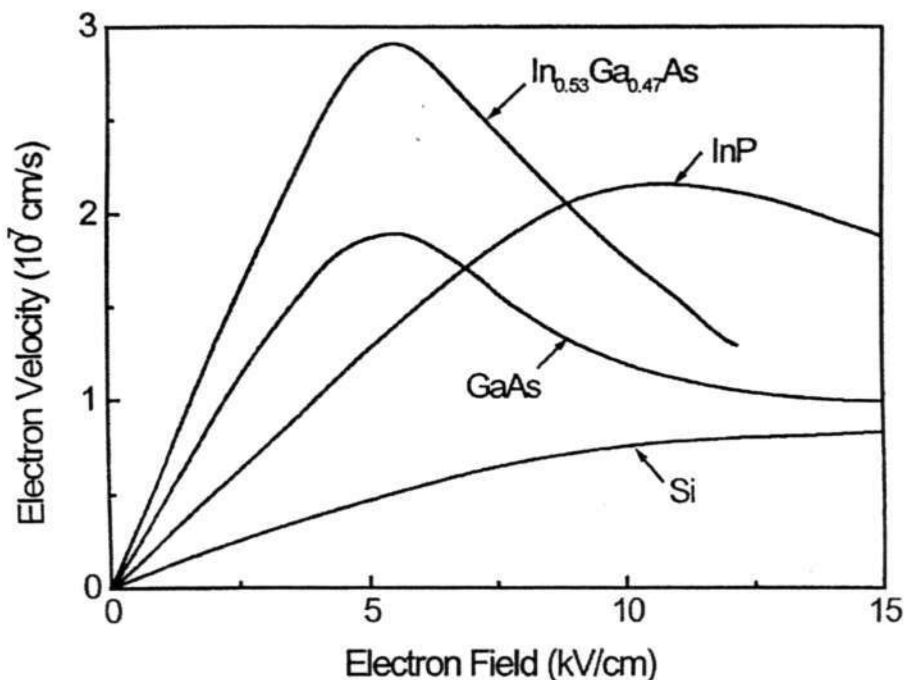

Fig.2.7 Equilibrium carrier velocity *vs*. electric field of various semiconductors.

2.5 Summary

In this chapter, a brief account of HBT operation theory has been presented. CBr_4 is regarded as a superior carbon source for SSMBE to CCl_4 and graphite filament. A brief review of carbon doping behavior in GaAs and InGaAs has been presented. And the material systems investigated in the thesis, i.e., GaInP/GaAs and InP/InGaAs, have been introduced.

ATTENTION: The Singapore Copyright Act applies to the use of this document. Nanyang Technological University Library

Chapter 3

Experimental techniques

In this chapter, a brief description of the SSMBE system and growth process is presented to explain the crystalline film preparation and growth process. The material characterization techniques, such as X-ray diffraction (XRD), photoluminescence (PL), atomic force microscopy (AFM), Hall measurement, and secondary ion mass spectroscopy (SIMS) are introduced.

3.1 Introduction to SSMBE

MBE is one of the oldest techniques for depositing solid films and is a valuable tool in the development of layer structures for sophisticated electronic and optoelectronic devices. Pioneered by A.Y. Cho at Bell Laboratories, MBE is an Ultra High Vacuum (UHV) deposition technique that has evolved from a surface physics study tool. The unique feature of MBE is the ability to prepare epitaxial layers with atomic dimensional precision down to a few angstroms. This ability allows the preparation of novel devices with multilayered epitaxial structures, and later has resulted in a host of highly efficient optical and electrical devices with superior characteristics. These include, to mention a few, strained Quantum Well (QW) lasers, vertical-cavity surface emitting lasers (VCSEL's), QW infrared photodetectors (QWIP), high electron mobility transistors (HEMT's), HBTs and Ga_2O_3-GaAs metal-oxide-semiconductor field-effect transistors (MOSFET's). These devices have found a wide range of applications in military, civilian and consumer systems. The MBE technique, developed originally for the AlGaAs/GaAs system, has rapidly expanded

ATTENTION: The Singapore Copyright Act applies to the use of this document. Nanyang Technological University Library

to include other III-V compounds along with group IV, II-VI and oxide materials. Meanwhile, to fulfill the need of producing complex heterostructures with high uniformity and reproducibility, various *in situ* real-time feedback growth control methods have been developed. This added capability allows the MBE technique to be used not only as a flexible research tool but also as a highly efficient production method. Currently, many industrial establishments have adopted the MBE technique for manufacturing optoelectronic as well as electronic devices.

3.1.1 The basic MBE process

The method of MBE is, in essence, a specialized form of vacuum deposition with several important characteristics [41]. The MBE growth of semiconductor films takes place by the reaction of molecular beams of the constituent elements with a crystalline substrate surface held at a suitable substrate temperature under UHV conditions. The molecular beams are generated from sources contained in effusion cells that are aimed at the heated substrate where the molecular beam flux intensity is accurately adjusted by the temperature within the effusion cell. The thermal beams emanating from effusion cells travel in rectilinear paths to the heated semiconductor substrate, where the atomic/molecular species migrate across the surface and combine to form successive layers of highly stoichiometric epilayers. To initiate or terminate the molecular beam flux, each source is provided with its own externally controlled mechanical shutter. Shutters in front of the orifices can be opened and closed within a tenth of a second, which is much shorter than the typical MBE growth rate of 1-2 monolayer/s, resulting in abrupt interfaces in the range of one atomic layer. Therefore, the sequence of opening and closing different shutters determines the multiplayer heterostructure in terms of both composition and doping profile.

ATTENTION: The Singapore Copyright Act applies to the use of this document. Nanyang Technological University Library

3.1.2 The SSMBE apparatus

All the samples studied in this investigation are grown by SSMBE system. The modern SSMBE system uses a modular configuration that contains a number of building blocks, such as the growth chamber, the sample exchange load-lock and the surface processing chamber, which are all interconnected by a UHV transfer tube. A basic SSMBE system for III-V compounds is shown in Fig.3.1.

The horizontally positioned UHV growth chamber is evacuated with a pumping stack that maintains a base pressure of 10^{-11} torr. The post popular pumping method for elemental sources is ion pumping or closed-cycle helium cryogenic pumping. In addition, a liquid-nitrogen-cooled shroud is used to enclose the entire growth area in order to minimize contamination from residual water vapor and hydrocarbons during epitaxy. The sample exchange load-lock permits the maintenance of UHV in the growth chamber while changing substrates between successive growth runs.

The substrate is typically mounted on a molybdenum (Mo) substrate holder attached to a sample manipulator for precise positioning within the growth chamber. Thermal radiation generated by resistance heating from behind the substrate holder is employed to heat the substrate. To maintain a stable substrate temperature, tungsten-rhenium thermocouples coupled with a temperature controller are used to regulate the input power to the substrate heater. On the back side of the manipulator there is an ion gauge for beam flux measurements.

ATTENTION: The Singapore Copyright Act applies to the use of this document. Nanyang Technological University Library

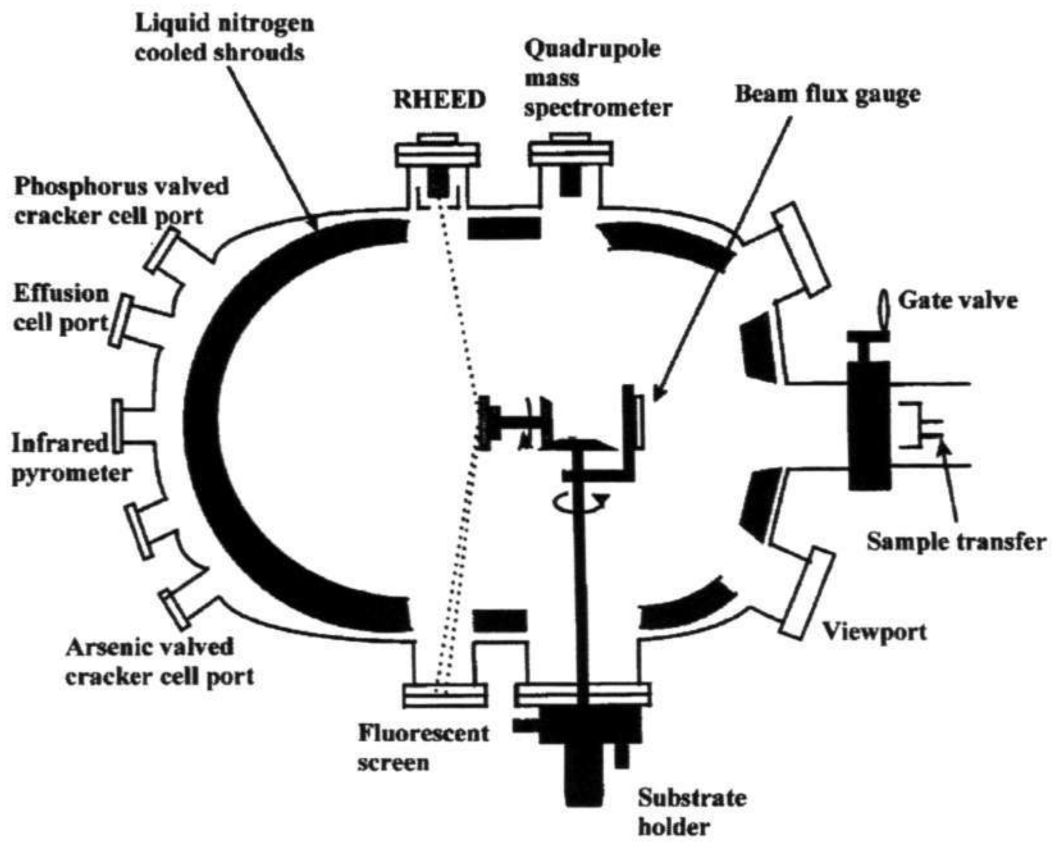

Fig.3.1 Schematic diagram of SSMBE growth chamber.

ATTENTION: The Singapore Copyright Act applies to the use of this document. Nanyang Technological University Library

In the growth chamber there is a quadrupole mass spectrometer for leak detection by measuring the residual gas composition in the vacuum system as well as calibrating the relative amount of molecular species emanating from the effusion cells.

The surface flange on the growth chamber contains a viewport and several ports for mounting effusion cells and/or gas injectors. Each of the effusion cell ports is equipped with an externally controlled mechanical shutter. Ultrahigh-purity elemental source materials loaded in pyrolytic boron nitride effusion cell crucibles are used to generate the desired molecular beams. The effusion cell temperatures are controlled to an accuracy of ± 1 °C to provide the precise amount of beam flux. Each effusion cell assembly is surrounded by a liquid-nitrogen-cooled shroud to minimize outgassing and to eliminate cross talk between neighboring cells. To prevent rapid depletion of volatile group V elements and to provide a means of rapid change of group V beam fluxes, valved-cracking effusion cells have been developed. The valved-cracking effusion cell consists of a low-temperature group V source container, a needle valve, and a high-temperature cracking heater.

The reflection high-energy electron diffraction (RHEED) apparatus is the most useful and important surface analysis instrument in the MBE growth chamber. It provides a very sensitive yet simple way to observe changes in the structure of the outermost layers of atoms in a crystal before and during growth as a function of growth conditions. It is possible to obtain information concerning substrate cleanliness, smoothness, and surface structure from the RHEED patterns.

ATTENTION: The Singapore Copyright Act applies to the use of this document. Nanyang Technological University Library

3.2 Material characterization techniques

3.2.1 X-Ray Diffraction (XRD)

XRD is widely used not only as a routine assessment to material structures but also as a high sensitive tool for detailed characterization of epitaxial layers, which are very thin crystalline films with the same crystalline orientation as the substrate [42]. It is a versatile, non-destructive analytical technique.

In a single crystal, the atoms are arranged in a regular three-dimensional array, which is known as the crystal lattice. The atoms within a lattice can be considered to be located on a series of equally spaced planes. When a monochromatic x-ray beam with wavelength λ is projected onto a crystalline material at an angle θ_B, diffraction occurs only when the distance traveled by the rays reflected from successive planes differs by a complete number n of wavelengths, which is known as Bragg's Law. That is:

$$\Delta l = n\lambda \tag{3.1}$$

i.e.

$$n\lambda = 2d\sin\theta_B \tag{3.2}$$

Fig.3.2 shows the path difference of the incident and diffracted X-ray beams. The diffracted radiation is said to have undergone the "(hkl) reflection" if the planes are separated by a_1/h, a_2/k and a_3/l, respectively, in the three axial directions, where h, k, and l are integers. Here, (hkl) is the so-called Miller indices representing a certain lattice plane. The interplanar spacing of a (hkl) reflection is then given by:

$$d_{hkl} = \frac{1}{\sqrt{h^2/a_1^2 + k^2/a_2^2 + l^2/a_3^2}} \tag{3.3}$$

ATTENTION: The Singapore Copyright Act applies to the use of this document. Nanyang Technological University Library

Here the a_1, a_2, and a_3 are the three dimensional lattice parameters, respectively. For a fixed wavelength λ and spacing d_{hkl}, a strong diffracted X-ray only occurs at a fixed angle.

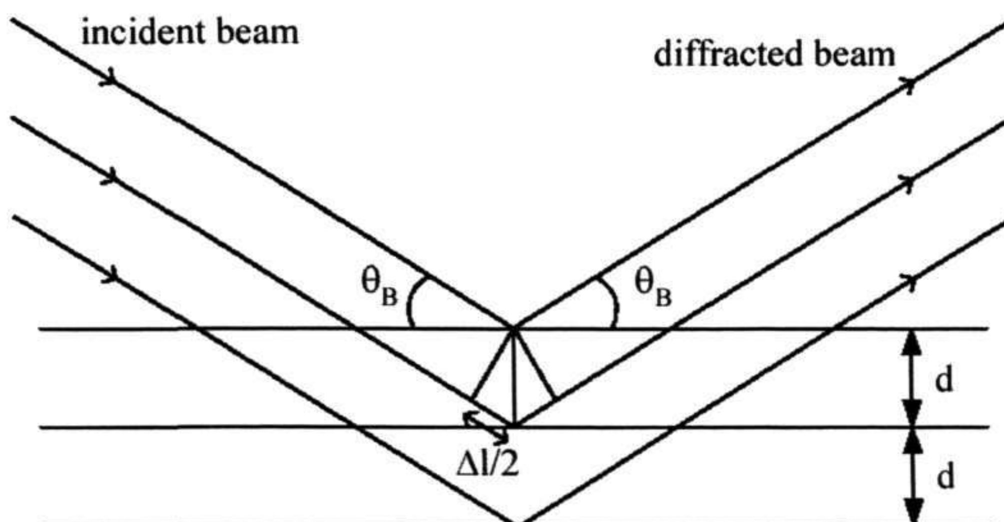

Fig.3.2 The diagram showing the path difference of the incident and diffracted X-ray beams.

Consider the case of a lattice-mismatched epitaxial layer grown on a substrate. Due to the different lattice spacing, the X-ray diffraction curve will generally exhibit two peaks corresponding to the Bragg angles of the epitaxial layer and the substrate. The separation of these peaks is directly related to the difference in lattice parameters. For the symmetric reflections, only the lattice mismatch along the surface can be determined by differentiating the Bragg'd Law:

$$\left(\frac{\Delta a}{a}\right)_{\perp} = \left(\frac{\Delta d}{d}\right)_{\perp} = -\Delta\theta \cdot \cot\theta_B \tag{3.4}$$

ATTENTION: The Singapore Copyright Act applies to the use of this document. Nanyang Technological University Library

where $\Delta\theta$ is the difference of Bragg angles between the epitaxial layer and the substrate, which can be precisely determined by X-ray diffraction.

To determine the lattice mismatch parallel to the sample surface, asymmetric reflections are necessary. For asymmetric reflections, the reflecting lattice planes are not parallel to the sample surface. For an arbitrary (hkl) reflection of a tetragonally distorted lattice with the lattice parameters $a_\perp$ and $a_\parallel$, where $a_\perp$ and $a_\parallel$ are the lattice parameters perpendicular and parallel to the layer plane, respectively, the following equations are given as [43]:

$$2\sin\theta_B \cos\varphi = \frac{l\cdot\lambda}{a_\perp} \tag{3.5}$$

$$2\sin\theta_B \sin\varphi = \frac{\sqrt{h^2+k^2}\cdot\lambda}{a_\parallel} \tag{3.6}$$

Here φ is the angle between the reflecting plane and the sample surface. From the lattice parameters determined by Eq. (3.5) and (3.6), the lattice mismatch both perpendicular and parallel to the surface can be derived as:

$$\left(\frac{\Delta a}{a}\right)_\perp = \frac{a_\perp - a_s}{a_s} \tag{3.7}$$

$$\left(\frac{\Delta a}{a}\right)_\parallel = \frac{a_\parallel - a_s}{a_s} \tag{3.8}$$

where a_s is the lattice parameter of the substrate. For a strain relaxed layer, the residual strain and strain relaxation ratio can also be calculated when the values of $a_\perp$ and $a_\parallel$ are determined by Eq. (3.7) and (3.8).

XRD measurements in this investigation were performed using Philips MRD high resolution X-ray diffractometer. This high resolution spectrometer system is equipped with a four-crystal monochromator in front of the specimen and a three-

ATTENTION: The Singapore Copyright Act applies to the use of this document. Nanyang Technological University Library

reflection Ge (220) channel-cut analyzer crystal for the diffracted beam, which is suitable not only for rocking curve measurement but also for reciprocal space mapping.

3.2.2 Photoluminescence (PL)

PL spectroscopy is a contactless, nondestructive method of probing the electronic structure of materials [44]. Specifically, light is directed onto a sample, where it is absorbed and imparts excess energy into the material in a process called "photo-excitation." One way this excess energy can be dissipated by the sample is through the emission of light, or luminescence. In the case of photo-excitation, this luminescence is called "photoluminescence." The intensity and spectral content of this photoluminescence is a direct measure of various important material properties.

More specifically, photo-excitation causes electrons within the material to move into permissible excited states. When these electrons return to their equilibrium states, the excess energy is released and may include the emission of light (a radiative process) or may not (a nonradiative process). The energy of the emitted light—or photoluminescence—is related to the difference in energy levels between the two electron states involved in the transition—that is, between the excited state and the equilibrium state. The quantity of the emitted light is related to the relative contribution of the radiative process.

The applications of PL spectrum is as the following aspects:

- Band gap determination. The most common radiative transition in semiconductors is between states in the conduction and valence bands, with the energy difference being known as the band gap. Band gap determination is particularly useful when working with new compound semiconductors.

ATTENTION: The Singapore Copyright Act applies to the use of this document. Nanyang Technological University Library

- Impurity levels and defect detection. Radiative transitions in semiconductors also involve localized defect levels. The photoluminescence energy associated with these levels can be used to identify specific defects, and the amount of photoluminescence can be used to determine their concentration.
- Recombination mechanisms. As discussed above, the return to equilibrium, also known as "recombination," can involve both radiative and nonradiative processes. The amount of photoluminescence and its dependence on the level of photo-excitation and temperature are directly related to the dominant recombination process. Analysis of photoluminescence helps to understand the underlying physics of the recombination mechanism.
- Material quality. In general, nonradiative processes are associated with localized defect levels, whose presence is detrimental to material quality and subsequent device performance. Thus, material quality can be measured by quantifying the amount of radiative recombination.

The PL measurements in this work were carried out using a SPEX system. Fig. 3.3 is the schematic diagram of the PL system. The excitation source is an Ar+ laser with the excitation power density of ~5 W/cm^2 and the wavelength is 514.5 nm. A chopper modulates the laser beam in order to process the signal by a lock-in amplifier. Samples are mounted in a vacuum chamber and can be cooled down to 4 K by a closed cycle He cryostat. The PL spectra are detected using a GaAs photo-multiplier tube (PMT) with a 1800 gr/mm grating spectrometer or a liquid nitrogen cooled Ge detector with a 1200 gr/mm grating spectrometer.

ATTENTION: The Singapore Copyright Act applies to the use of this document. Nanyang Technological University Library

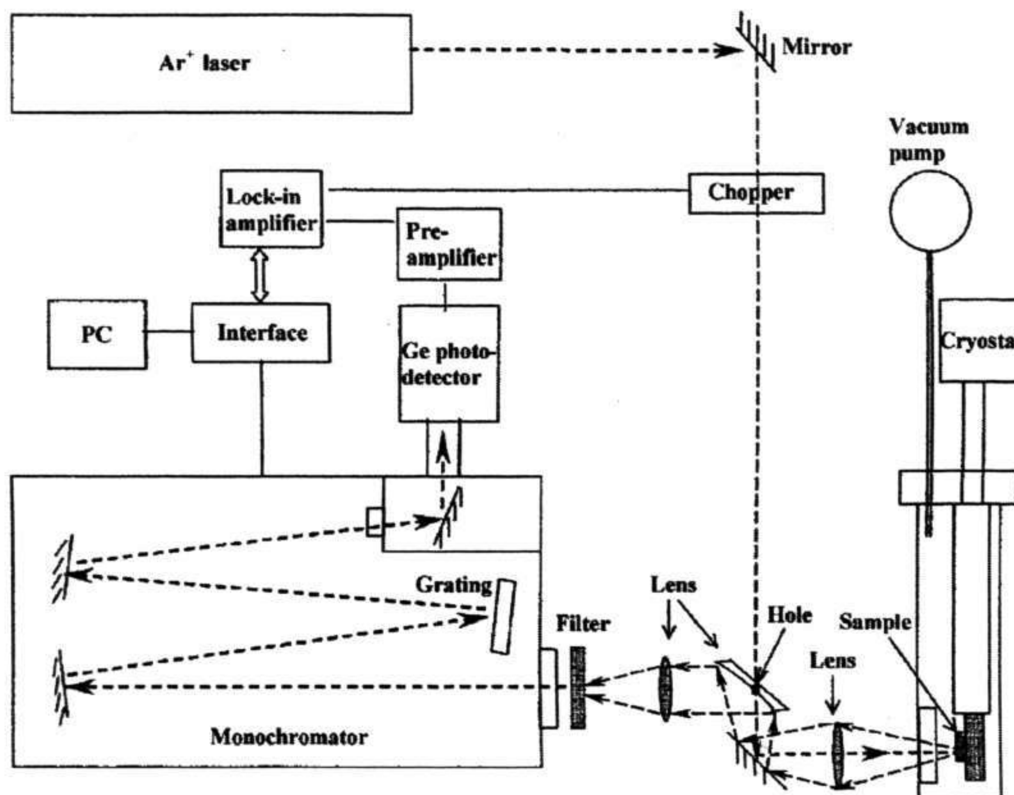

Fig.3.3 The schematic diagram of the PL experimental apparatus.

3.2.3 Atomic Force Microscopy (AFM)

AFM [45,46] is a powerful tool for high-resolution imaging of surfaces, which was developed quickly based on the invention of the scanning tunneling microscope (STM). Similar to STM, the AFM probes the sample surface using a sharp tip, which is several microns long and often less than 100Å in diameter. The tip is located at the free end of a cantilever. Unlike STM, which applies bias voltage on the tip and monitors the tunneling current between the tip and the sample, the AFM detects the interatomic force between the sample surface and the tip, which rises if the tip is placed very close to the surface. The force can cause the cantilever to bend, or deflect, which can be detected by a detector. When the tip is scanned over the sample, or the

ATTENTION: The Singapore Copyright Act applies to the use of this document. Nanyang Technological University Library

sample is scanned under the tip, measured cantilever deflection allows a computer to generate a map of surface topography. AFM can be used to study insulators and semiconductors as well as electrical conductors.

In this thesis, all samples were characterized by contact mode AFM using Shimadzu SPM scanning probe microscope. A standard Si_3N_4 tip was employed for the surface scan. No special sample preparation was required. The detection of the cantilever deflection was achieved by a laser beam irradiating on the back of the cantilever and reflecting into a position-sensitive photodetector (PSPD). Fig.3.4 is the schematic diagram of the AFM.

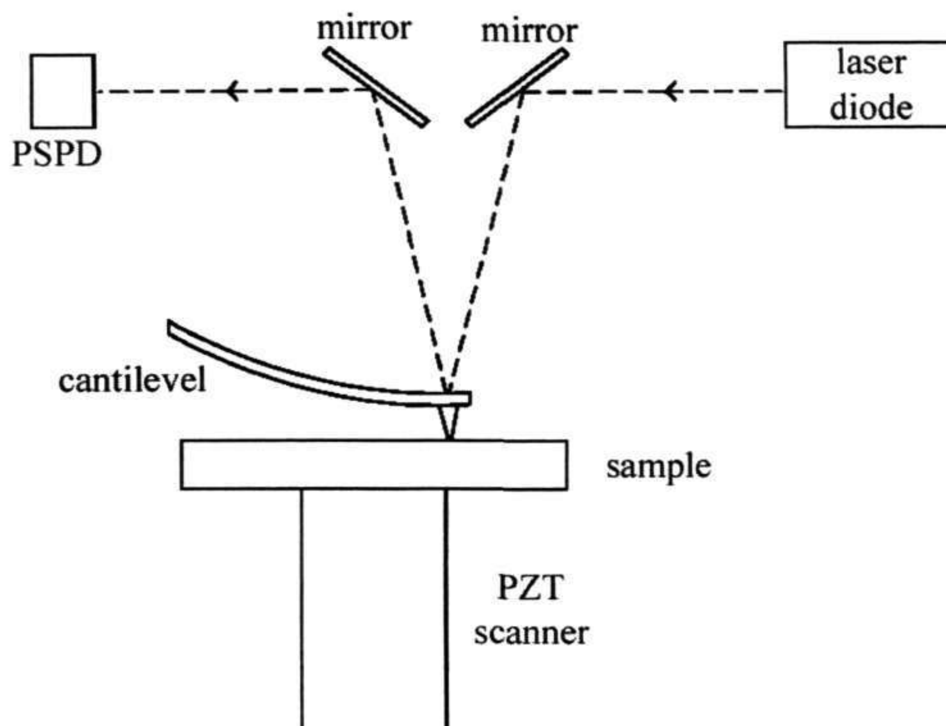

Fig.3.4 Schematic diagram of AFM.

ATTENTION: The Singapore Copyright Act applies to the use of this document. Nanyang Technological University Library

3.2.4 Hall measurement

In semiconductors, when the carriers move perpendicular to the direction of the magnetic filed or at an oblique angle, the Lorentz force will make the carriers deflected from the direction of motion, which is caused by the effect known as Hall effect [47]. The deflection of the carrier will cause a Hall voltage. The Hall effect measurement is a useful tool to determine the carrier concentration and the Hall mobility of the semiconductor. Such measurements are extremely useful in the analysis of the electrical properties of semiconductors.

In this work, the Hall measurement was carried out using a Bio-Rad system with Van der Pauw Hall method. The measurement was performed at room temperature, and the magnetic field applied was 0.32 T. Prior to the measurement, ohmic contacts were formed by annealing pure indium on the samples in nitrogen ambient at 380 ^{o}C for 60 seconds. The size of all the samples for Hall measurement was kept at 1×1 cm^2.

3.2.5 Secondary Ion Mass Spectrometry (SIMS)

Secondary ion mass spectrometry (SIMS) [48] is a technique that measures elements at a surface with detection sensitivity as low as a few parts per billion. The technique of SIMS is the most sensitive of all the commonly employed surface analytical techniques. In an ultra high vacuum environment, a beam of energetic oxygen or cesium ions is directed to a surface to be analyzed. These bombarding ions force atomic and molecular particles to be ejected from the surface, a process called sputtering. When the primary ion strikes the sample there is a momentum transfer to the target atom. This occurs because the primary ion penetrates the sample surface, travels into the sample for some distance, and then collides with the target atom. The

ATTENTION: The Singapore Copyright Act applies to the use of this document. Nanyang Technological University Library

collisions repeat until the energy transfer is insufficient to displace any more target atoms. The ejection or sputtering of target atoms occurs because much of the momentum transfer is redirected towards the surface by recoil within this collision sequence. This makes this method of analysis destructive because the sample is actually eroded, or etched on an atomic level. Since some of these sputtered particles carry a charge, a mass spectrometer can be used to measure their mass and charge. Continued sputtering measures the elements exposed as material is removed to construct elemental depth profiles. SIMS instruments can produce two-dimensional elemental maps of the original surface or at a particular depth (after sputtering).

3.3 Summary

In this chapter, a brief description of the SSMBE system and growth process has been presented to explain the crystalline film preparation and growth process. The material characterization techniques used in this thesis have been introduced. XRD is widely used not only as a routine assessment to material structures but also as a high sensitive tool for detailed characterization of epitaxial layers. PL spectroscopy is a contactless, nondestructive method of probing the electronic structure of materials. AFM is a powerful tool for high-resolution imaging of surfaces. The Hall effect measurement is a useful tool to determine the carrier concentration and the Hall mobility of the semiconductor. SIMS is a technique that measures elements at a surface with detection sensitivity as low as a few parts per billion.

ATTENTION: The Singapore Copyright Act applies to the use of this document. Nanyang Technological University Library

Chapter 4
Growth and characterization of C-doped GaAs

In this chapter, the installation of the carbon source and the calibration of CBr_4 flux are described. Material properties of C-doped GaAs are also presented in detail. The C-doped PN junctions have been grown and fabricated.

4.1 Introduction

In GaAs, the carbon impurity sits on the arsenic sublattice and introduces a shallow acceptor level that produces p-type GaAs with a high hole mobility [49]. Carbon in GaAs exhibits low thermal diffusivity and high solubility, enabling sharp dopant profiles at high doping levels that are appropriate for electronic devices.

4.1.1 Brief review of C-doped GaAs grown by various techniques

Very high carbon doping concentrations in GaAs have been obtained by different growth techniques. Table 4.1 shows the brief history of carbon doping in GaAs grown by several techniques. The highest hole concentration of C-doped GaAs obtained was 1×10^{21} cm^{-3}.

ATTENTION: The Singapore Copyright Act applies to the use of this document. Nanyang Technological University Library

Table 4.1 Development of C-doped GaAs grown by various techniques.

Year	Growth technique	Maximum hole concentration (cm^{-3})	Carbon source	Reference
1988	MOMBE	5.8×10^{20}	TMGa	[50]
1991	GSMBE	1×10^{20}	CBr_4	[51]
1991	MOCVD	1.5×10^{20}	CCl_4	[52]
1991	MOMBE	1×10^{21}	TMGa	[53]
1991	SSMBE	5×10^{19}	Graphite filament	[54]
1993	MOCVD	1×10^{21}	TMGa	[55]
1993	SSMBE	1.5×10^{20}	CBr_4	[56]
1994	CBE	6×10^{20}	CBr_4	[57]
1997	GSMBE	5×10^{20}	CBr_4	[58]

4.1.2 Heavy doping issue in C-doped GaAs

It has been reported that the net hole concentration in C-doped GaAs is relatively low at a high total carbon concentration ($>5\times10^{19}$ cm^{-3}). The main reasons have been found to be the following:

- Interstitial carbon donors [59,60];
- For those growth techniques with hydrogen rich environment, the unintentional hydrogen passivation of carbon acceptors during growth and the post-growth cool down [61].

Carbon doping levels $>10^{20}$ cm^{-3} can be easily obtained in CBE with almost 100% activation, good surface morphology, and with reduced hydrogen incorporation compared with MOCVD grown C-doped GaAs [62]. SSMBE offers the advantage of hydrogen free environment, eliminating the passivation of carbon acceptor by hydrogen [57].

ATTENTION: The Singapore Copyright Act applies to the use of this document. Nanyang Technological University Library

4.2 CBr_4 source installation and flux calibration

4.2.1 CBr_4 gas handling system

In this work, the high-purity solid CBr_4 source is contained in a sealed stainless-steel cylinder immersed in a constant temperature bath for regulating its vapor pressure. The cylinder is well evacuated and the distribution line well purged with nitrogen before the introduction of sublimed CBr_4 into the MBE chamber. CBr_4 was delivered from its container to the leak valve through gas line. The gas line was kept at 100 °C to prevent condensation of CBr_4. A UHV leak valve is used to control the CBr_4 flux to be injected into the growth chamber. No carrier gas was used to transport the CBr_4 into the MBE system. As convention, the flux of CBr_4 is measured with the beam flux monitor. Fig.4.1 shows a schematic illustration of the CBr_4 gas handling and injection system. The maximum attainable flux of CBr_4 is limited by the maximum conductance of the leak valve. The maximum vapor pressure of CBr_4 (at temperature lower than 60 °C) shown from a beam flux monitor is 1.3×10^{-6} torr.

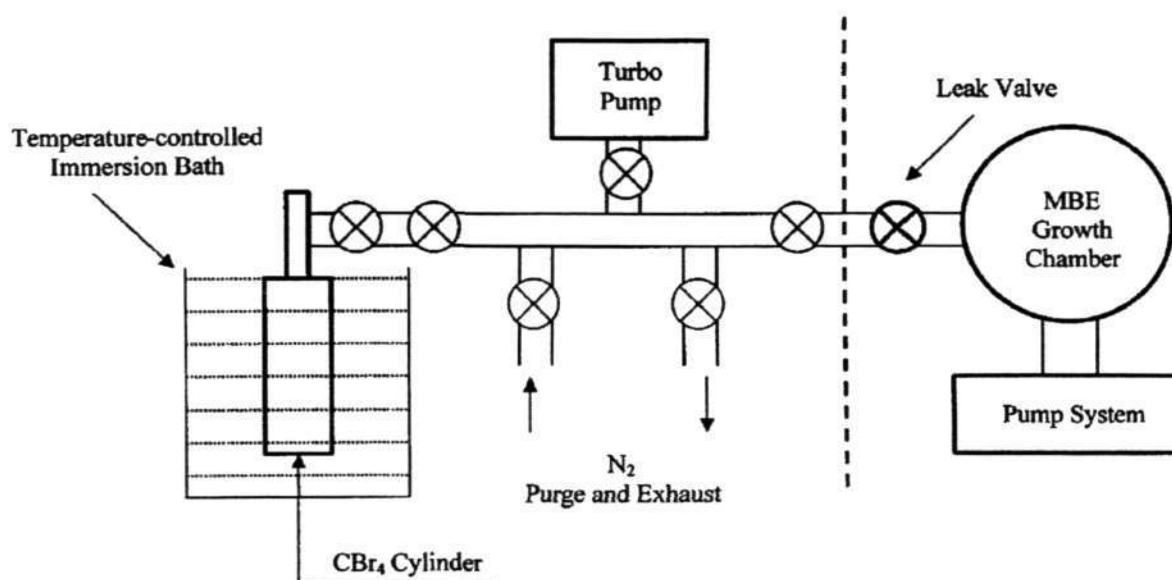

Fig.4.1 Schematic illustration of the CBr_4 gas handling system.

ATTENTION: The Singapore Copyright Act applies to the use of this document. Nanyang Technological University Library

4.2.2 CBr_4 Flux control

Initially, the leak valve position and the CBr_4 flux obtained were investigated with the CBr_4 source keeping at a given temperature. Fig.4.2 shows the CBr_4 relative flux as a function of leak valve position at 2 °C of CBr_4 source. It can be seen that there was no CBr_4 flux when the leak valve was opened below 2 turns and it saturated when the leak valve was opened above 6 turns.

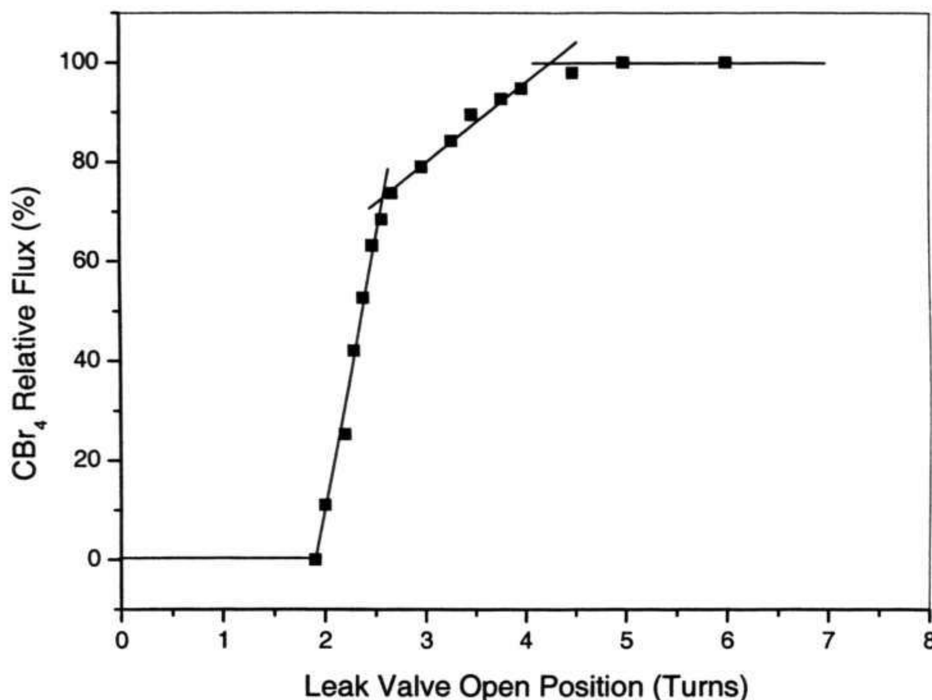

Fig.4.2 CBr_4 relative flux versus leak valve open position with CBr_4 source keeping at a given temperature.

Then, the leak valve position and the CBr_4 flux obtained were investigated with the CBr_4 source keeping at different temperature. Fig.4.3 plots the CBr_4 flux versus the leak valve opening position at three different temperatures. The CBr_4 flux increases rapidly, followed by saturation, with increase in the leak valve position (i.e.

ATTENTION: The Singapore Copyright Act applies to the use of this document. Nanyang Technological University Library

number of opening turns). A wide range of CBr_4 flux can be obtained by increasing the cylinder temperature from 2 °C to 20 °C, as the valve position is varied from fully close to fully open. At 2 °C, the CBr_4 flux ranges from ~ 1.0×10^{-8} to ~ 9×10^{-8} torr, and at 20 °C, it ranges from ~ 6×10^{-8} to ~ 1×10^{-6} torr. A sustainable and stable CBr_4 flux is essential, especially for long growth time during which homogenous carbon doping is required. Measurement of CBr_4 flux before and after sample growth shows essentially the same value with variation lower than 2.5%, indicating good flux stability and sustainability during the entire doping process. For example, a typical CBr_4 flux of 4.6×10^{-8} torr only has an uncertainty of ~ 0.1×10^{-8} torr within the growth duration of 1 hour.

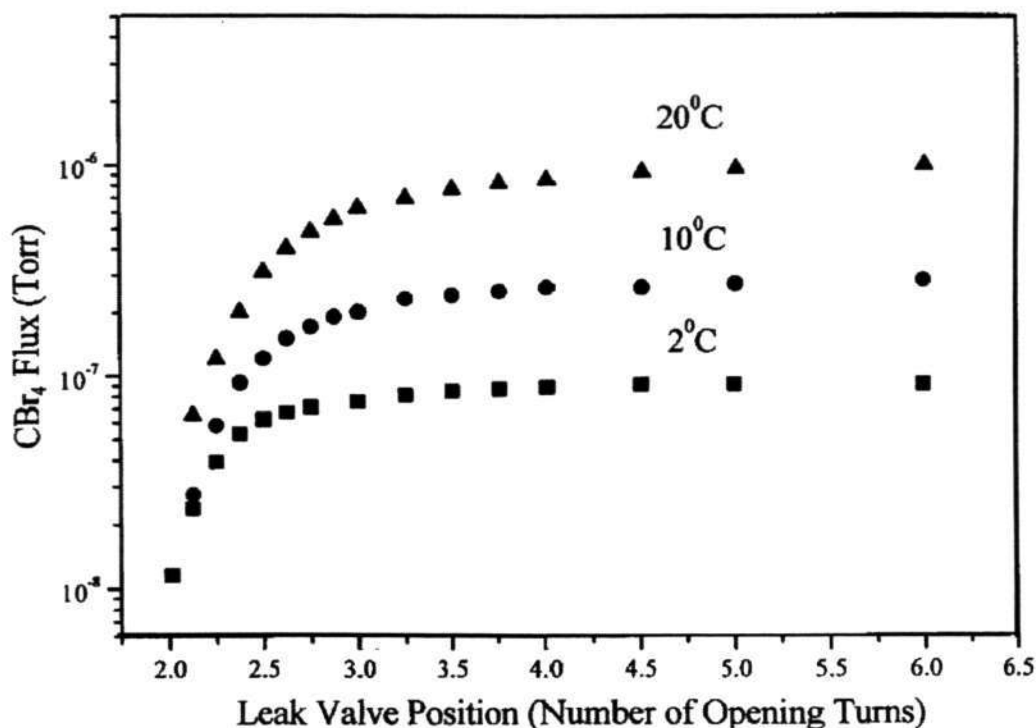

Fig.4.3 Plot of CBr_4 flux versus leak valve opening position at different cylinder temperature.

ATTENTION: The Singapore Copyright Act applies to the use of this document. Nanyang Technological University Library

4.2.3 Investigation of memory effect

The memory effect was investigated roughly through comparison between the unintentionally doped GaAs films grown one day before CBr_4 doping as well as two hours and one day after CBr_4 doping. It can be seen that small memory effect existed. For the first batch of samples, the unintentionally doped hole concentration (after 2 hours of CBr_4 doping up to 1×10^{20} cm^{-3}) reached 2.05×10^{16} cm^{-3} as shown in Table 4.2. However, for the doping level commonly used for HBTs (~ 5×10^{19} cm^{-3}), the memory effect is negligible, as can be seen from the results of the second and third batch of samples.

Table 4.2 Investigation of memory effect.

	Batch	1 Day before CBr_4 doping	CBr_4 doping	2 Hours after CBr_4 doping	1 Day after CBr_4 doping
Hole concentration	1	3.55×10^{15}	1×10^{20}	**2.05×10^{16}**	3.48×10^{15}
		(382)	(20)	(261)	(299)
(cm^{-3})	2	/	7.5×10^{19}	6.39×10^{15}	1.78×10^{15}
(mobility)		/	(44)	(330)	(386)
(cm^2/Vs)	3	/	3.3×10^{19}	2.74×10^{15}	1.3×10^{15}
		/	(89)	(395)	(409)

4.3 Growth and characterization of C-doped GaAs

The C-doped GaAs samples were grown using SSMBE on GaAs (100) semi-insulating (S.I.) substrates. Initially, the GaAs growth rate was maintained at 1 μm/h and growth temperature at 600 °C. The CBr_4 source was kept at 2-20 °C. The As_4/Ga flux ratio used was about 18. The thickness of the GaAs buffer layer and C-doped

ATTENTION: The Singapore Copyright Act applies to the use of this document. Nanyang Technological University Library

GaAs epilayer was 1000 Å and 4000 Å, respectively. Conventional procedures were used for substrate preparation, degassing and oxide desorption.

The C-doped GaAs materials were characterized by various methods. The hole concentration and mobility at room temperature were measured using the van-der-Pauw Hall effect technique. High resolution XRD was used to measure the lattice parameters of the C-doped GaAs epilayers. PL measurements were performed at 4 K and at different temperatures to investigate the optical properties. SIMS measurements were conducted to provide information on atomic concentration and dopant depth profile.

4.3.1 Hall results of C-doped GaAs

The variation of hole concentration at room temperature as a function of CBr_4 flux in our C-doped GaAs samples is shown in Fig.4.4. It can be seen that the hole concentration increases following increase in CBr_4 flux and reaches a maximum of 1.86×10^{20} cm^{-3} at CBr_4 flux of 2.6×10^{-7} torr. The SIMS results show that at CBr_4 flux level below 2.6×10^{-7} torr, the hole concentration and the number of carbon atoms incorporated into GaAs are in good agreement. This indicates that the carbon atoms incorporated into GaAs are nearly fully activated. However, as shown in Fig.4.4, the hole concentration decreases rather significantly beyond CBr_4 flux of 2.6×10^{-7} torr. The total carbon atomic density from SIMS should have continued to increase as the CBr_4 flux was increased above 2.6×10^{-7} torr. Due to equipment and time constraint, SIMS data are not available in Fig.4.4 when CBr_4 flux was above 2.6×10^{-7} torr. However, results from other literature show the trend that carbon atom density does continue to increase although the hole concentration begins to deviate from the carbon atom concentration at ~1×10^{20} cm^{-3} [63, 64]. And this trend is not constraint by

ATTENTION: The Singapore Copyright Act applies to the use of this document. Nanyang Technological University Library

growth techniques. The C-doped GaAs samples grown at CBr_4 fluxes beyond the maximum hole concentration exhibited spotty RHEED pattern with much reduced intensity. So far there have been few reports on the electrical and structural characteristics of highly C-doped GaAs samples [65] in terms of degradation in material properties and different mechanisms occurring during growth.

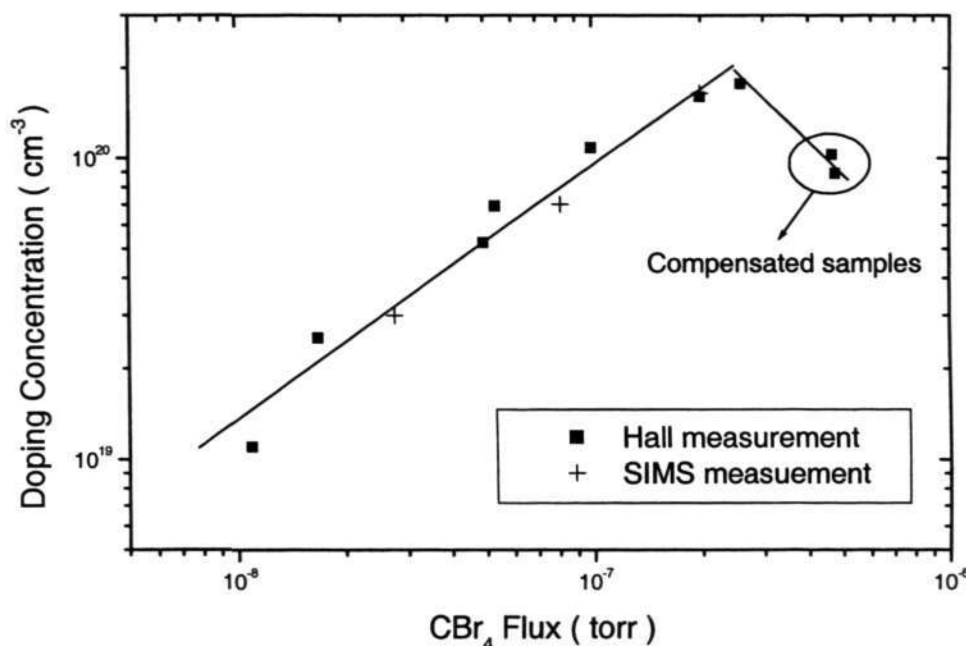

Fig.4.4 Doping concentration versus CBr_4 flux. A comparison between Hall effect and SIMS measurement.

Cheong *et al.* [63] have conducted theoretical calculations on C-doped GaAs, and suggested the reason for hole concentration saturation under high C doping conditions. The saturation in hole concentration is attributed to the compensation of split-interstitial C-C pairs in the form of dicarbon defects. According to their calculation, the defect density of the C-C pairs increases very rapidly following increase in the C concentration. At doping levels above $10^{20}cm^{-3}$, the C-C pairs become the main compensating defects, resulting in significant compensation for the

ATTENTION: The Singapore Copyright Act applies to the use of this document. Nanyang Technological University Library

hole carriers from C_{As} acceptors. The existence of such dicarbon defects in C-doped GaAs was first demonstrated experimentally by Wagner *et al*. from Raman scattering measurements [64]. In our case, when the CBr_4 flux exceeds 2.6×10^{-7} torr, further increase in the C atomic concentration causes the formation and rapid increase in dicarbon defects. Hence, the hole concentration decreases due to the compensating effects of the C-C pairs. The mechanism involved can be explained in detail as follows.

At high CBr_4 flux levels exceeding 2.6×10^{-7} torr, the high density of CBr radicals greatly enhances the probability of collision between the CBr radicals. This could promote the formation of energetically more stable carbon pairs on the growth surface. This surface reaction can be described as [66]:

$$CBr + CBr = Br_2 + C\text{-}C \quad (4.1)$$

Due to the fact that the dicarbon defect behaves as a single deep level donor, the holes provided by carbon on arsenic sites (C_{As}), which behave as acceptors, are significantly compensated. The dicarbon defect is formed by moving an interstitial carbon atom, which is then captured by the C_{As}. Therefore, there are actually two effects that could induce the reduction in hole concentration. On one hand, part of the C_{As} is incorporated into the C-C pair; while on the other hand, the C-C pair behaves as a donor. Therefore, there exists a relationship as follows [67]:

$$N_{C_{As}} - N_{CC} = N_{Hall} \quad (4.2)$$

$$N_{C_{As}} + 2N_{CC} = N_C \quad (4.3)$$

where, $N_{C_{As}}$ and N_{CC} are the concentration of C_{As} and dicarbon defects, respectively. N_{Hall} is the Hall carrier concentration, and N_C is the concentration of C atoms incorporated into GaAs, which can be obtained from SIMS measurement. In Fig.4.4, the two samples with dicarbon defects are denoted as "compensated samples".

ATTENTION: The Singapore Copyright Act applies to the use of this document. Nanyang Technological University Library

The hole mobility versus concentration at room temperature is plotted in Fig.4.5. The hole mobility ranges from 101 cm^2/Vs at hole concentration of 1.02×10^{19} cm^{-3} to 45 cm^2/Vs at 1.86×10^{20} cm^{-3}. This data is comparable to that from beryllium-doped GaAs reported by Hoke *et al.* [68]. Beyond the maximum hole concentration of 1.86×10^{20} cm^{-3}, the mobility dropped drastically to ~ 20 cm^2/Vs for the two compensated samples, compared to the mobility at the same carrier concentration using a smaller CBr_4 flux.

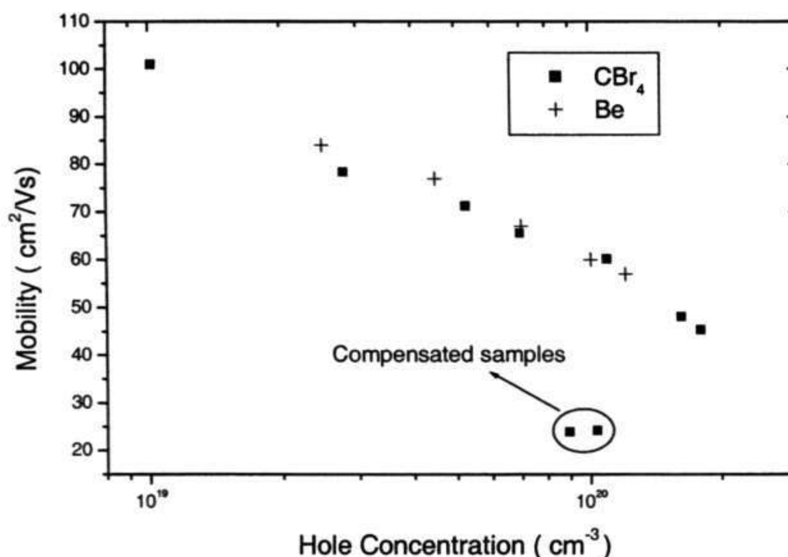

Fig.4.5 Mobility versus hole concentration at 300 K. The mobility data of the Be-doped samples are from ref. [68].

4.3.2 XRD results of C-doped GaAs

Figure 4.6 plots the lattice mismatch variation as function of CBr_4 flux. The mismatch drops significantly for the two "compensated samples" due to formation of C-C pairs. This indicates that dicarbon defects result in increase in lattice parameter. The lattice mismatch versus hole concentration is plotted in Fig.4.7. From Vegard's Law, the lattice mismatch is given by [55]:

ATTENTION: The Singapore Copyright Act applies to the use of this document. Nanyang Technological University Library

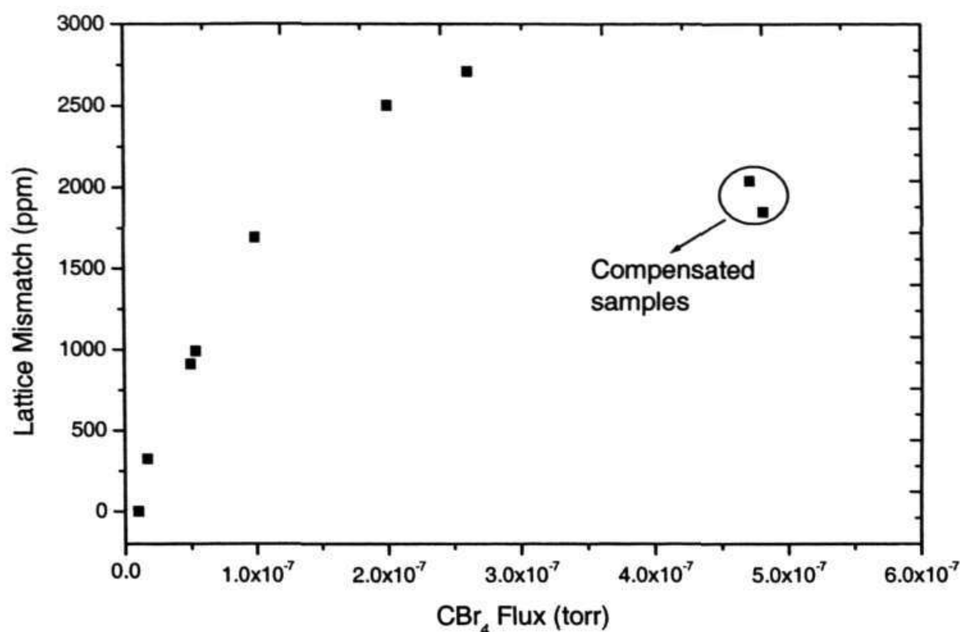

Fig.4.6 Plot of lattice-mismatch versus CBr_4 flux.

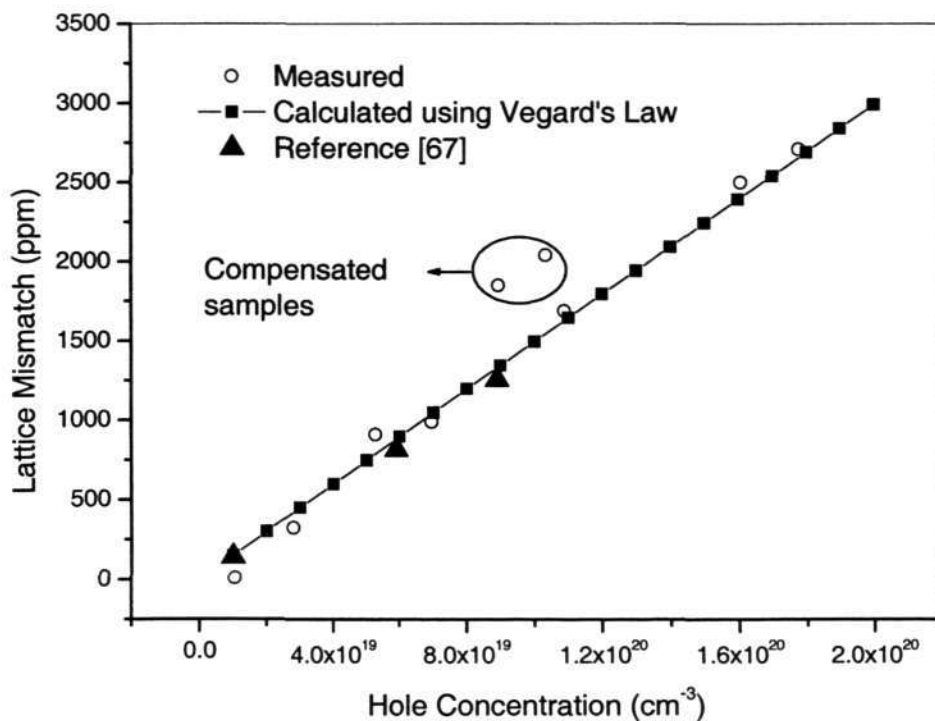

Fig.4.7 Plot of lattice-mismatch versus hole concentration.

ATTENTION: The Singapore Copyright Act applies to the use of this document. Nanyang Technological University Library

$$\frac{\Delta a}{a_0} = \frac{4[N_{C_{Ga}}(r_C - r_{Ga}) + N_{C_{As}}(r_C - r_{As})](1+\upsilon)}{\sqrt{3}(2.21\times10^{22})a_0(1-\upsilon)} \quad (4.4)$$

where, Poisson's ratio $\nu = 0.31$, tetrahedral covalent radius of C atom r_C=0.774 Å, and tetrahedral covalent radius of As atom r_{As}=1.20 Å. r_{Ga} denotes the tetrahedral covalent radius of Ga atom. $N_{C_{As}}$ and $N_{C_{Ga}}$ denotes the density of C atoms on As sites, and density of C atoms on Ga sites, respectively. $N_{C_{Ga}}$ is assumed to be 0.

The solid squares in Fig.4.7 are the mismatch values calculated using Eq.(4.4). The open circles denote the experimental mismatch data. It can be seen that the mismatch data of most samples agree well with Vegard's Law (Eq.(4.4)), except for the two "compensated samples", which were grown at high CBr_4 flux exceeding 2.6×10^{-7} torr. As presented earlier, the two "compensated samples" are the ones with C-C pairs (dicarbon defects). To further understand the intrinsic mechanisms involved in Fig.4.7, a detailed discussion of the lattice structure of dicarbon defects is necessary.

As we know, the lattice parameter of the C-C pair is larger than that of the substitutional carbon atom C_{As} [63]. Thus, compensation of the hole concentration, which is caused by transformation from C_{As} to dicarbon defect, may lead to reduction in lattice contraction. There are mainly two possible structures of dicarbon defects: (i) Cheong *et al.* [63] have reported that the dicarbon defects are mainly oriented along the [100] crystal direction. In this direction, the lattice parameter of the C-C pair is smaller than that of the As atom. (ii) Tan *et al.* [67] have reported that the dicarbon defects in compensated C-doped GaAs induced by the high substrate temperature are mainly oriented along the [111] crystal direction. In this direction, the lattice parameter of the C-C pair is larger than the As atom. Table 4.3 shows the size comparison of C atom, As atom and the C-C pairs on different crystal orientation.

ATTENTION: The Singapore Copyright Act applies to the use of this document. Nanyang Technological University Library

Here, d_{xxx} denotes the distance between the C-C pairs along [xxx] crystal direction and the nearest Ga atom.

Table 4.3 Size comparison of C atom, As atom and the C-C pairs on different crystal orientation.

	r_C	r_{As}	$d_{100}-r_{Ga}$	$d_{110}-r_{Ga}$	$d_{111}-r_{Ga}$
Size (Å)	0.774	1.20	1.12	1.356	1.548

As shown in Eq.(4.2) and Eq.(4.3), for the compensated samples, $N_{C_{As}}$ is larger than N_{Hall}, the lattice mismatch induced by $N_{C_{As}}$ (denoted by $M_{C_{As}}$) is larger than the mismatch induced by N_{Hall} (denoted by M_{Hall}). For [100]-$(C\text{-}C)^+$ pairs, the final mismatch should be larger than M_{Hall}. Therefore, the mismatch data should lie above the Vegard's Law line denoted by solid squares. However, for [111]-$(C\text{-}C)^+$ pairs, $M_{C_{As}}$ is compensated by [111]-$(C\text{-}C)^+$ pairs. Hence, whether the lattice mismatch of compensated C-doped GaAs lies below or above the Vegard's Law line is uncertain, and it depends on the magnitude of compensation. Our results show that the mismatch in the two heavily compensated samples lie in the region well above the Vegard's Law line (Fig.4.7). Hence, our analysis finally suggests two possible phenomena in our samples: (i) dicarbon defects are mainly oriented along the [100] direction; (ii) dicarbon defects are oriented along the [111] direction, and the extent of compensation is small. The lattice mismatch data of compensated samples with dicarbon defects reported in ref. [67] are plotted in Fig.4.7 for comparison. The samples in ref. [67] were grown at high substrate temperature, and the dicarbon defects are mainly oriented along the [111] direction with high compensation level.

ATTENTION: The Singapore Copyright Act applies to the use of this document. Nanyang Technological University Library

Figure 4.8 shows the XRD (004) rocking curve of a typical sample grown at CBr_4 flux of 2.5×10^{-7} torr. A C-doped GaAs peak and some interference fringes are clearly observed. This indicates that the sample is of high epitaxial quality.

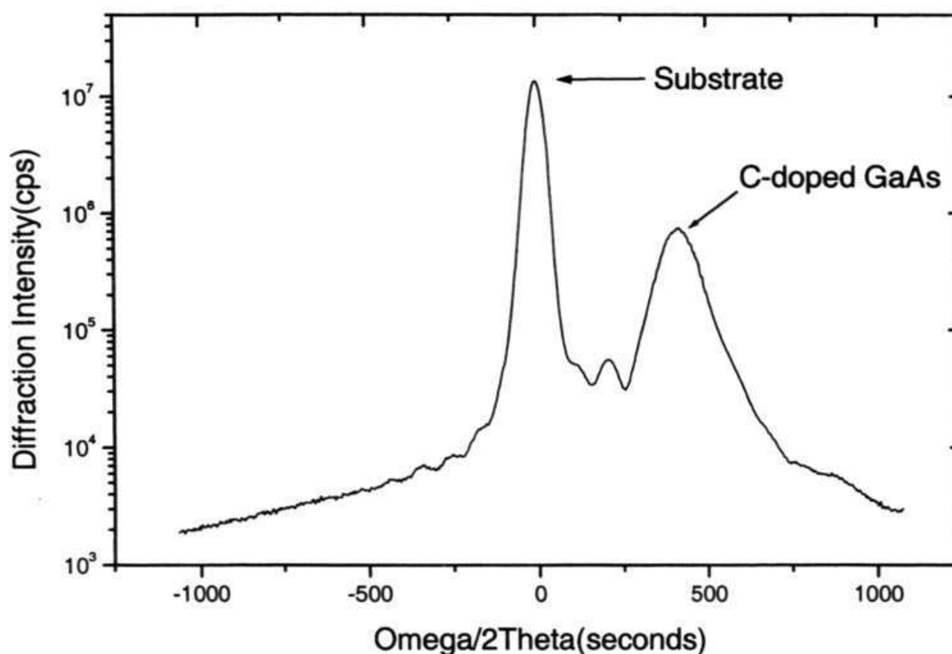

Fig.4.8 Experimental X-Ray Bragg Diffraction patterns (004 reflection) of the C-doped GaAs grown at CBr_4 flux of 2.5×10^{-7} torr.

4.3.3 AFM results of C-doped GaAs

Figure 4.9 shows the AFM surface morphology images of C-doped GaAs samples grown at different CBr_4 flux levels; (a) 5×10^{-8} torr, (b) 2×10^{-7} torr, and (c) 4.8×10^{-7} torr, respectively. For samples depicted in Fig.4.9 a) and b), the surface is generally smooth, with average root mean square (rms) roughness of approximately 3 Å and 5 Å, respectively. During growth, the reflection high-energy electron diffraction (RHEED) patterns were observed to be streaky. Clear intensity oscillations

ATTENTION: The Singapore Copyright Act applies to the use of this document. Nanyang Technological University Library

in the RHEED pattern were observed; indicative of two-dimensional (2D) layer-by-layer growth mode. In the C-doped GaAs sample depicted in Fig.4.9 c), which was grown at high CBr_4 flux of 4.8 $\times 10^{-7}$ torr, the effect on surface morphology is very significant. The surface morphology is affected badly by the high CBr_4 flux level, and there are signs of three-dimensional (3D) island formation. The rms surface roughness of this sample is ~ 680 Å. Following our earlier discussions, at such high CBr_4 flux, C-C pairs are formed and this greatly affects the properties of the material, such as reducing the hole concentration and increasing the lattice parameter. The AFM images suggest a possible relationship between the significant increase in surface roughness and formation of dicarbon defects. However, detailed physical mechanisms relating the effect of C-C pairs on surface morphology and growth mode requires further investigation. Since surface roughness has significant effect on device performance [69], device applications of C-doped GaAs should consider CBr_4 flux below 2.6×10^{-7} torr. An acceptable hole concentration level in the C-doped GaAs base layer of the HBT is 4×10^{19} cm^{-3}. For such hole level, CBr_4 flux of 3.4×10^{-8} torr should be adequate for HBT structure grown in our MBE system.

ATTENTION: The Singapore Copyright Act applies to the use of this document. Nanyang Technological University Library

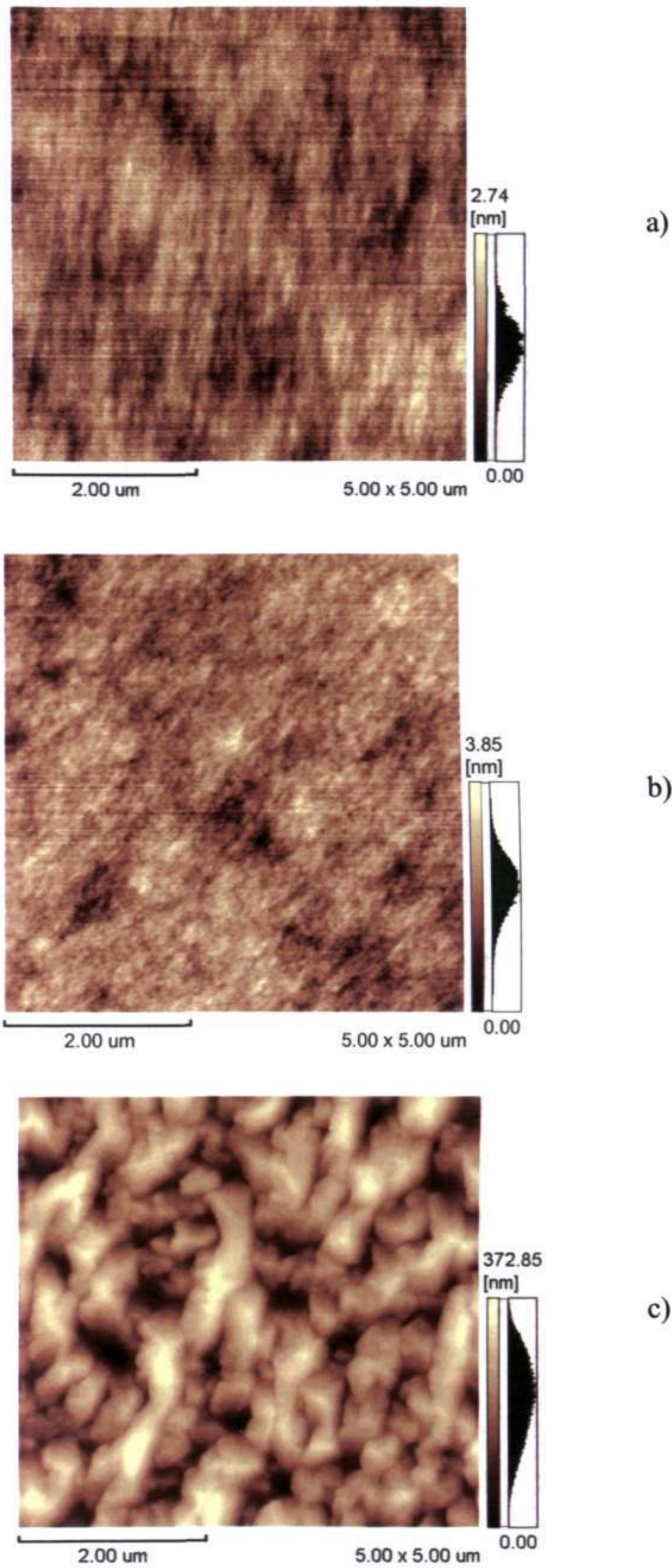

Fig.4.9 AFM micrographs of C-doped GaAs surface grown at CBr_4 flux of: a) 5×10^{-8} torr, b) 2×10^{-7} torr, and c) 4.8×10^{-7} torr.

ATTENTION: The Singapore Copyright Act applies to the use of this document. Nanyang Technological University Library

4.3.4 PL results of C-doped GaAs

The 4 K PL spectra of the GaAs samples grown at different C doping levels are shown in Fig.4.10. The spectrum of the unintentionally doped GaAs sample (curve (a)) with hole concentration of 6.39×10^{15} cm^{-3} shows the usual features of band edge emission consisting of acceptor-bound excitons (A^0-X) and band-to-acceptor (e-A^0) transitions [70]. At increasing C doping level (hole concentration > 10^{18} cm^{-3}), the excitonic features vanish, and the e-A^0 transition peak broadens to become two distinct peaks, indicated as peak 1 and 2, as shown in Fig.4.10. Peak 1 becomes increasingly broader and concurrently shifts to lower energy as the hole concentration increases. Its energy position shifts from ~1.480 eV at concentration of 1.02×10^{19} cm^{-3} to ~ 1.452 eV at 6.95×10^{19} cm^{-3}. This effect can be attributed to band gap shrinkage following increase in carrier concentration. The energy position of peak 2 remained relatively unchanged at ~ 1.493eV. A similar phenomenon was observed in zinc-doped GaAs grown by MOCVD [71,72] and C-doped GaAs grown by MOCVD [73,74]. Some controversy exists concerning the origin of peak 2 in the PL spectrum. Olego *et al.* [71] proposed that peak 2 arose from non-*k* conserving transitions from conduction band to Fermi level, which lies well inside the valence band for such highly-doped p-type samples. Lee *et al.* [73], however, related peak 2 not to luminescence from the C-doped epilayer, but to the S.I. GaAs substrate. Alternatively, Kim *et al.* [74] proposed that peak 1 and peak 2 are made up of two peaks arising from conduction band (CB) to heavy hole (HH) valence band (VB) and CB to light hole (LH) valence band transitions, respectively. They calculated the PL spectrum of C-doped GaAs with hole concentration of 9×10^{19} cm^{-3} at different temperatures. In our study, the PL spectrum at different temperatures was measured on a C-doped sample with hole concentration of 1.02×10^{19} cm^{-3}. Figure 4.11 shows the normalized

ATTENTION: The Singapore Copyright Act applies to the use of this document. Nanyang Technological University Library

PL spectra as a function of temperature. By comparison with the calculated results of Kim *et al.* [74], our results seem to support their proposed model. The contribution of the CB-LH transition in the PL spectra is very dominant in heavily C-doped GaAs, and even more so at low temperature. Following increase in temperature, the relative intensity of the CB-LH transition is more rapidly quenched and broadened, compared to that of the CB-HH transition. This results in virtual disappearance of peak 2 and increases the full-width at half maximum (FWHM) of its PL spectrum. According to this model, the transition mechanism changes from e-A^0 at low doping level, to CB-HH and CB-LH at high doping level (see Fig.4.10). It is coincidental that the position of peak 2 is close to that of e-A^0 transition.

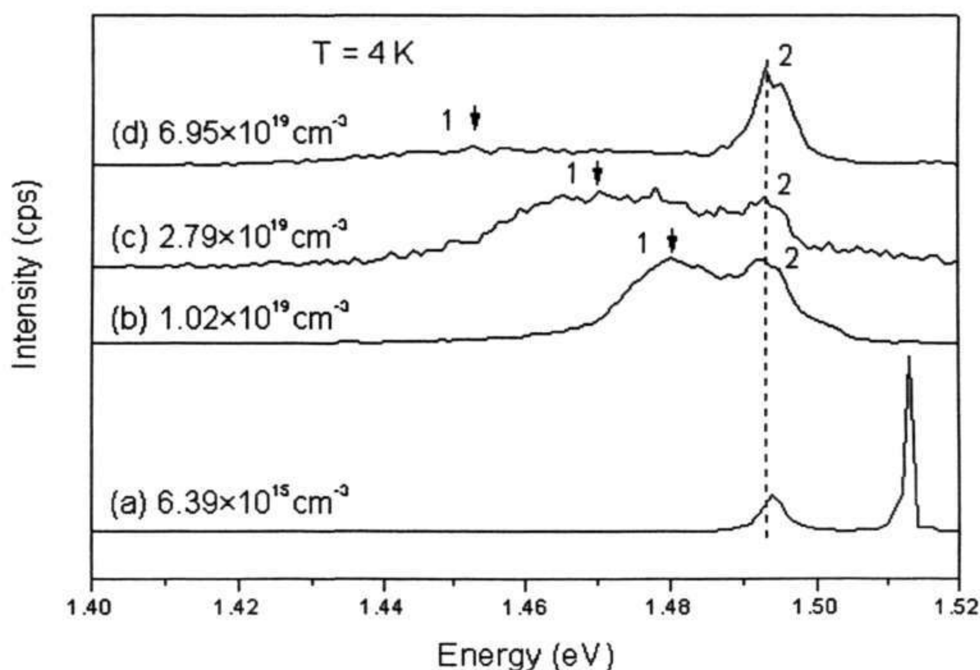

Fig.4.10 Normalized PL spectra of C-doped GaAs samples for various doping levels.

ATTENTION: The Singapore Copyright Act applies to the use of this document. Nanyang Technological University Library

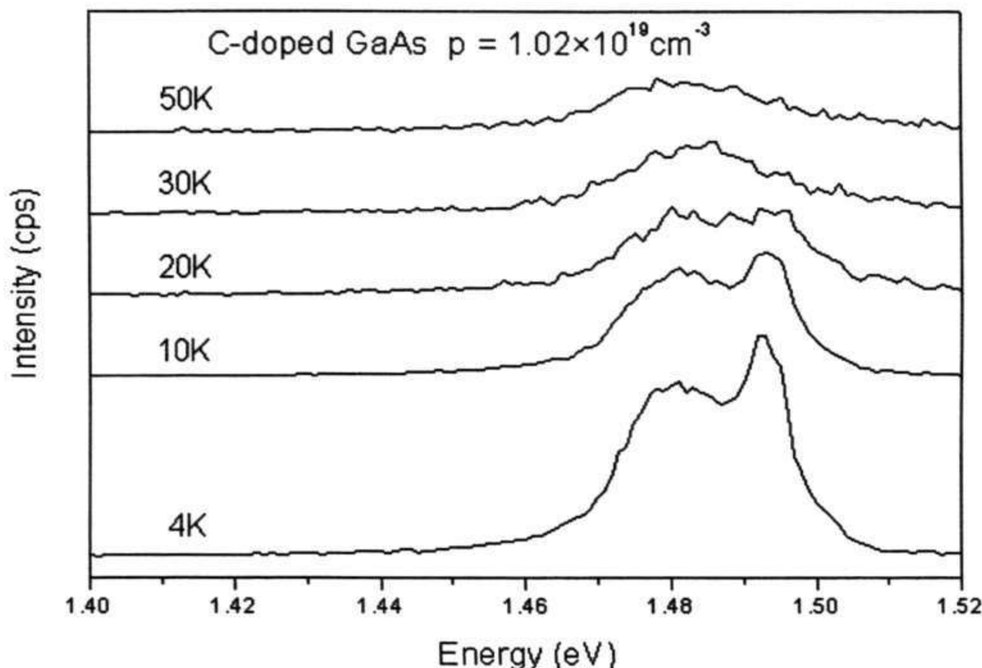

Fig.4.11 Normalized PL spectra for various temperatures of a C-doped GaAs sample with hole concentration of 1.02×10^{19} cm^{-3}.

4.3.5 SIMS results of C-doped GaAs

The modulation control of the C doping process was investigated using a test structure comprising alternating 1700 Å-thick C-doped GaAs layer, followed by 1700 Å-thick unintentional-doped GaAs layer. Three C doping levels corresponding to CBr_4 flux of 2×10^{-7} torr, 8.2×10^{-8} torr and 2.8×10^{-8} torr, respectively, was used in the test structure. The sample was subjected to SIMS measurement, which revealed a pulsed profile of C doping with concentration $< 6\times10^{16}$ cm^{-3} (limited by the lower sensitivity limit of SIMS measurement of carbon impurities) between the peaks of the three C doping pulses, as shown in Fig.4.12. Close agreement between the nominal thickness of the sample structure and the SIMS depth profile was obtained. No growth

ATTENTION: The Singapore Copyright Act applies to the use of this document. Nanyang Technological University Library

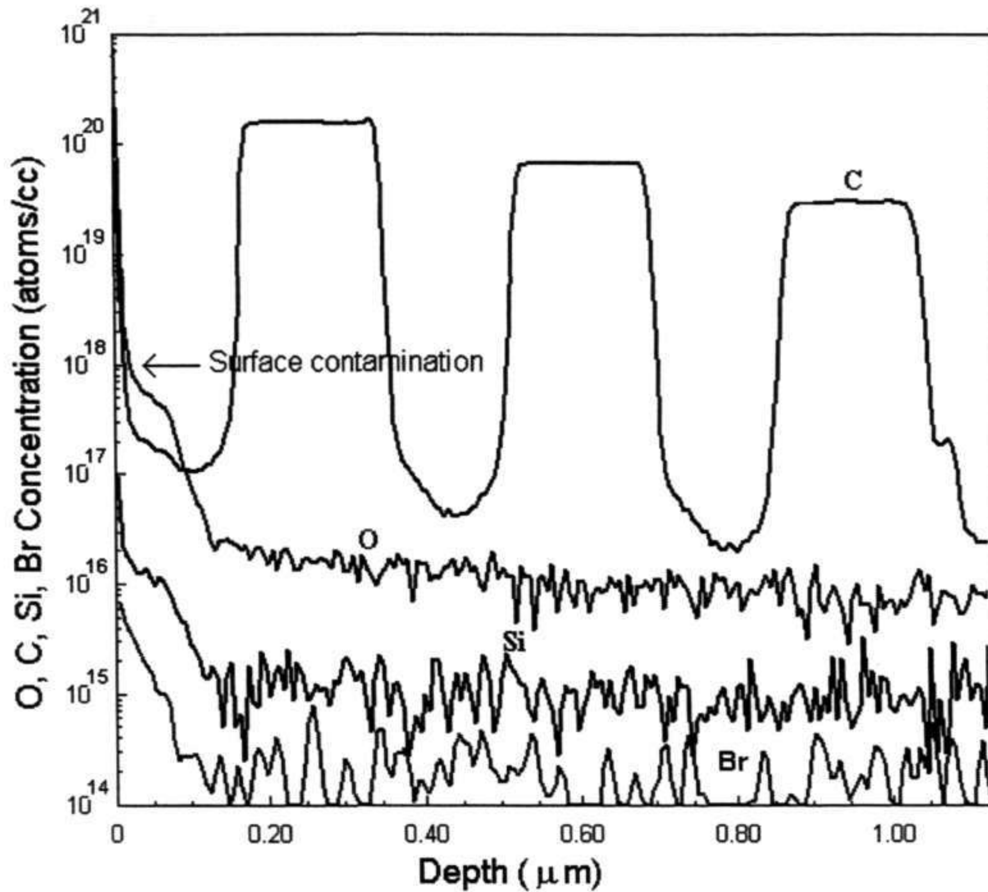

Fig.4.12 Pulsed C-doping profile of a GaAs sample measured by SIMS.

interruptions were employed during the growth of the modulated C-doped structure. It is expected that further improvement in the doping control can be achieved if growth interruptions are employed. Some background elements of O, Si and Br are also detected in the material, whose concentration is ~ 10^{16} cm^{-3}, 10^{15} cm^{-3} and 10^{14} cm^{-3}, respectively. The Br value is comparable to that in published literature [75]. The increase in O, Si and Br levels near the sample surface is probably due to surface contamination.

ATTENTION: The Singapore Copyright Act applies to the use of this document. Nanyang Technological University Library

4.4 C-doped GaAs PN junction

4.4.1 Epitaxial structure & schematic of the PN junction

Using carbon as p-type dopant, GaAs PN junctions were grown by SSMBE. Table 4.4 shows the epitaxial structure of the PN junction. The PN junction was fabricated using conventional lithography and wet etch. Au/Ge/Ni/Au (28/7/8.8/84 nm) metals were deposited on the n = 5×10^{18} cm^{-3} GaAs cap layer as n-type ohmic contact. The n-type ohmic contact was annealed at 430 °C for 10sec in a rapid thermal processor. The GaAs cap layer and the GaAs n-type (5×10^{17} cm^{-3}) layer were etched to form the mesa. The p-type ohmic contact was made using Ti/Au (50/250 nm) metallization deposited on the p-type C-doped GaAs. Figure 4.13 shows the schematic cross section of the C-doped GaAs PN junction.

Table 4.4 Epitaxial structure of the PN junction.

Thickness (Å)	Material	Dopant	Concentration (cm^{-3})
1600	GaAs	Si	5×10^{18}
800	GaAs	Si	5×10^{17}
800	GaAs	C	5×10^{19}
GaAs buffer			
S.I. GaAs substrate			

ATTENTION: The Singapore Copyright Act applies to the use of this document. Nanyang Technological University Library

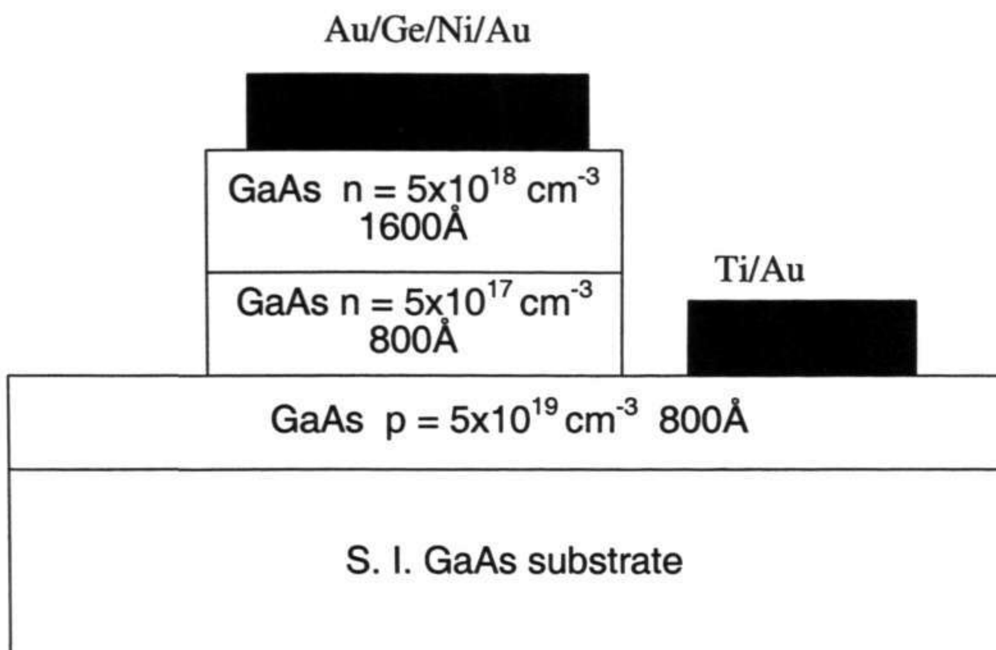

Fig.4.13 Schematic of the PN junction.

4.4.2 Electrical properties of the PN junction

The electrical properties of the PN junctions were measured using Semiconductor Parameters Analyzer. Figure 4.14 shows the typical I-V and breakdown characteristics of the PN junction. The turn-on voltage is about 1.16 V. The breakdown voltage is about 6.5 V, which is nearly equal to the calculated value. Figure 4.15 shows the reverse leakage currents of the PN junction at elevated temperature ranging from 27°C to 200 °C. As the temperature increases, the reverse leakage current becomes less sensitive to reverse bias and approaches the classical Shockley-Read-Hall (SRH) I-V characteristics, that show gentle dependence on the bias voltage. Fig.4.16 and Fig.4.17 show the ideality factor at the medium current and low current, respectively. The ideality factor is 1.76 at low current as compared to 1.3 at medium current, which indicates that the recombination current is more prominent

ATTENTION: The Singapore Copyright Act applies to the use of this document. Nanyang Technological University Library

at low voltage. The good electrical properties of the PN junctions show that the use of CBr_4 in SSMBE is promising for the growth of p-type base layer in the HBT device.

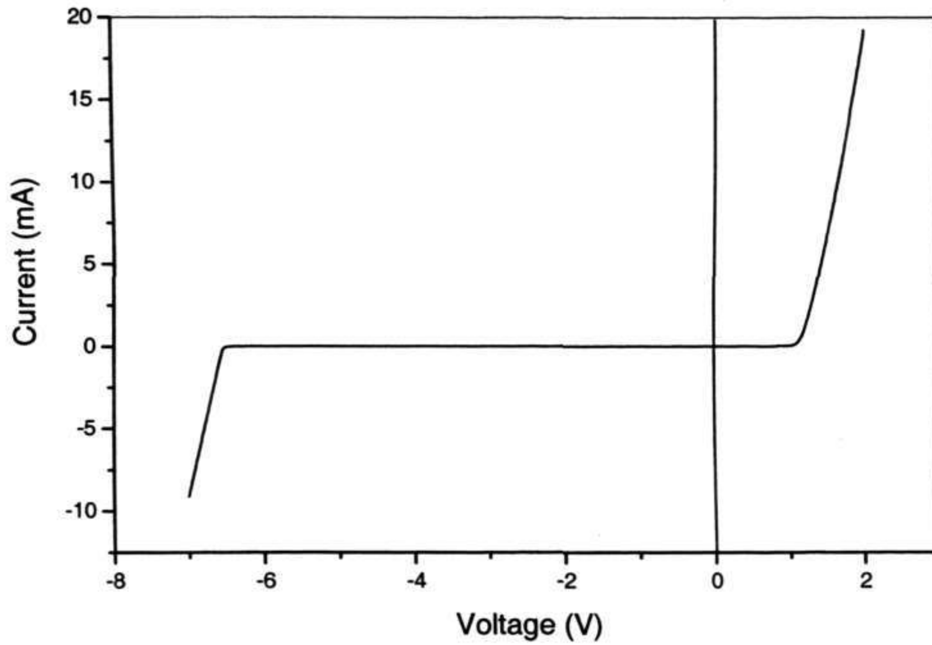

Fig.4.14 I-V and breakdown characteristic of the PN junction.

ATTENTION: The Singapore Copyright Act applies to the use of this document. Nanyang Technological University Library

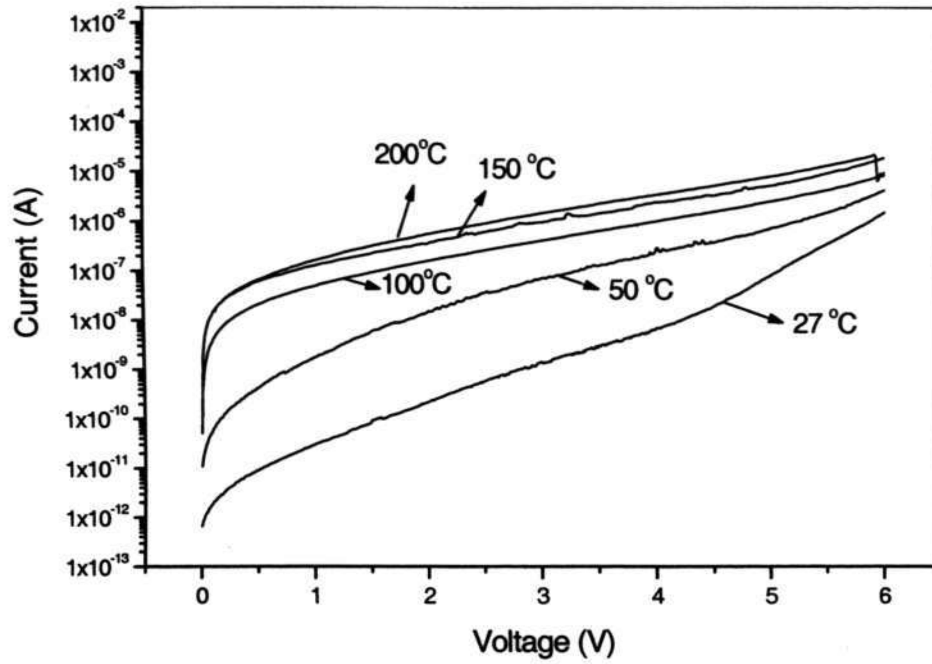

Fig.4.15 Reverse leakage current at different temperature.

ATTENTION: The Singapore Copyright Act applies to the use of this document. Nanyang Technological University Library

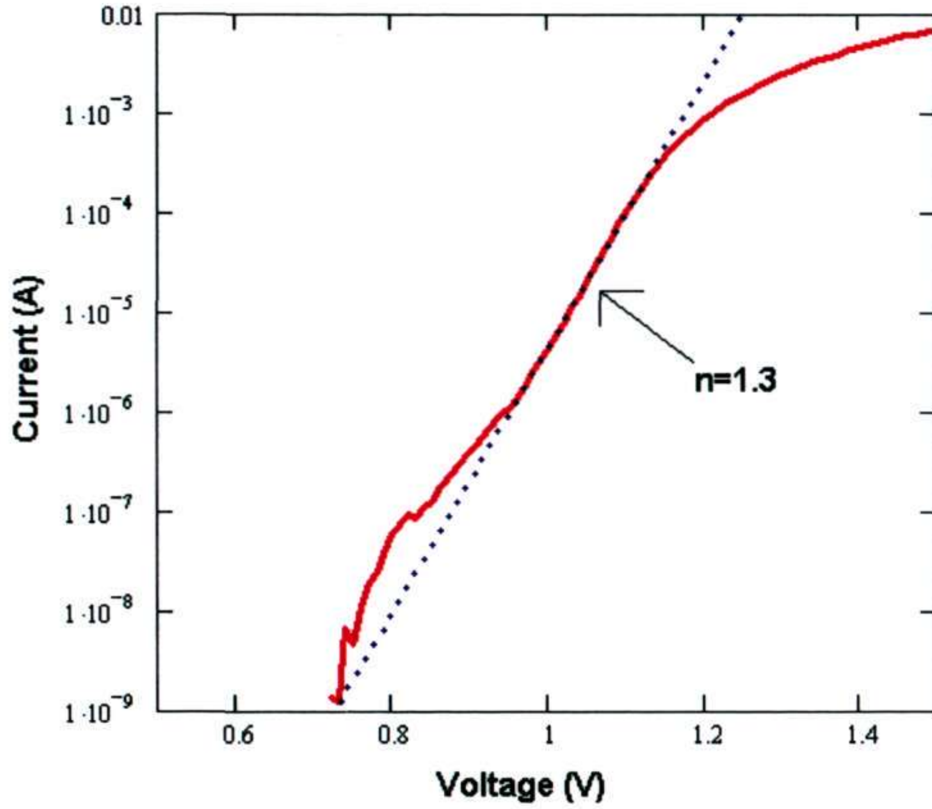

Fig.4.16 Ideality factor of the PN junction at medium current.

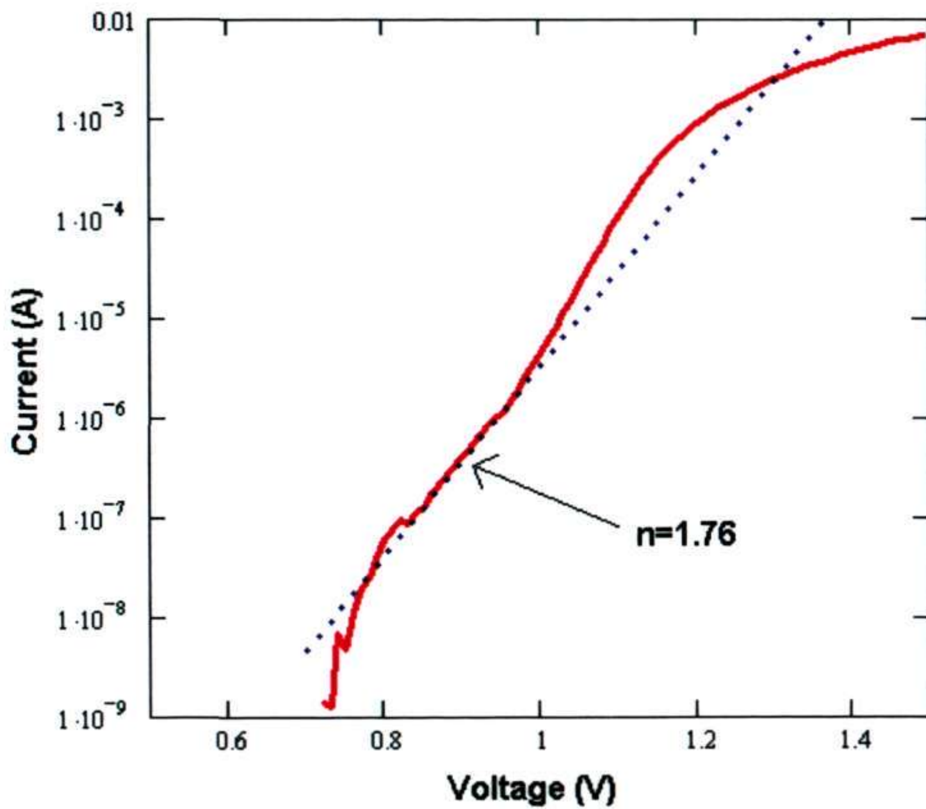

Fig.4.17 Ideality factor of the PN junction at low current.

ATTENTION: The Singapore Copyright Act applies to the use of this document. Nanyang Technological University Library

4.5 Summary

In this chapter, successful installation of CBr_4 source and growth of C-doped GaAs by SSMBE using CBr_4 is reported. Sustainable and stable CBr_4 flux with variation lower than 2.5% has been obtained. The memory effect has been investigated. For the doping level commonly used for HBTs (~ 5×10^{19} cm^{-3}), the memory effect is negligible.

Various techniques have been applied to characterize the C-doped GaAs layers. It has been observed that hole concentration increases following increase in CBr_4 flux and reaches a maximum of 1.86×10^{20} cm^{-3} at CBr_4 flux of 2.6×10^{-7} torr, beyond which, it decreases rather significantly. The SIMS results show that the carbon atoms incorporated into GaAs are nearly fully activated at CBr_4 flux level below 2.6×10^{-7} torr. At room temperature, the C-doped samples showed mobility of 101 to 45 cm^2/Vs at hole concentration of 1.02×10^{19} cm^{-3} to 1.86×10^{20} cm^{-3}, respectively, comparable to samples doped with beryllium (Be). When the CBr_4 flux exceeds 2.6×10^{-7} torr, further increase in the C atomic concentration causes the formation and rapid increase in dicarbon defects. The compensating effects of the dicarbon defects induce the decrease in hole concentration, drop in mobility, and increase in lattice parameter. Unlike the samples grown at CBr_4 flux below 2.6×10^{-7} torr, the lattice mismatch data of the compensated samples, which were grown at high CBr_4 flux exceeding 2.6×10^{-7} torr, deviate from Vegard's Law. However, the structure of dicarbon defects formed under high CBr_4 flux needs further investigation. AFM images of surface morphology show signs of growth mode transformation from 2D to 3D island formation following increase in CBr_4 flux. The results suggest a possible relationship between significant increase in surface roughness and formation of dicarbon defects in C-doped GaAs.

ATTENTION: The Singapore Copyright Act applies to the use of this document. Nanyang Technological University Library

Low temperature (4K) PL measurements show a reduction in bandgap and broadening of the PL spectrum following increase in the doping concentration. The main PL peak shifts from ~ 1.480 eV at concentration of 1.02×10^{19} cm^{-3} to ~ 1.452 eV at 6.95×10^{19} cm^{-3}. Variable temperature PL measurements show the existence of two peaks, which could arise from conduction band (CB) to heavy hole (HH) valence band and CB to light hole (LH) valence band transitions. Reasonably good C pulsed doping profile has been achieved and verified by SIMS measurement on samples grown without the use of growth interruption. C-doped PN junctions have been grown and fabricated. Good I-V characteristics and ideality factors have been obtained. The results show that the use of CBr_4 in SSMBE is promising for the growth of p-type base layer in the HBT device.

The basic characteristics of the C-doped GaAs layers have been studied systematically in this chapter. These results not only help to obtain the insight and understanding of the material properties and the mechanisms involved, but also form the basis for further optimization and device fabrication, as described in the following chapters.

ATTENTION: The Singapore Copyright Act applies to the use of this document. Nanyang Technological University Library

Chapter 5

Optimization of growth conditions for C-doped GaAs

In this chapter, the effect of growth conditions, such as substrate temperature, growth rate and V/III ratio on properties of heavily C-doped GaAs was investigated to search for optimum growth conditions based on our experimental setup. The results serve as a useful baseline growth process for the development of HBT devices using C-doped GaAs as the highly doped base layer.

For the use of C-doped GaAs as base layer of HBTs, the quality of the base layer is very important. The growth conditions greatly affect the material quality. The growth conditions need to be optimized for the device applications. In this chapter, three series of samples of C-doped GaAs grown with various growth temperatures, growth rates, and V/III ratios have been studied. Hall measurements were used to characterize the samples at room temperature. The surface morphology of the samples was measured using AFM in contact mode. The study reveals the effect of these factors to the material quality of the C-doped GaAs layers, and finds the optimized growth condition. The optimization will benefit the design and fabrication of C-doped HBT device applications.

5.1 Sample growth

The C-doped GaAs samples were grown on GaAs (100) S.I. substrates by SSMBE using CBr_4 as p-type doping precursor. As described in Chapter 4, the CBr_4 source was sublimed from 2-20 °C. The CBr_4 flux was measured before each run by

ATTENTION: The Singapore Copyright Act applies to the use of this document. Nanyang Technological University Library

using beam flux monitor, and then the same precision leak valve position was used during the run. Over the course of each run the CBr_4 flux kept stable. The thickness of all C-doped GaAs samples was 2300 Å in this investigation.

5.2 Effect of substrate temperature

To investigate the effect of substrate temperature on C-doped GaAs, two groups of samples were grown at CBr_4 flux of 2.2×10^{-8} torr and 4.6×10^{-8} torr, respectively. At CBr_4 flux of 2.2×10^{-8} torr, six samples were grown at 500 °C, 530 °C, 560 °C, 590 °C, 620 °C, and 650 °C, respectively. At CBr_4 flux of 4.6×10^{-8} torr, five samples were grown at 500 °C, 560 °C, 590 °C, 620 °C, and 650 °C, respectively. The growth rate (1μm/h) and V/III ratio (18) were kept unchanged.

Figure 5.1 plots the dependence of hole concentration on substrate temperature. At CBr_4 flux of 2.2×10^{-8} torr, the hole concentration is relatively insensitive to changes in substrate temperature. However, at higher CBr_4 flux of 4.6×10^{-8} torr, substrate temperature above 620 °C causes a reduction in hole concentration. Similar results were reported by other groups [66, 75], indicating the formation of C-C pairs at high substrate temperature. Tan *et al.* [67] have reported that the dicarbon defects formed at high substrate temperature are mainly oriented along the [111] direction. Regardless of the orientation direction of the dicarbon defects, they result in reduction of the hole concentration. Therefore, high CBr_4 flux and/or high substrate temperature can both induce formation of dicarbon defects. However, the dicarbon defects formed under these two conditions may not have the same orientation.

ATTENTION: The Singapore Copyright Act applies to the use of this document. Nanyang Technological University Library

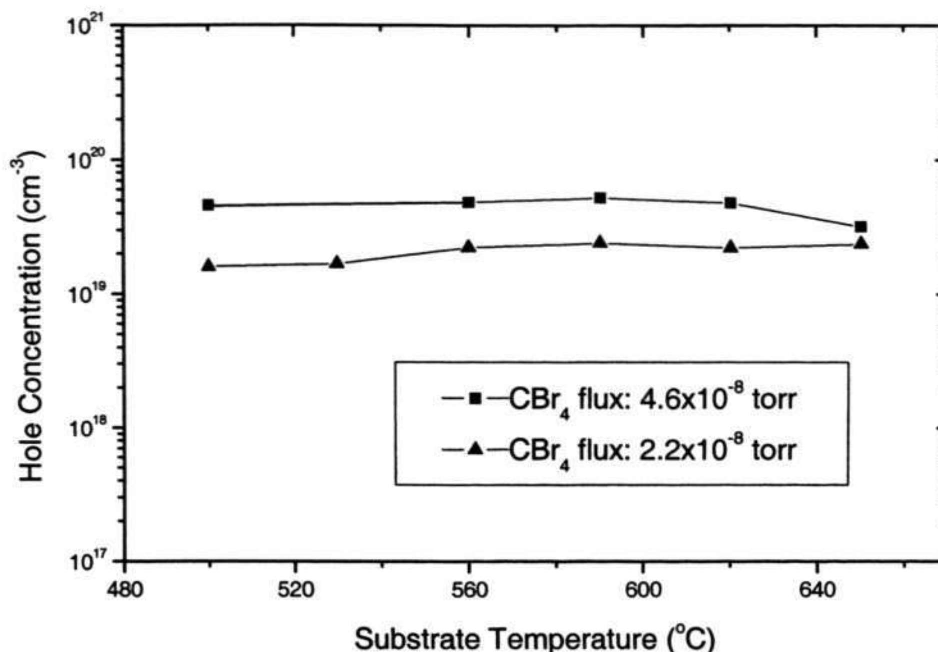

Fig.5.1 Plot of hole concentration versus substrate temperature.

Figure 5.2 plots the rms surface roughness (with error bars) as function of substrate temperature at two CBr_4 flux levels: 2.2×10^{-8} torr and 4.6×10^{-8} torr, respectively. At each flux level, the surface roughness shows signs of increase at substrate temperatures above 590 °C. At CBr_4 flux of 4.6×10^{-8} torr, the surface roughness increases drastically above 620 °C, and the highest surface roughness was recorded at 650 °C, within the range of substrate temperatures investigated. At CBr_4 flux of 2.2×10^{-8} torr, the surface roughness was the highest at 650 °C, but its value is ~4 times lower compared to the highest surface roughness value at CBr_4 flux of 4.6×10^{-8} torr. Since good surface morphology is important for HBT application, the substrate temperature for C-doped GaAs should be maintained between 560 °C to 590 °C within the range of CBr_4 flux investigated in our MBE system.

ATTENTION: The Singapore Copyright Act applies to the use of this document. Nanyang Technological University Library

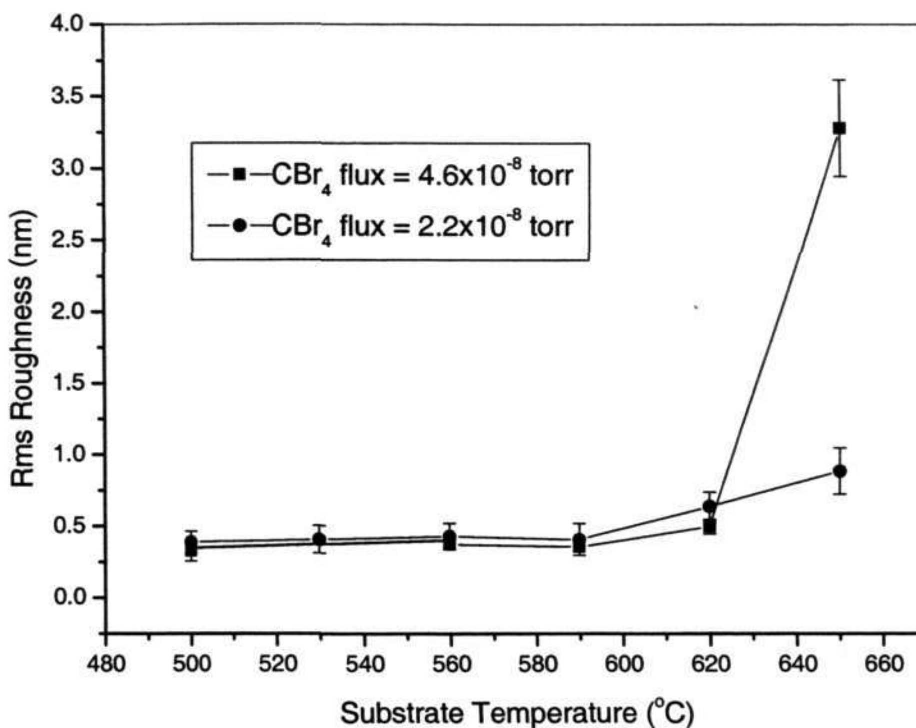

Fig.5.2 Plot of rms surface roughness (with error bars) versus substrate temperature.

5.3 Effect of growth rate

Keeping V/III ratio of 18, and substrate temperature of 580 °C, C-doped GaAs samples grown at 0.5 μm/h using CBr_4 flux of 4.6×10^{-8} torr, yield hole concentration of 6×10^{19} cm^{-3}. This hole concentration is nearly the same as that in samples grown at 1μm/h under the same CBr_4 flux. The presence of the same hole concentration in samples grown at 1:2 growth rate ratio suggests that only half of the carbon atoms reaching the growth surface are incorporated. The results suggest that the carbon species behave like As during the C-doped GaAs growth process. This is different from carbon doping in CBE using CBr_4 as p-dopant precursor [76], in which all carbon atoms reaching the growth surface are incorporated and no accumulation of

ATTENTION: The Singapore Copyright Act applies to the use of this document. Nanyang Technological University Library

carbon species at the growth front occurs. In our experiment, the surface roughness is ~ 3 Å and the lattice mismatch is consistent with Vegard's Law. Thus, the results so far suggest that the growth rate of 0.5 μm/h has no significant deteriorating effect on the material quality.

5.4 Effect of V/III ratio

To investigate the effect of V/III ratio, three samples were grown using the same substrate temperature of 580 °C and growth rate of 1 μm/h at CBr_4 flux of 4.6×10^{-8} torr. As shown in Fig.5.3, the V/III ratio (in the range of 10 to 18) has negligible effect on the hole concentration and the hole mobility. However, as seen in Fig.5.4, the rms surface roughness results from the AFM measurements show that at low V/III ratio of 10, the surface of C-doped GaAs becomes significantly rougher.

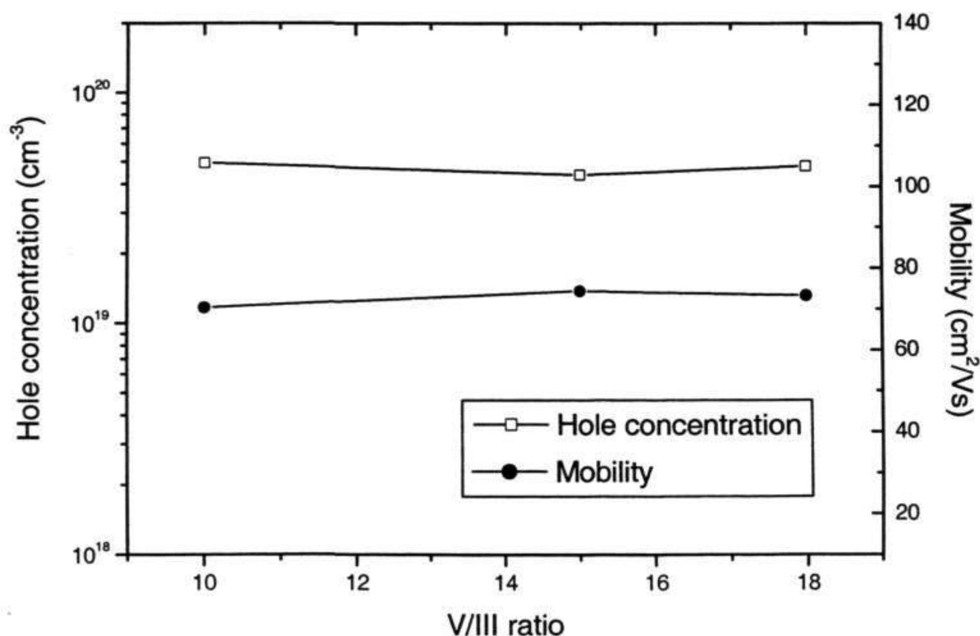

Fig.5.3 Plot of hole concentration and hole mobility versus V/III ratio.

ATTENTION: The Singapore Copyright Act applies to the use of this document. Nanyang Technological University Library

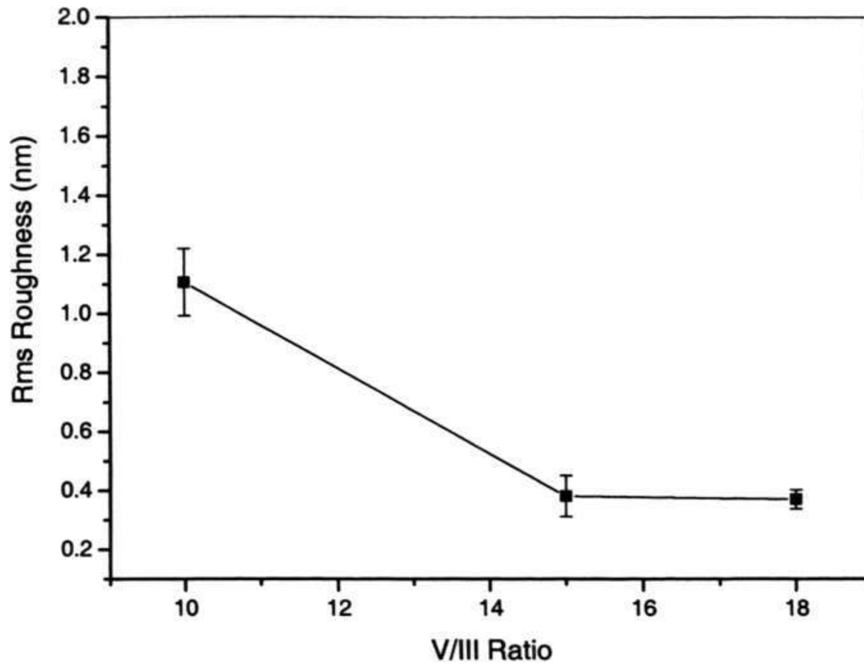

Fig.5.4 Plot of rms surface roughness (with error bars) versus V/III ratio.

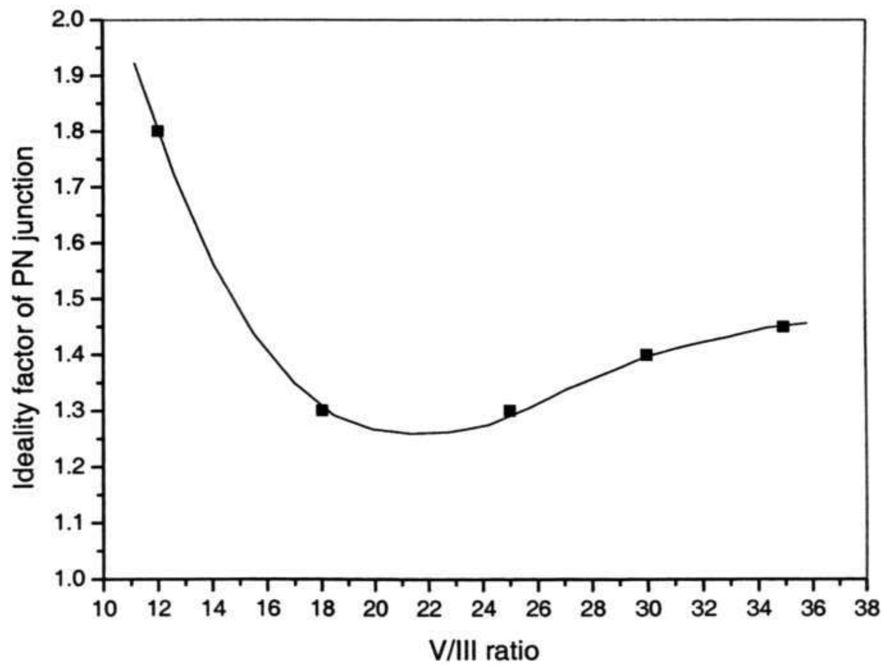

Fig.5.5 Plot of ideality factor of PN junctions versus V/III ratio.

ATTENTION: The Singapore Copyright Act applies to the use of this document. Nanyang Technological University Library

Some PN junctions were grown using higher V/III ratio of 35, 30, and 25 and one with a V/III ratio less than 15. From the ideality factors of the PN junctions as shown in Fig.5.5 (the ideality factor data at V/III ratio of 18 was obtained from Chapter 4), the ideality factor became higher at V/III ratio either above 25 or below 18. Therefore, the optimum V/III ratio for the growth of C-doped GaAs is between 18 and 25.

5.5 Summary

The effect of substrate temperature, growth rate, and V/III ratio on C-doped GaAs grown by SSMBE was investigated. High substrate temperature can also induce the formation of dicarbon defects in C-doped GaAs, which results in reduction in hole concentration. The surface roughness shows signs of increase at substrate temperature above 590 °C, indicating a possible relationship between the significant increase in the surface roughness and the formation of dicarbon defects, which is consistent with that in Chapter 4. The presence of the same amount of hole concentration in samples grown at 1:2 growth rate ratio suggests that only half of the carbon atoms reaching the growth surface are incorporated. At low V/III ratio of 10, the surface of C-doped GaAs becomes significantly rougher; the ideality factor of PN junctions becomes higher at V/III ratio above 25 or below 18. Within the range of experimental conditions in our MBE system, substrate temperature between 560 °C - 590 °C, growth rate of 1 μm/h or 0.5 μm/h and V/III ratio between 18 and 25 are suitable parameters for C-doped GaAs growth for HBT applications.

ATTENTION: The Singapore Copyright Act applies to the use of this document. Nanyang Technological University Library

Chapter 6
Results of C-doped GaInP/GaAs HBTs

In this chapter, the grown of C-doped GaInP/GaAs HBTs by SSMBE using CBr_4 as p-type dopant precursor is reported. The preliminary results are reported and the poor DC characteristics studied. The carrier transport mechanisms were revealed through temperature-dependant investigation and the material quality was assessed.

At the beginning of the 1990's, the commercial development of wireless communications was greatly encouraged and more applications were found for HBTs. The most notable among them was GaAs HBT power amplifier for cell phones. The GaAs HBT process is now the leading semiconductor technology for RF power products and has over 30% of the total market share up to date.

6.1 Brief review of GaInP/GaAs HBTs

The first GaInP/GaAs HBT was reported by Mondry and Kroemer in 1985 [77]. This npn device was grown by MBE and had a 1500 Å GaAs base layer with Be doping concentration of 1×10^{19} cm^{-3}. Current gain of 30 was obtained for this device. The first microwave characterization of MOCVD grown C-doped GaInP/GaAs HBT was reported in 1991 [78]. The f_t and f_{max} were 30 GHz and 45 GHz, respectively. In 1993, the current gain of 2690 was reported for GaInP/GaAs HBT with a 1000 Å GaAs base layer (Be-doped, 5×10^{18} cm^{-3}) grown by MOMBE [79]. The highest f_t

ATTENTION: The Singapore Copyright Act applies to the use of this document. Nanyang Technological University Library

and f_{max} of C-doped GaInP/GaAs HBTs reported were 156 GHz and 255 GHz, respectively, in 1998, that were grown by GSMBE [80].

6.2 SSMBE growth of C-doped GaInP/GaAs HBTs

The GaInP/GaAs HBT structure with abrupt emitter-base junction was grown on (100)-oriented semi-insulating GaAs substrates in the SSMBE system. The CBr_4 flux was generated in a temperature-controlled canister, and the flux was delivered into the MBE chamber via a system of ultra-clean piping, as described previously in Chapter 4. The magnitude of the CBr_4 flux introduced into the MBE chamber was regulated by a high precision leak valve. The C-doped GaAs base layer was grown at substrate temperature of 580 °C, growth rate of 1 μm/h and nominal V/III ratio of 18. A 3-min growth interruption was used after the p-type base layer growth to alleviate possible carbon-doping memory effect, during which the CBr_4 flux is terminated.

Table 6.1 shows the layer structure of the HBT. The epitaxial layers consists of 5200 Å n = 4×10^{18} cm^{-3} GaAs sub-collector, a 200 Å GaInP which is inserted in the sub-collector to serve as etch stop layer, a 6000 Å n = 1×10^{16} cm^{-3} GaAs collector, a 520 Å p = 5×10^{19} cm^{-3} GaAs base layer, a 500 Å n = 3×10^{17} cm^{-3} $Ga_{0.51}In_{0.49}P$ emitter, a 1200 Å n = 4×10^{18} cm^{-3} GaAs cap, a 400 Å n = 1×10^{19} cm^{-3} $In_xGa_{1-x}As$ graded cap layer (x=0-0.6), and a 400 Å n = 1×10^{19} cm^{-3} $In_{0.6}Ga_{0.4}As$ ohmic contact layer.

ATTENTION: The Singapore Copyright Act applies to the use of this document. Nanyang Technological University Library

Table 6.1 Layer structure of GaInP/GaAs HBT.

Layer	Material	Component	Thickness (Å)	Dopant	Concentration (cm^{-3})
Cap	$In_xGa_{1-x}As$	x = 0.6	400	Si	1×10^{19}
Cap	$In_xGa_{1-x}As$	x = 0-0.6	400	Si	1×10^{19}
Cap	GaAs		1200	Si	4×10^{18}
Emitter	$Ga_{0.51}In_{0.49}P$		500	Si	3×10^{17}
Base	GaAs		520	C	5×10^{19}
Collector	GaAs		6000	Si	1×10^{16}
Sub-collector I	GaAs		500	Si	4×10^{18}
Etch stop	$Ga_{0.51}In_{0.49}P$		200	Si	1×10^{18}
Sub-collector II	GaAs		4700	Si	4×10^{18}
Buffer	$Al_xGa_{1-x}As$	x = 0.8	2000	/	/
S.I. GaAs substrate					

6.3 Fabrication of C-doped GaInP/GaAs HBTs

In order to minimize the effects of surface recombination, which are more dominant in small emitter area HBTs, large emitter area ($50 \times 50\ \mu m^2$) devices were fabricated in this study. The HBT devices were fabricated using conventional photolithography and wet chemical etching. The main steps for the fabrication of GaInP/GaAs HBT are: 1) formation of emitter, base and collector mesas, 2) formation of ohmic contacts to emitter, base and collector. The key features of each processing step are described as follows.

ATTENTION: The Singapore Copyright Act applies to the use of this document. Nanyang Technological University Library

6.3.1 Mesa formation

Mesa-type structure was employed for the fabrication of GaInP/GaAs HBT devices. A 3:1:40 mixture of H_3PO_4:H_2O_2:H_2O was used to etch the GaAs and InGaAs layers. The etch rate was around 120 nm/minute and 150 nm/minute, respectively. The GaInP layer was etched using 1:1 mixture of HCl:H_2O, which gives a etch rate of about 30 nm/minute. One major advantage of using the above mentioned etching solution is the ability to selectively etch GaAs (or InGaAs) and GaInP. The sequence of forming emitter, base and collector mesas is described as below:

1) The GaInP/GaAs HBT structure is cleaned using acetone, isopropyl alcohol and DI water. After dehydration-bake in 110 °C for 30 minutes, the wafer is coated with photoresist, and then soft-baked at 105 °C. The emitter mesa pattern is defined by the mask aligner with an exposure of 20 seconds at a UV light intensity of 14.0 mW/cm^2. The wafer is then developed in the developer until the patterns are clear as seen under microscope. Hard bake at 110 °C is necessary to harden the photoresist to improve the adhesion with the mesa islands.

2) The highly doped InGaAs and GaAs cap layers are removed using H_3PO_4:H_2O_2:H_2O, and then HCl:H_2O is used to selectively etch GaInP emitter stopping on the p+ GaAs base layer. The emitter etching is verified by performing I-V measurement of surface breakdown using a pair of tungsten probe tips. The breakdown voltage of Schottky diodes formed on the p+ GaAs base is much lower than that on GaInP emitter layer.

3) The base is then patterned and the GaAs base and collector layers are etched using H_3PO_4:H_2O_2:H_2O until the GaInP etch stop layer in the sub-collector is exposed. After that the GaInP etch stop layer is removed using HCl:H_2O. The mesa

ATTENTION: The Singapore Copyright Act applies to the use of this document. Nanyang Technological University Library

depth is confirmed by using a surface profiler. Finally, the collector isolation mesa is patterned and etched by H_3PO_4:H_2O_2:H_2O.

6.3.2 Formation of ohmic contacts

After the mesa formation, ohmic contacts must be made on the emitter, base and collector regions. The metallization is patterned by transferring the designed mask pattern to photoresist and then to the metal layer. Conventional lift-off technique is used in this work. This technique involves deposition of the ohmic contact metal layers directly on the top of the patterned photoresist, followed by lifting off unwanted metal by dissolving the underlying photoresist with acetone. For the lift-off method, it requires an overhang of the photoresist to prevent the continuity between the metal on the material surface and that on the photoresist, which is not only to allow solvent to penetrate and dissolve the photoresist, but also to prevent ragged edges due to peeling of the metal. An image reversal lithography process using AZ 5214 photoresist is developed to form the overhang of the resist. After the pattern definition, the wafer is dipped in a HCl:H_2O (1:10) solution to remove the residual oxide, and rinsed in DI water. Ni/Ge/Au/Ni/Au (5/25/100/20/250 nm) were used for emitter and collector ohmic contacts. The n-type ohmic contact was annealed at 430 °C for 10 secs in a rapid thermal processor. The p-type ohmic contact was made using Ti/Au (50/250 nm) metallization. Figure 6.1 shows the SEM image of the fabricated GaInP/GaAs HBT.

After fabrication, the temperature dependence of device DC characteristics was measured using a semiconductor parameter analyzer in conjunction with a probe station.

ATTENTION: The Singapore Copyright Act applies to the use of this document. Nanyang Technological University Library

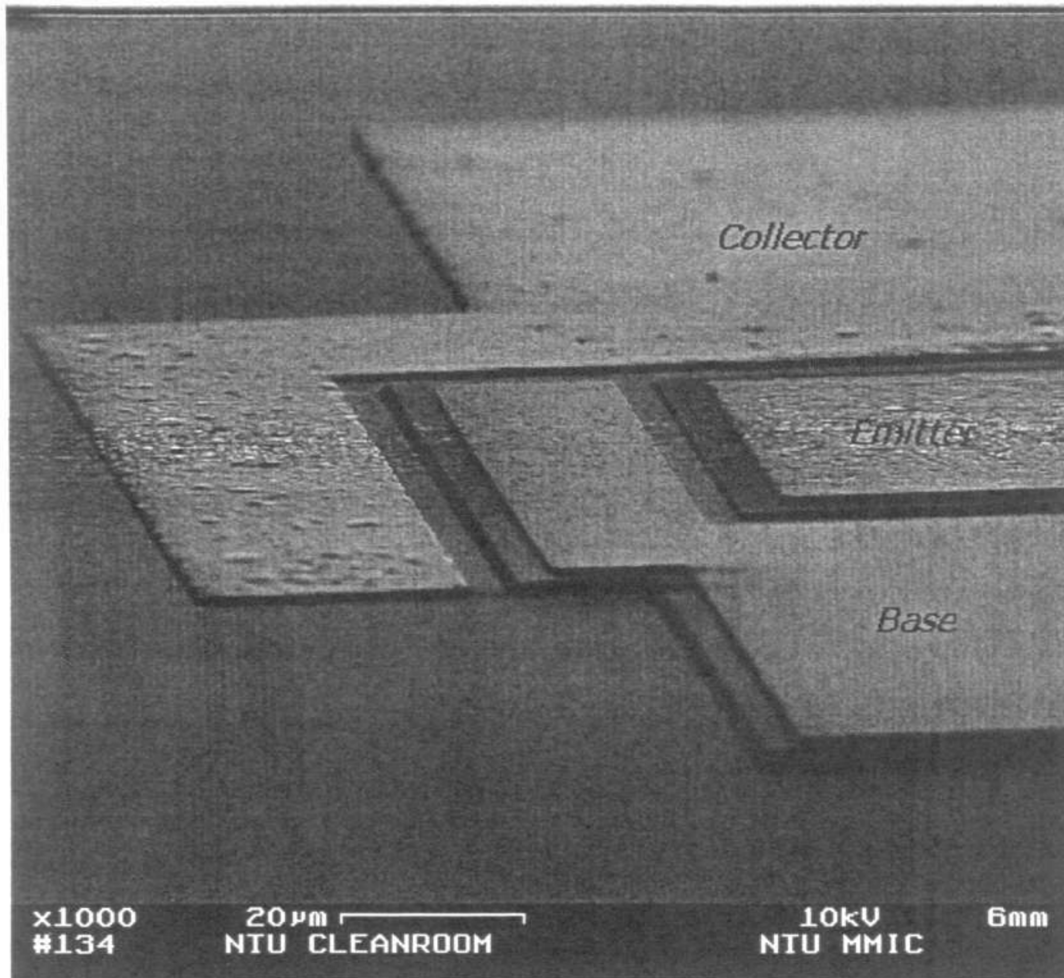

Fig.6.1 SEM image of C-doped GaInP/GaAs HBT grown by SSMBE.

ATTENTION: The Singapore Copyright Act applies to the use of this document. Nanyang Technological University Library

6.4 DC characteristics of C-doped GaInP/GaAs HBTs

The base sheet resistance of the GaInP/GaAs HBT was measured using the transmission line method (TLM). Typical TLM patterns had a width W of 100 μm. The TLM gaps L ranged from 5 to 25 μm. The resistance dependence on TLM gap size was evaluated and plotted. It is well known that the total resistance R between two TLM contacts with gap L is:

$$R = 2R_C + \frac{R_{sh}}{W} \cdot L \tag{6.1}$$

where R_C is the contact resistance, R_{sh} is the sheet resistance of the base layer. Plot of total resistance as a function of TLM pad gap size for GaInP/GaAs HBT base layer is shown in Fig.6.2.

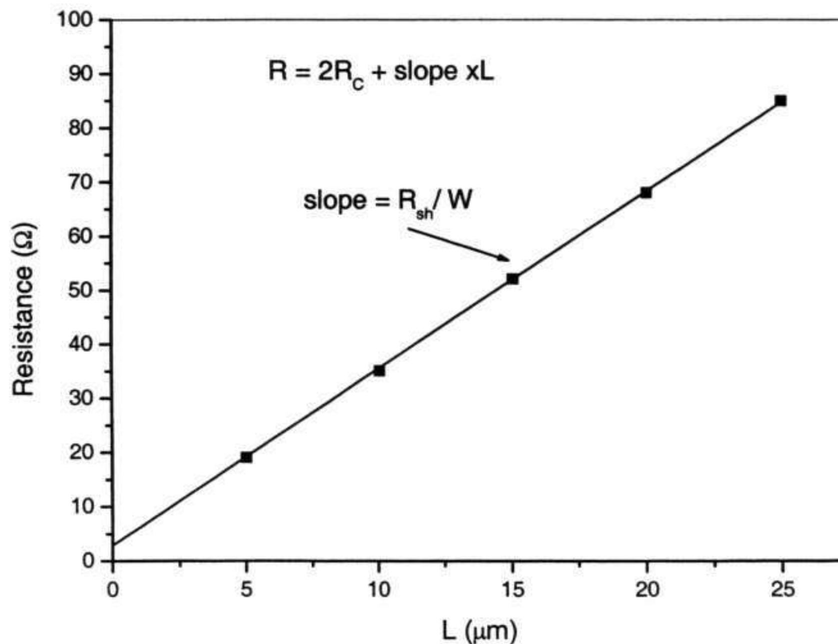

Fig.6.2 Plot of total resistance as a function of TLM pad gap size for GaInP/GaAs HBT base layer.

ATTENTION: The Singapore Copyright Act applies to the use of this document. Nanyang Technological University Library

From TLM measurements, the base sheet resistance R_{sh} of the GaInP/GaAs HBT was found to be 330 Ω/ . This value is inversely proportional to the base thickness. Using the simple expression:

$$R_{sh} = \frac{\rho_B}{W_B} = \frac{1}{p \cdot q \cdot \mu_p} \cdot \frac{1}{W_B} \tag{6.2}$$

where, R_{sh} is the sheet resistance of the base layer, ρ_B the specific resistance of the base layer, p the hole concentration, q the electronic charge, and μ_p the hole mobility at room temperature. From Eq. (6.2), the hole mobility at room temperature of the C-doped base layer was found to be 72 cm^2/Vs. As previously shown in Chapter 4, Figure 4.5 plots the room temperature hole mobility versus concentration for the C-doped GaAs samples. The hole mobility ranges from 101 cm^2/Vs at concentration of 1.02×10^{19} cm^{-3} to 45 cm^2/Vs at 1.86×10^{20} cm^{-3}. Further increase in CBr_4 flux results in significant reduction in hole mobility due to dopant compensation effects. The mobility value in the HBT base layer obtained from TLM is consistent with that from our calibrated C-doped GaAs samples in Fig.4.5. This indicates that the majority carrier mobility of C-doped base layer in the HBT structure is within the normal range.

The common emitter characteristics of the GaInP/GaAs HBT device are shown in Fig.6.3. The offset voltage is 0.3V. The breakdown voltage is about 13V. It can be seen that the device exhibits good output characteristics with low output conductance and low knee voltage.

ATTENTION: The Singapore Copyright Act applies to the use of this document. Nanyang Technological University Library

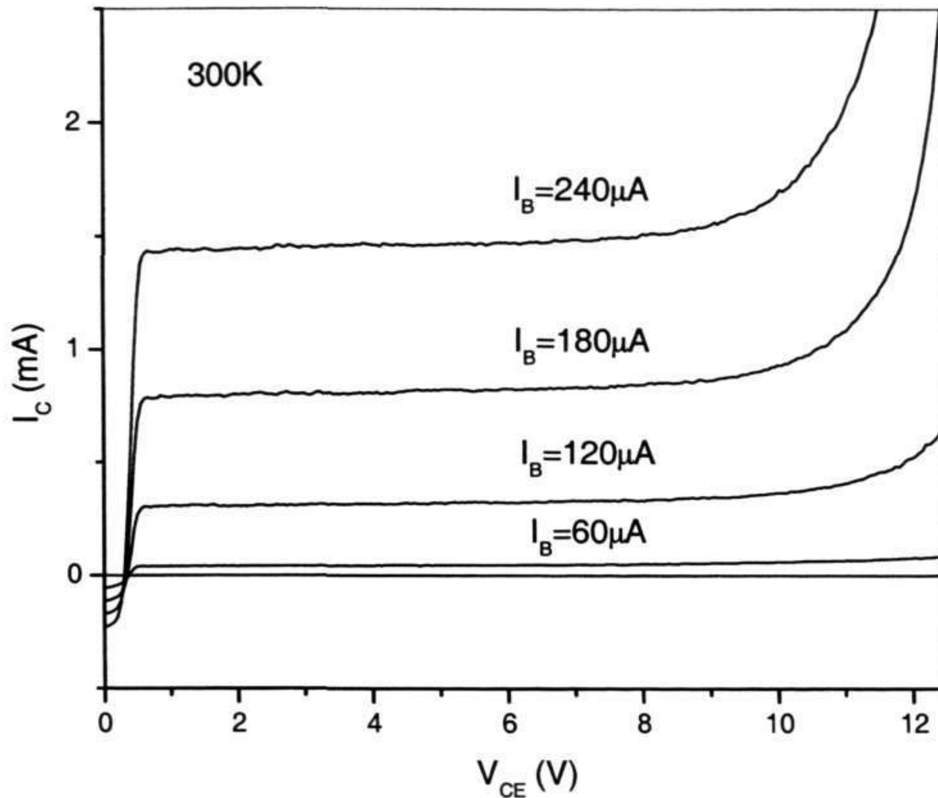

Fig.6.3 Common-emitter I-V characteristics of GaInP/GaAs HBT.

Figure 6.4 shows the temperature dependence of DC current gain (β) versus collector current (I_C) characteristics. At 300 K, the DC gain is 30 at collector current density of 3200 A/cm^2. At high I_C level of above 1×10^{-2} A, a slight degradation of β can be seen in the plot. However, at low I_C level of below 1×10^{-2} A, a slight increase in β is observed. This can be well understood by comparing the device Gummel plots within temperature range from 300K to 380K.

ATTENTION: The Singapore Copyright Act applies to the use of this document. Nanyang Technological University Library

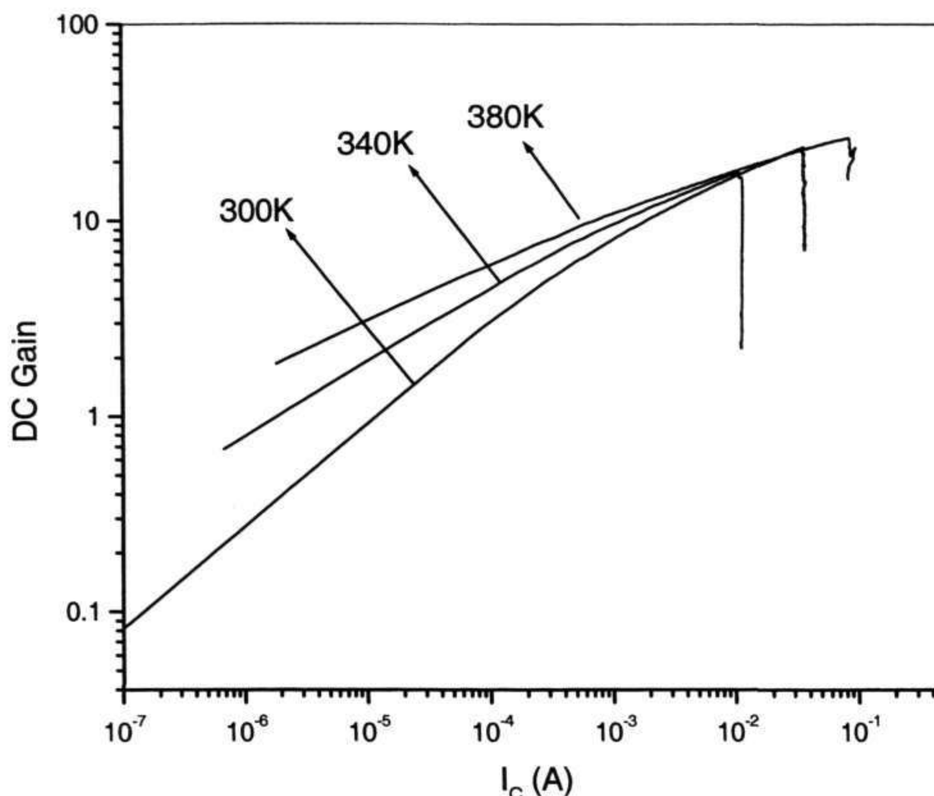

Fig.6.4 Plot of current gain versus collector current characteristics at different temperatures.

Figure 6.5 shows the Gummel plots measured from 300 K to 380 K. At elevated temperatures, both the base current and the collector current increase. The current gain is influenced by competition between the base current and collector current. At low current level, the collector current increases more rapidly than the base current, which induces an increase in current gain with temperature. At high current level, the base current increases more rapidly than collector current, which induces a decrease in current gain with temperature. To further understand the carrier transport characteristics of the device, a detailed discussion of the base current mechanism and analysis of the temperature dependence of the Gummel plot is necessary.

ATTENTION: The Singapore Copyright Act applies to the use of this document. Nanyang Technological University Library

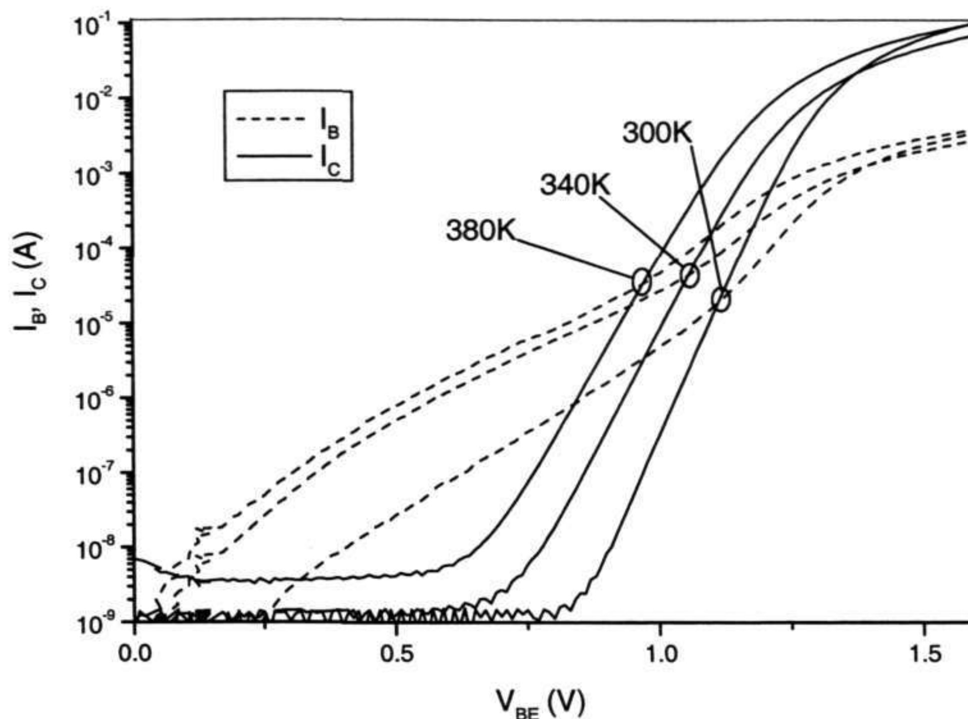

Fig.6.5 Gummel plot of GaInP/GaAs HBT at different temperatures.

For base current in the HBT, the effects of Shockley-Read-Hall (SRH) recombination, Auger recombination and radiative recombination should be considered [81]. In SRH recombination, an electron recombines with a hole through a mid-gap recombination center. This effect has been widely studied in compound semiconductor HBTs, because compound semiconductors generally have relatively large bulk defect densities. It is well known that the base current due to SRH recombination shows a $\sim(2kT)^{-1}$ behavior, while the base current induced by Auger recombination, or band-to-band radiative recombination has a $\sim(kT)^{-1}$ behavior.

At 300 K, the ideality factor of the base and collector current of the device is 1.9 and 1.1, respectively. The relatively high base current ideality factor indicates that the recombination current in the space charge region (SCR), which is determined by

ATTENTION: The Singapore Copyright Act applies to the use of this document. Nanyang Technological University Library

the SRH recombination process, is dominant in the base current. The base current ideality factor increases gradually up to 3.3 at 380 K, and collector current ideality factor increases up to 1.3 at 380 K. Recombination enhanced defect reactions (REDRs) as described by Henderson [82] and modeled by Welser *et al.* [83] are believed to be the driving force behind this phenomenon. The excess base current contributed by its high ideality factor of n ~ 3.3, suggests the possibility of a carrier tunneling mechanism due to the presence of large interface defect state density. The base-emitter turn-on voltage decreases following increase in the temperature. This decrease in turn-on voltage is mainly due to increase in the intrinsic carrier concentration in the emitter and base layers as temperature increases [84].

Figure 6.6 a) compares the reverse leakage current of the base-collector junction from 300 K to 380 K. At elevated temperatures, the reverse leakage current of the base-collector junction shows lower dependence on the bias voltage, indicating that SRH generation-recombination process [85] could be the dominant mechanism. The temperature dependent characteristics of the reverse leakage current of the base-emitter junction are shown in Fig.6.6 b). The reverse leakage current of the base-emitter junction is about 3 orders larger compared to that of the base-collector junction. The relatively low dependence of the base-emitter leakage current on temperature variation suggests that carrier tunneling from emitter to base could be the dominant mechanism. This tunneling current is most probably related to the presence of defects in the space charge region of the base-emitter junction. This gives further evidence that the poor material quality at the base-emitter junction could be responsible for the poor DC characteristics of the device.

ATTENTION: The Singapore Copyright Act applies to the use of this document. Nanyang Technological University Library

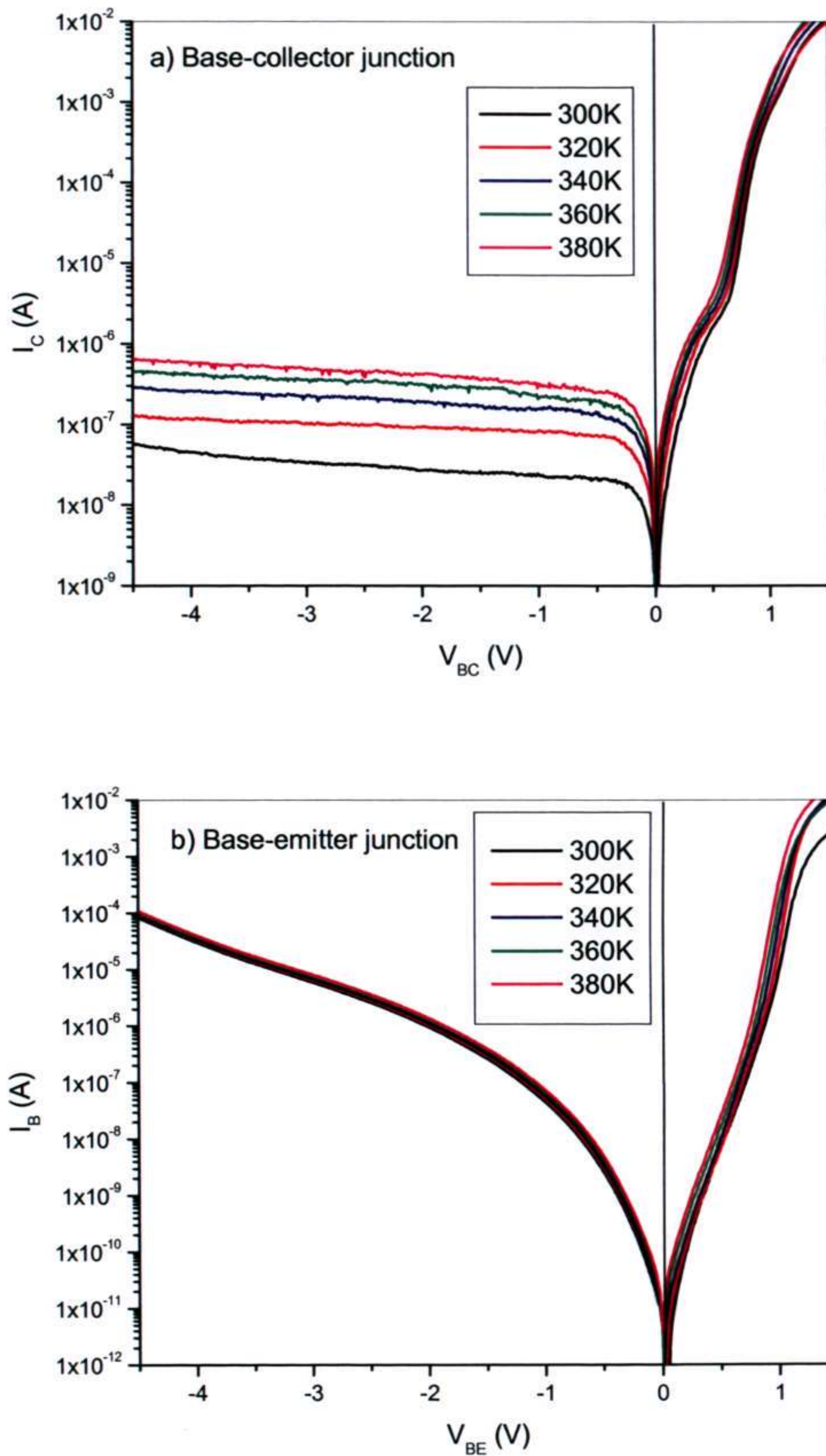

Fig.6.6 Temperature dependence of: a) base-collector junction, b) base-emitter junction characteristics.

ATTENTION: The Singapore Copyright Act applies to the use of this document. Nanyang Technological University Library

6.5 Investigation on root cause for poor characteristics of GaInP/GaAs HBT

Further investigation found that the poor characteristics of GaInP/GaAs HBT was due to the actually lower V/III ratio than the optimum range (18~25). This was resulted from the mechanical problem of the As shutter. Further process optimization is needed to improve the material quality and device performance.

6.6 Summary

C-doped GaAs grown by SSMBE using CBr_4 as p-type dopant precursor was used as the base layer of GaInP/GaAs HBT. Devices with base layer thickness of 520 Å showed DC current gain of 30 at collector current density of 3200 A/cm^2. The hole mobility obtained from the base layer sheet resistance is consistent with that of C-doped GaAs bulk layer. The temperature dependence of DC current gain versus collector current showed a slight decrease in current gain at high collector current, and increase in current gain at low collector current. The Gummel plot from 300 K to 380 K suggests that trap-related recombinations played a significant role in the poor device DC characteristics. The reverse leakage current of the base-collector junction suggests that the dominant mechanism could be related to the SRH generation-recombination process. On the other hand, the reverse leakage current of the base-emitter junction could be dominated by carrier tunneling effects. Further process optimization is needed to improve the device performance.

ATTENTION: The Singapore Copyright Act applies to the use of this document. Nanyang Technological University Library

Chapter 7

Improved characteristics of C-doped GaInP/GaAs HBTs

In this chapter, improved properties of C-doped GaInP/GaAs HBTs with base doping concentration of 4×10^{19} cm^{-3} were obtained through better control of growth process. The DC characterization of the device temperature–dependant performance was investigated and the carrier transport was studied. The DC characteristics of C-doped GaInP/GaAs HBT with base doping concentration of 2×10^{19} cm^{-3} were also reported.

7.1 Growth and fabrication of C-doped GaInP/GaAs HBT with improved performance

Chapter 6 has reported the poor material quality for the GaInP/GaAs HBTs due to lower V/III ratio. In this chapter, with better control of the growth process (including shutter control) using V/III ratio of 25, C-doped GaInP/GaAs HBT with improved characteristics was grown by SSMBE.

The C-doped GaInP/GaAs HBT structure with an abrupt emitter-base junction and base doping concentration of 4×10^{19} cm^{-3} was grown on (100)-oriented semi-insulating GaAs substrates. Table 7.1 shows the layer structure of the HBT.

ATTENTION: The Singapore Copyright Act applies to the use of this document. Nanyang Technological University Library

Table 7.1 Layer structure of GaInP/GaAs HBT with improved performance.

Layer	Material	Thickness (Å)	Dopant	Concentration (cm^{-3})
Cap	$In_{0.2}Ga_{0.8}As$	200	Si	1×10^{19}
Cap	GaAs	1200	Si	4×10^{18}
Emitter	$Ga_{0.51}In_{0.49}P$	500	Si	3×10^{17}
Base	GaAs	600	C	4×10^{19}
Collector	GaAs	7000	Si	1×10^{16}
Sub-Collector I	GaAs	500	Si	4×10^{18}
Etch stop	$Ga_{0.51}In_{0.49}P$	200	Si	1×10^{18}
Sub-collector II	GaAs	5500	Si	4×10^{18}
GaAs buffer 5000 Å				
S.I. GaAs substrate				

The actual doping profile was measured using SIMS measurement. Figure 7.1 shows the SIMS depth profile of the HBT structure. The Si and C levels cross at the GaInP/GaAs interface, indicating correct placement of the junction, in agreement with the electrical characteristics. The Br level was kept below 10^{15} cm^{-3}. Till now there are no reports of the degradation of material quality associated with the presence of halogens in the growth system.

ATTENTION: The Singapore Copyright Act applies to the use of this document. Nanyang Technological University Library

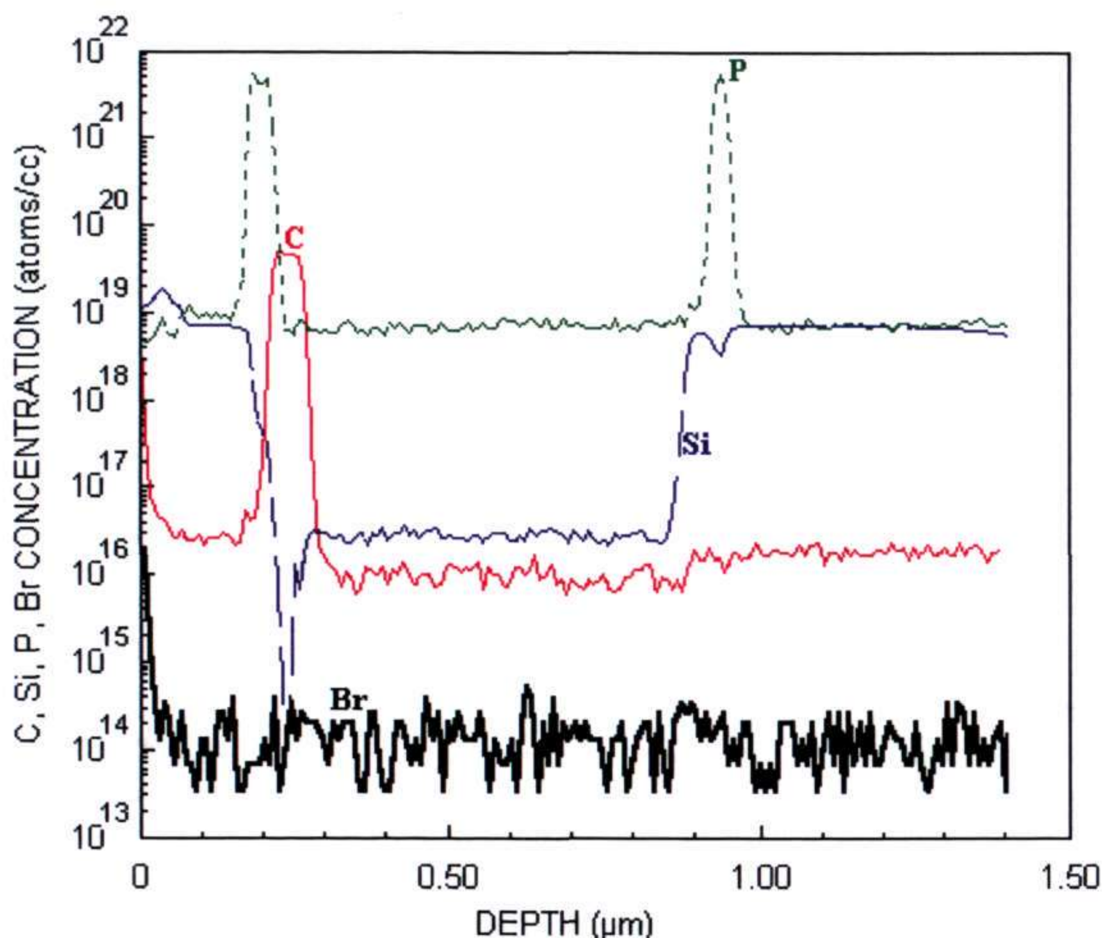

Fig.7.1 SIMS profiles of C, Si, P, and Br concentration in the GaInP/GaAs HBT structure with abrupt emitter-base junction and base doping concentration of 4×10^{19} cm^{-3}. The depth data in the profile are approximate values.

The HBT devices were fabricated using the same mask set and same process as in chapter 6. Large emitter area (50×50 μm^2) devices were fabricated in this study for DC characterization. Figure 7.2 shows the schematic cross section of the GaInP/GaAs HBT. The devices were dipped into a diluted HF solution for 1 min (at room temperature) for passivation. After HF treatment, a detailed DC characterization of the device performance at elevated temperature ranging from 300 K to 380 K was carried out. The temperature dependence of device DC characteristics was measured using a semiconductor parameter analyzer in conjunction with a probe station.

ATTENTION: The Singapore Copyright Act applies to the use of this document. Nanyang Technological University Library

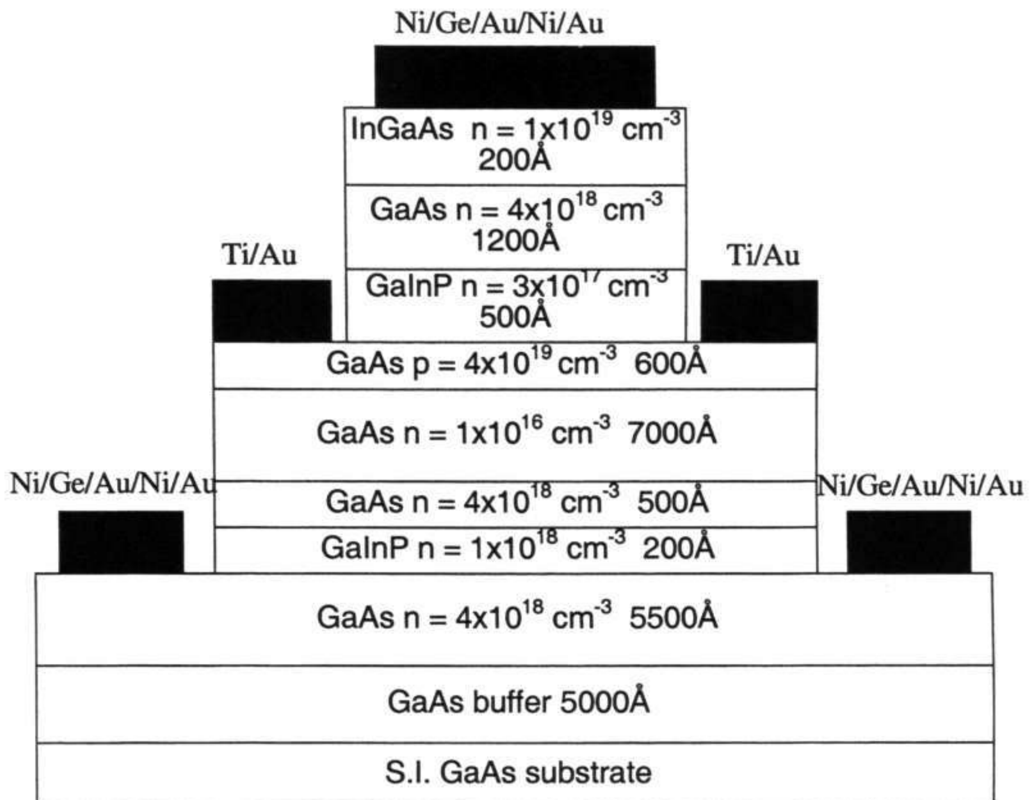

Fig.7.2 Schematic cross section of the GaInP/GaAs HBT.

ATTENTION: The Singapore Copyright Act applies to the use of this document. Nanyang Technological University Library

7.2 Improved DC characteristics of C-doped GaInP/GaAs HBT with base doping concentration of 4×10^{19} cm^{-3}

Figure 7.3 shows the Gummel plot of the C-doped GaInP/GaAs HBT before and after HF treatment. It can be seen that at base bias voltages below 0.9 V, the base current after HF treatment was greatly reduced, which indicated that the extrinsic base surface recombination current was greatly reduced. The base current and collector current ideality factors are 1.12 and 1.01, respectively. This indicated that the space-charge region recombination current is insignificant in the base current. The base current is dominated by radiative recombination current and/or the Auger recombination current.

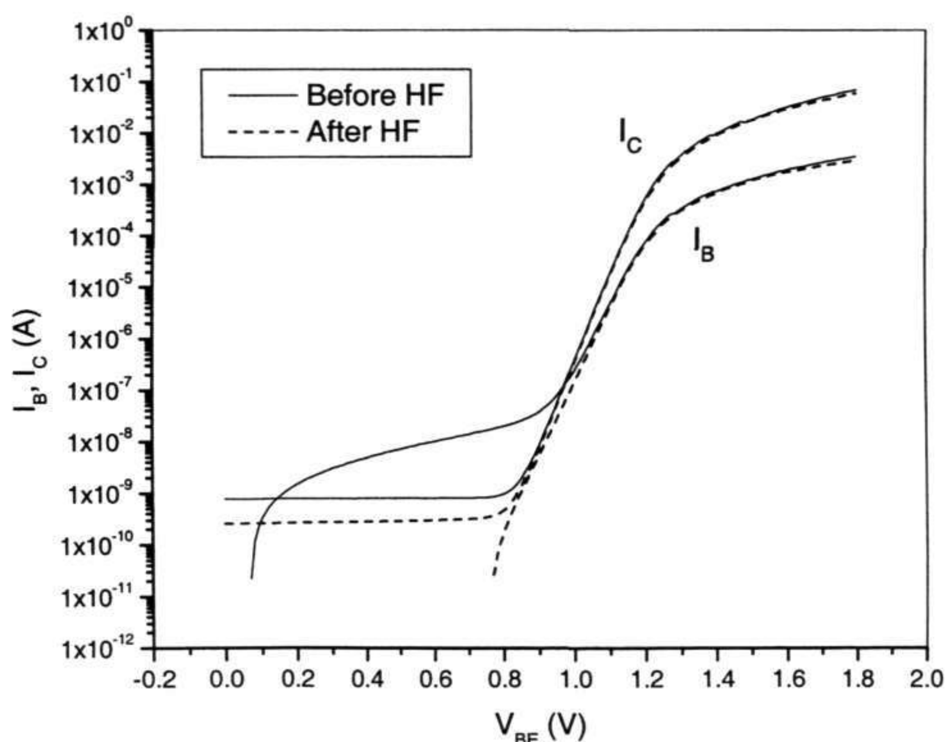

Fig.7.3 Gummel plot of GaInP/GaAs HBT before and after HF passivation.

ATTENTION: The Singapore Copyright Act applies to the use of this document. Nanyang Technological University Library

The common emitter I-V characteristics at 300 K and 380 K are shown in Fig.7.4. It can be seen that the device exhibits good output characteristics with low output conductance. Base-emitter (B-E) and base-collector (B-C) junction characteristics measured from 300 K to 380 K are shown in Fig.7.5. The temperature dependence for B-E and B-C junctions behaves similarly. As the temperature increases, the increase of the junction leakage current can be observed. However, no significant changes of bias sensitivity of the leakage current was found which indicates that the dominated transport mechanism for the junction reverse current is not changed in this temperature range.

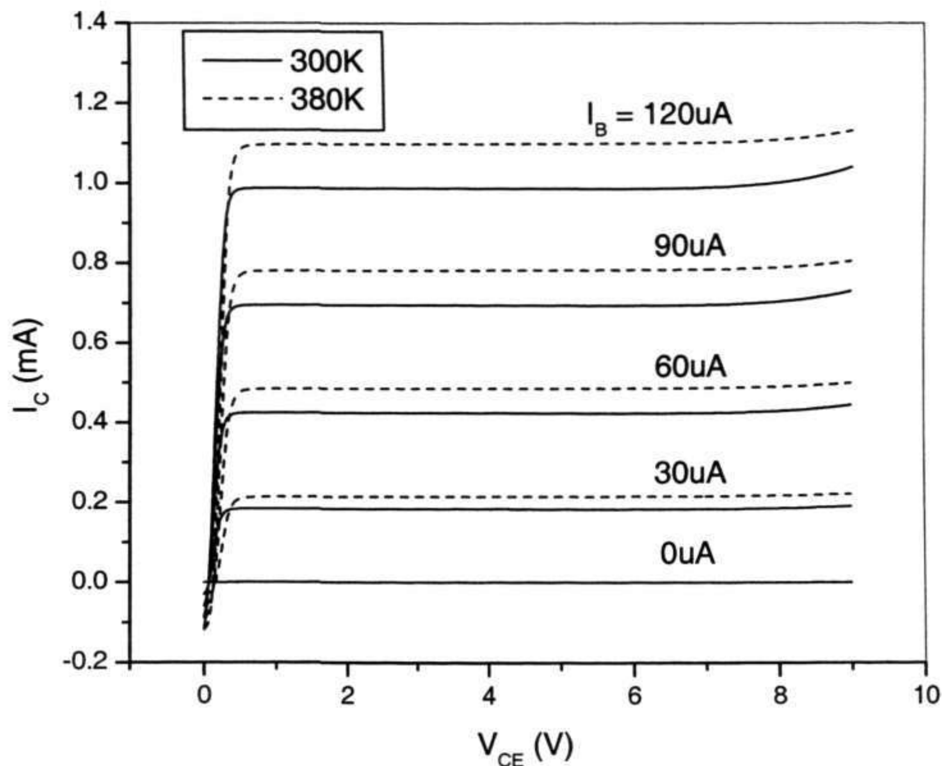

Fig.7.4 Plot of GaInP/GaAs HBT common-emitter I-V characteristics at 300 K and 380 K.

ATTENTION: The Singapore Copyright Act applies to the use of this document. Nanyang Technological University Library

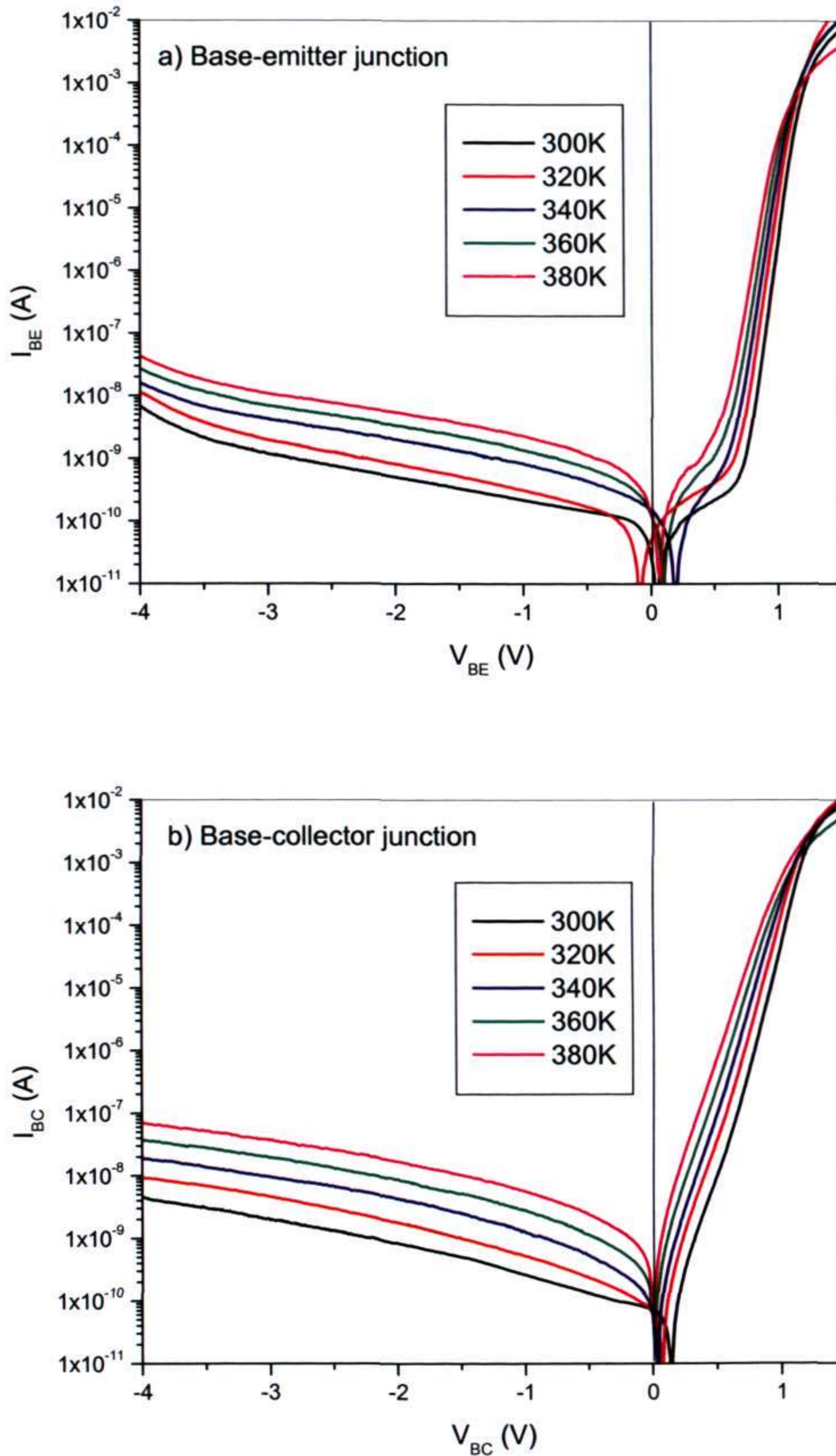

Fig.7.5 Temperature dependent characteristics of: a) base-emitter junction, and b) base-collector junction.

ATTENTION: The Singapore Copyright Act applies to the use of this document. Nanyang Technological University Library

The temperature dependence of Gummel plot measured at $V_{CB} = 1$ V is shown in Fig.7.6. It can be seen that no obvious changes of base and collector ideality factors are observed. As the temperature increases, the base-emitter turn-on voltage largely decreases. The decrease of turn-on voltage is mainly due to the increase of the intrinsic carrier concentration in the emitter and base layer as the temperature is increased [84].

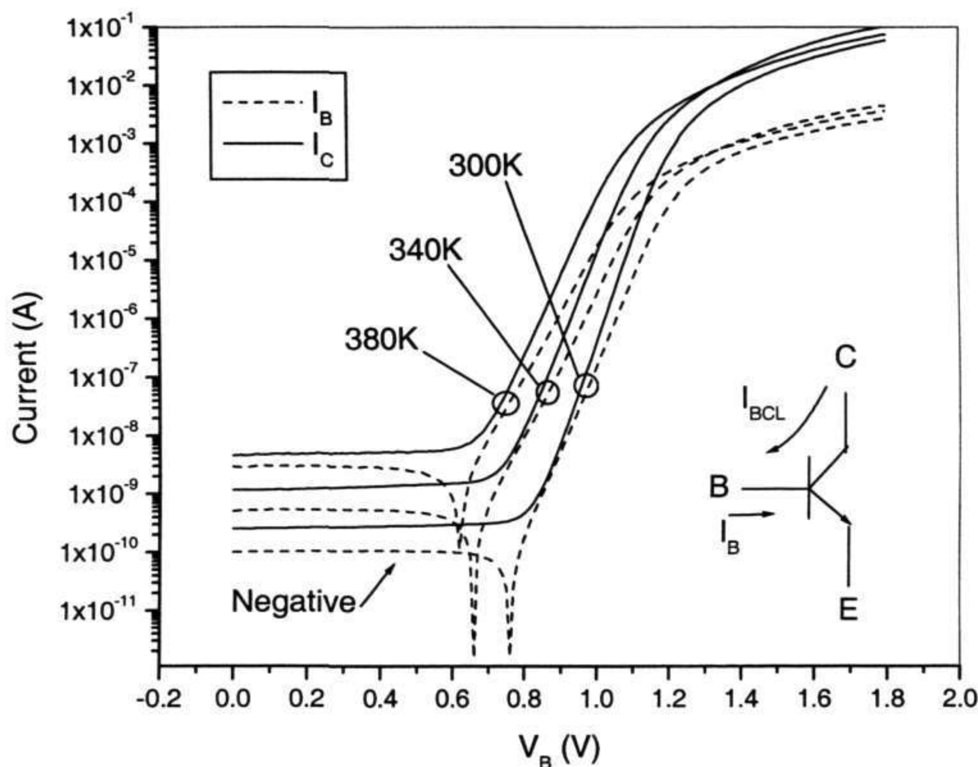

Fig.7.6 Gummel plot of GaInP/GaAs HBT at different temperature.

To gain a better understanding of the carrier transport properties in the device, collector and base currents in Gummel plots at different temperatures were extrapolated to $V_{BE} = 0$ V to obtain the values of zero bias collector current I_{C00} and base current I_{B00} [81]. Activation energies were determined from the slope of Arrhenius plots of I_{C00} and I_{B00} as shown in Fig.7.7. For the collector current, the

ATTENTION: The Singapore Copyright Act applies to the use of this document. Nanyang Technological University Library

activation energy is 1.4 eV, which is close to the bandgap of the GaAs base. This indicates that the collector current is determined by drift-diffusion process, in which an energy barrier same as the base bandgap should be overcome by the electrons before they are collected by the collector. For the base current, the activation energy is also 1.4 eV, which is close to the bandgap of the GaAs base, indicating that band-to-band recombination plays a dominant role in determining the base current. No trap-related recombination is observed for the base and collector currents, which further indicates the good base material quality for the HBT structures.

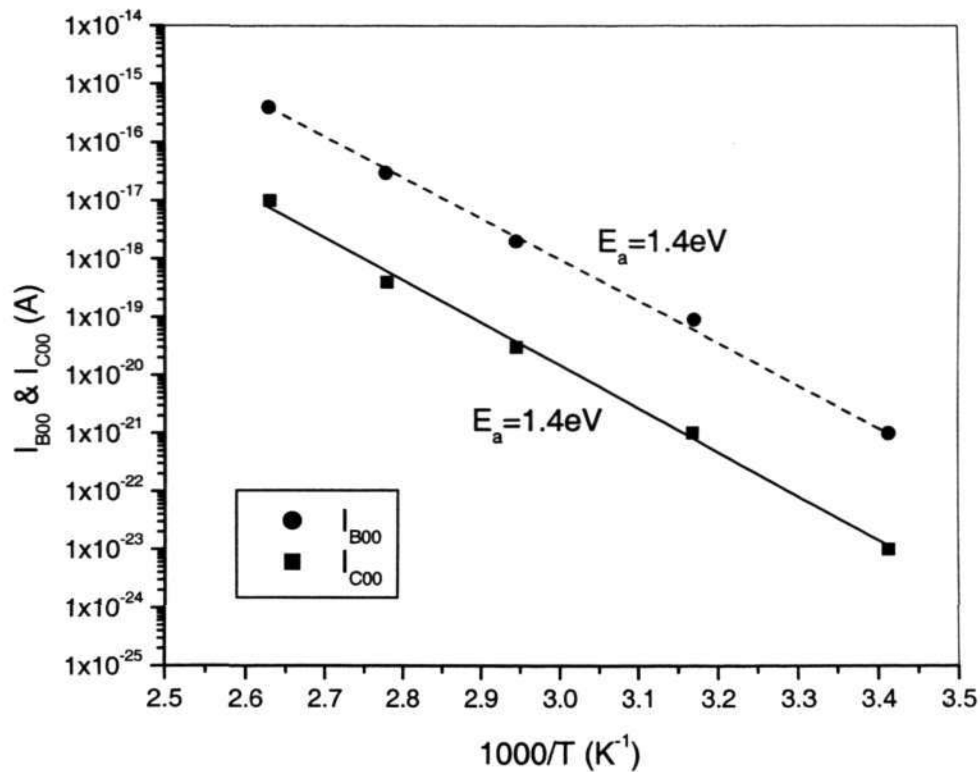

Fig.7.7 Activation energy plots for collector and base currents extrapolated to $V_{BE} = 0$ V.

ATTENTION: The Singapore Copyright Act applies to the use of this document. Nanyang Technological University Library

A plot of current gain (β) versus collector current (I_C) at different temperatures measured at $V_{CE} = 3$ V is shown in Fig.7.8. At 300 K, the DC gain is 28 at a collector current density of 3200 A/cm^2. At low I_C level, a slight increase in β with the increase of temperature can be seen in the plot. However, at high I_C level, a slight degradation of β is observed.

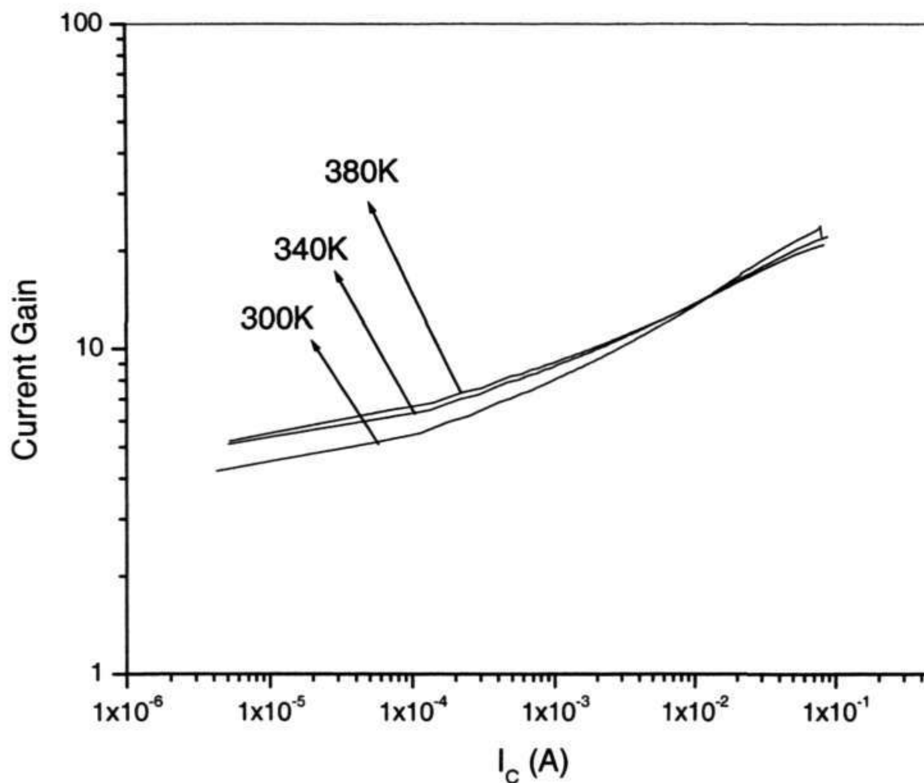

Fig.7.8 Plot of current gain *vs.* collector current characteristics at different temperatures.

To further analyze the mechanism involved in the change of current gain, it is essential to correlate it with the Gummel plot at different temperatures. It can be seen that at high I_C level, both base current and collector current increased with temperature. Thus, the change of β is determined by the competition between base

ATTENTION: The Singapore Copyright Act applies to the use of this document. Nanyang Technological University Library

current and collector current. The base current increased more rapidly following increase in temperature than the collector current did at high I_C level. Therefore, β decreased with temperature. On the other hand, we give a physical explanation. Due to the near unity value of base current ideality factor, it is reasonable to assume that bulk base recombination dominates the base current. Therefore,

$$\beta \approx \tau_e / \tau_b \qquad (7.1)$$

where τ_e is the minority electron lifetime in the p-type GaAs base and τ_b is the base transit time [86]. The temperature dependence of the base bulk recombination dominated current gain will therefore depend on the temperature dependence of τ_e and τ_b. As discussed earlier, the base current is dominated by radiative recombination current and/or the Auger recombination current. In radiative recombination process, it is known that the recombination lifetime increases with increasing temperature [87]. In the Auger recombination process, the recombination lifetime decreases with increasing temperature [88,89]. However, the general consensus is that the total recombination lifetime, τ_e, decreases with increasing temperature [86,90]. On the other hand, for diffusive base transport, τ_b is given by: $W_B^2 / 2D_n$. Here the diffusion coefficient, $D_n = \mu_e^p kT / q$, and μ_e^p is the minority electron mobility in the p-type GaAs base of width W_B. The temperature dependence of the minority electron mobility indicates that μ_e^p is approximately proportional to $1/T$ up to room temperature [91,92]. However, the data presented in [91,92] indicate that μ_e^p tends to become less sensitive to temperature above 300K [86]. Thus, D_n would increase or remain constant with increasing temperature, and hence τ_b would decrease or remain constant. Consequently, β is expected to change with temperature according to the

ATTENTION: The Singapore Copyright Act applies to the use of this document. Nanyang Technological University Library

relative rates of change of τ_e and τ_b. In our device, τ_e decreased more rapidly than τ_b, therefore, β decrease at high I_C level.

However, at low I_C region, in our device, the base current at low V_{BE} is dominated by B-C junction leakage, since the values for the negative I_B are close to those for I_C as shown in Fig.7.6. Following increase in temperature, the B-C junction reverse leakage current greatly increased. The increase of the B-C junction leakage current contributes to the reduction of the total base current as shown in the inset of Fig.7.6 [93]. It subsequently causes the increase of the ratio of I_C/I_B, i.e. β, in the low I_C range.

7.3 C-doped GaInP/GaAs HBT with base doping concentration of 2×10^{19} cm^{-3}

C-doped GaInP/GaAs HBT structure with base doping concentration of 2×10^{19} cm^{-3} was grown using V/III ratio of 25. The HBT devices were fabricated using the same mask set. Figure 7.9 shows the Gummel plots of the C-doped GaInP/GaAs HBT with base doping concentration of 2×10^{19} cm^{-3}. The ideality factor of base current and collector current is 1.30 and 1.01, respectively. The base-collector leakage current of the HBT with base doping concentration of 2×10^{19} cm^{-3} is nearly two orders lower than that of the HBT with base doping concentration of 4×10^{19} cm^{-3}. As seen in Fig.7.10, the current gain of GaInP/GaAs HBT with base doping concentration of 2×10^{19} cm^{-3} reaches 138 at $I_C = 0.1$ A, which is much higher than that of the HBT with base doping concentration of 4×10^{19} cm^{-3}. High-performance C-doped GaInP/GaAs HBTs with different doping levels grown by SSMBE using CBr_4 as p-type precursor have been obtained, which indicate the capability and stability of the C-doping growth technique in our group.

ATTENTION: The Singapore Copyright Act applies to the use of this document. Nanyang Technological University Library

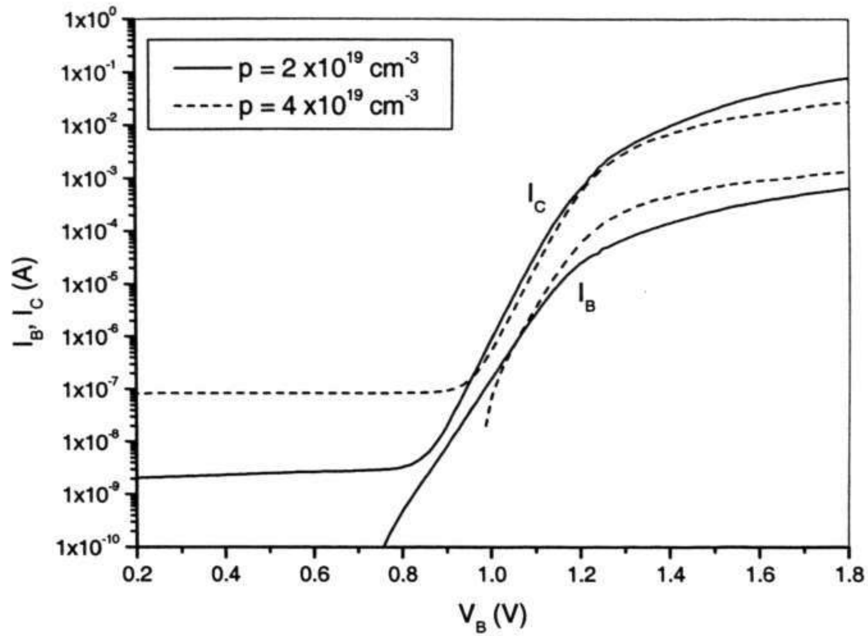

Fig.7.9 Gummel plots of C-doped GaInP/GaAs HBTs with base doping concentration of 2×10^{19} cm^{-3} and 4×10^{19} cm^{-3}.

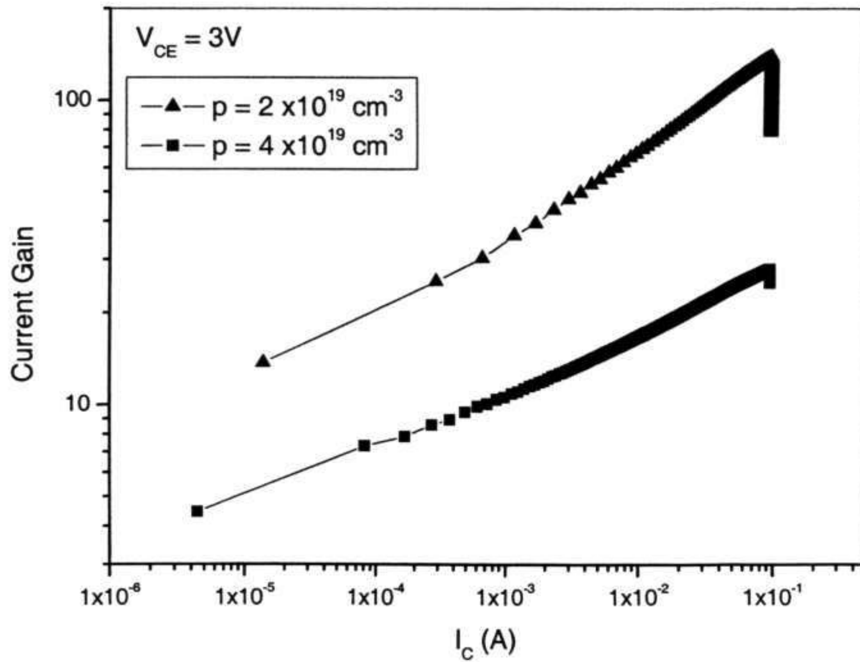

Fig.7.10 Current gain vs. collector current for C-doped GaInP/GaAs HBTs with base doping concentration of 2×10^{19} cm^{-3} and 4×10^{19} cm^{-3}.

ATTENTION: The Singapore Copyright Act applies to the use of this document. Nanyang Technological University Library

7.4 Summary

C-doped GaInP/GaAs HBT with base doping concentration of $4\times10^{19}\,cm^{-3}$ has been grown by SSMBE using CBr_4 as p-type precursor with improved device performance. HF treatment greatly reduced the extrinsic base surface recombination current at low base bias voltages. After HF treatment, a detailed DC characterization of the devices in the temperature range of 300 K 380 K has been carried out. The base current and collector current ideality factors at 300 K were 1.12 and 1.01, respectively, which indicates that space charge region recombination current is insignificant in the base current. From the temperature dependent Gummel plot, the activation energies of collector current and base current were obtained. For the collector current, the activation energy is 1.4 eV, which is close to the bandgap of the GaAs base. This indicates that the collector current is determined by drift-diffusion process. For the base current, the activation energy is also 1.4 eV, indicating that band-to-band recombination plays a dominant role in determining the base current. No trap-related recombination is observed for the base and the collector currents, which further indicates the good base material quality of the HBT structures. Properties of current gain versus collector current at different temperatures were also investigated. At low I_C level, a slight increase in β with the increase of temperature can be seen in the plot. However, at high I_C level, a slight degradation of β is observed. The physical mechanisms involved were analyzed in detail. High-performance C-doped GaInP/GaAs HBTs with base doping concentration of $2\times10^{19}\,cm^{-3}$ grown by SSMBE using CBr_4 as p-type precursor have also been obtained. Maximum current gain of 138, as well as base current and collector current ideality factors of 1.30 and 1.01,

ATTENTION: The Singapore Copyright Act applies to the use of this document. Nanyang Technological University Library

respectively, was achieved. The above results indicate the capability and stability of the C-doping epitaxial growth technique in our group.

ATTENTION: The Singapore Copyright Act applies to the use of this document. Nanyang Technological University Library

Chapter 8

C-doped InGaAs and InP/InGaAs HBTs

C-doped InGaAs lattice matched to InP, InP/InGaAs single heterojunction bipolar transistor (SHBT) and double heterojunction bipolar transistor (DHBT) have been grown by SSMBE using CBr_4 as p-type dopant precursor. Material properties of C-doped $In_{0.53}Ga_{0.47}As$, such as hole mobility, and effect of V/III ratio on the PL properties have been investigated. DC characteristics of InP/InGaAs composite collector DHBT have been compared with the SHBT. Furthermore, this study elucidates the complex breakdown mechanisms in the composite collector DHBTs.

8.1 Introduction

8.1.1 Applications of InP-based HBT technology

InP-based HBTs were first marketed in military programs due to their superior transport characteristics. With the continuing increase of communication speed and capacity, InP-based HBTs have found a variety of applications, especially in the area of optical communication systems such as OC192 (10 Gb/s) and OC768 (40 Gb/s). InP-based HBTs are of great interest for the development of microwave point to point links with the emerging 60 GHz band and possible 90 GHz band applications. InP-based HBTs are also of great interest in commercial wireless communications. Although they have not been widely adopted by commercial foundries due to substrate cost, concern over breakage, and possible lack of 6" wafers, the low turn-on voltage offered by the low energy bandgap of InGaAs made them very desirable for

ATTENTION: The Singapore Copyright Act applies to the use of this document. Nanyang Technological University Library

operations at low power supply voltages without compromising power added efficiency. This is the key for portable electronics to extend the battery lifetime without sacrificing the performance.

8.1.2 State-of-the art of C-doped $In_{0.53}Ga_{0.47}As$ and InP-based HBTs

In MOCVD [94], GSMBE [95] and MOMBE [96], hydrogen atoms incorporated into InGaAs along with carbon reduces the hole concentration. In recent years, the hydrogen passivation level for C-doped InGaAs has been in good control with lower than 10% by GSMBE and MOMBE. The use of CBE allows the reduction of the hydrogen incorporation problem [97]. SSMBE offers the advantage of a hydrogen-free environment for the growth of carbon-doped III-V semiconductor layers, eliminating the passivation of carbon acceptors by hydrogen. Table 8.1 shows the state-of-the art of C-doped $In_{0.53}Ga_{0.47}As$ grown by different techniques. The highest doping level has reached 2×10^{20} cm^{-3}. The hydrogen (H) passivation level is also shown in the table.

Table 8.1 State-of-the art of C-doped $In_{0.53}Ga_{0.47}As$.

Growth Technique	Doping Precursor	Maximum Hole Concentration (cm^{-3})	H Passivation Level	Year	Reference
MOCVD	CCl_4	8×10^{19}	~ 40%	1994	[98]
MOMBE	CBr_4	8×10^{19}	≤ 10%	1996	[99]
GSMBE	CBr_4	9×10^{19}	< 10%	1999	[95]
CBE	CBr_4	2×10^{20}	Insignificant	2002	[97]
SSMBE	CBr_4	2.1×10^{20}	No	1999	[100]

ATTENTION: The Singapore Copyright Act applies to the use of this document. Nanyang Technological University Library

Record f_{max} of 478 GHz [101] has been achieved by InP/InGaAs SHBT with a 400Å C-doped base (p = 6×10^{19} cm^{-3}) grown by SSMBE (IntelliEPI Inc.). Record f_t of 509 GHz [102] has been achieved by InP/InGaAs SHBT with a 250 Å compositionally graded C-doped base (p = 6×10^{19} cm^{-3}) grown by MBE (University of Illinois at Urbana-Champaign). Record $f_t + f_{max} = 673$ GHz [103] has been obtained by InP/InGaAs SHBT with a 300 Å compositionally graded C-doped base grown by MBE (University of Illinois at Urbana-Champaign).

8.1.3 InP/InGaAs SHBT and DHBT

InP/InGaAs single heterojunction bipolar transistors (SHBTs) are limited by low breakdown voltage and high output conductance due to the high impact ionization rate in the narrow bandgap InGaAs collector. Double heterojunction bipolar transistor (DHBT) structures, in which the wide bandgap InP is used as the collector, provide improvement in breakdown performance. However, due to the large conduction band discontinuity between the InGaAs base and InP collector, InP/InGaAs DHBTs typically suffer from the current blocking effect. So far various design schemes have been proposed to suppress the current blocking effect; such as those using a composite collector [104,105,106], pn-pair doping [107], InGaAsP graded layers [108] and staggered energy band lineup of InP/GaAsSb heterojunction [109]. Although the last two approaches are ideal, as far as potential barrier due to conduction band discontinuity is concerned, special and complex optimization for the growth conditions is needed to obtain good step-graded InGaAsP or GaAsSb materials. Following the composite collector approach, there have been reports on the use of a thin n$^+$-InP insertion layer between the p$^+$-InGaAs base and n$^-$-InP collector [104], and undoped InGaAs and n$^+$-InP insertion layers [106]. We adopted the latter design of

ATTENTION: The Singapore Copyright Act applies to the use of this document. Nanyang Technological University Library

composite collector to grow and fabricate the DHBT device using our baseline InP HBT process. Table 8.2 shows the state-of-the art of InP/InGaAs DHBTs.

Table 8.2 State-of-the art of InP/InGaAs DHBTs.

Year	f_t (GHz)	f_{max} (GHz)	BV_{CE0} (V)	Current gain	Base doping (cm^{-3})	Reference
2001	341	---	~ 3	---	6×10^{19} (300Å)	NTT [110]
2001	~ 200	~ 300	~ 6	~ 50	4×10^{19} (500Å)	NEC [111]
2003	> 300	492	~ 5	~ 20	6×10^{19} (300Å)	NTT [112]
2003	---	---	> 15	120	5×10^{18} (1000Å)	[106]

8.2 Growth and characterization of C-doped $In_{0.53}Ga_{0.47}As$

C-doped $In_{0.53}Ga_{0.47}As$ bulk layers were grown by SSMBE on InP semi-insulating (S.I.) substrate at 450 °C. The CBr_4 flux is generated in a temperature-controlled canister, and the flux is delivered into the MBE chamber *via* a system of ultra-clean pipes, as described previously in Chapter 4. The magnitude of the CBr_4 flux introduced into the MBE chamber is regulated by a high precision leak valve. The hole concentration was controlled by the CBr_4 flux.

The hole concentration and mobility were measured at room temperature using the Hall effect system. PL measurements were performed at 4 K using the 514.5 nm line of an Ar^+ ion laser.

ATTENTION: The Singapore Copyright Act applies to the use of this document. Nanyang Technological University Library

Figure 8.1 shows the hole mobility at room temperature for C-doped InGaAs layers grown by SSMBE as function of net hole concentration. As-grown data of C-doped InGaAs grown by GSMBE [95], MOCVD [98], and SSMBE [113] reported by other workers is included for comparison. The hole motilities in our SSMBE-grown C-doped InGaAs layers are comparable to those grown by GSMBE, MOCVD and other groups.

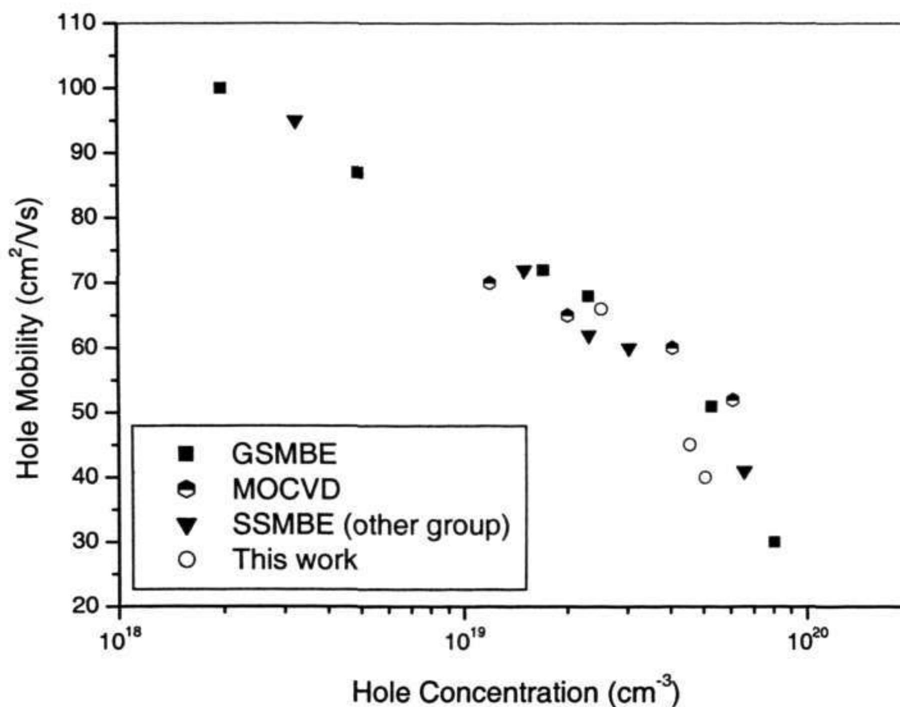

Fig.8.1 Room temperature hole mobility *vs.* hole concentration in C-doped InGaAs. The GSMBE data are from Ref. [95], MOCVD data from Ref. [98], and SSMBE data (other groups) from Ref. [113].

The V/III ratio used for the growth of C-doped InGaAs greatly affects the material quality. Figure 8.2 shows the PL of C-doped InGaAs layers grown at different V/III ratios of 20, 25, and 35, respectively. The same CBr_4 flux was used in all the samples.

ATTENTION: The Singapore Copyright Act applies to the use of this document. Nanyang Technological University Library

According to the Hall measurement results, the hole concentration remains unchanged at 4.5×10^{19} cm^{-3}. At 4 K, the PL spectrum yields two peaks, which are due to the valence band splitting into light-hole and heavy-hole bands. This results in both conduction band to light-hole and conduction band to heavy-hole transitions [114]. From the point of view of material quality, the presence of defects and impurities can lead to nonradiative recombination centers which will decrease the PL intensity. Higher PL intensity indicates higher material quality, which corresponds to better minority carrier lifetime [115]. When C-doped InGaAs is used as the base layer of HBTs, the current gain is determined mainly by the minority carrier lifetime in the base layer. As shown in Fig.8.2, both the highest PL intensity and the narrowest FWHM of 50 meV were obtained at V/III ratio of 25, suggesting this value as optimum for growth of C-doped InGaAs base layer for HBT application. To the best

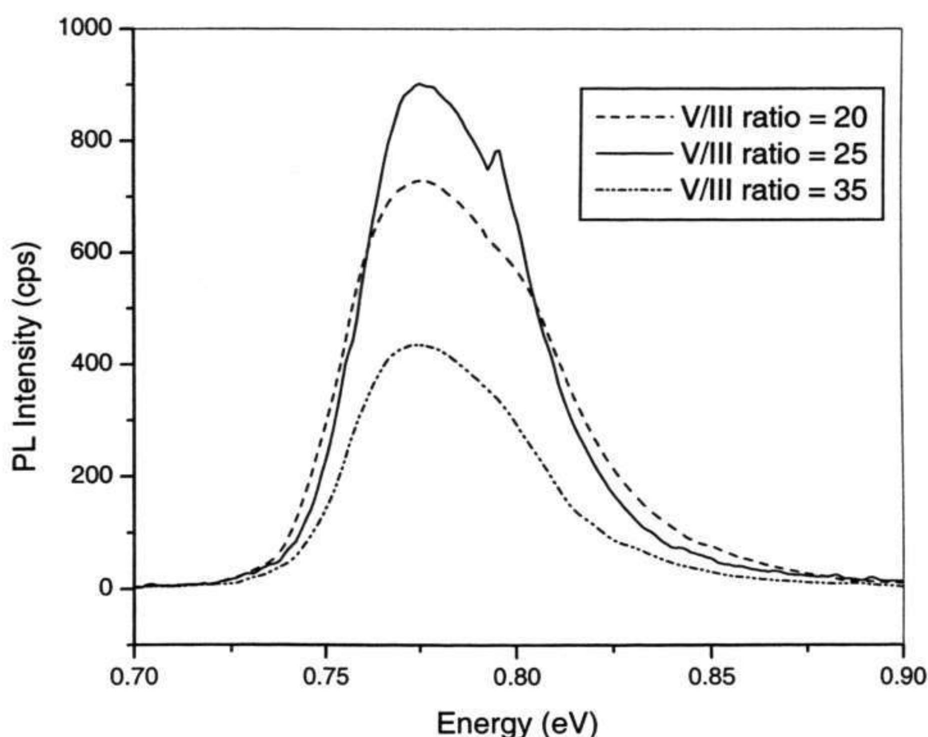

Fig.8.2 4K PL spectra of C-doped InGaAs grown at different V/III ratios.

ATTENTION: The Singapore Copyright Act applies to the use of this document. Nanyang Technological University Library

of the author's knowledge, there are few reported PL data from SSMBE grown C-doped InGaAs. Therefore, for comparison purpose, the PL result from MOCVD grown C-doped InGaAs at 10 K as shown in Ref. [116] is used. The FWHM of their PL is around 47 meV at 10 K, which is comparable to the result in this work.

8.3 Growth and fabrication of C-doped InP/InGaAs SHBTs and DHBTs

C-doped InP/InGaAs SHBT and DHBT structures were grown by SSMBE on InP S.I. substrate at 450 °C. To suppress the current blocking effect in the DHBT, a composite collector structure, which comprises 100 Å undoped InGaAs layer and 50 Å n^+-InP layer, is used. The epitaxial layer structures of the SHBT and DHBT are listed in Table 8.3 a) and b), respectively.

Table 8.3 Epitaxial layer structure of: a) InP/InGaAs SHBT; b) composite collector DHBT.

a)

Layer	Material	Thickness (Å)	Doping Level (cm^{-3})
Cap	$In_{0.53}Ga_{0.47}As$	1400	Si: 1×10^{19}
Cap	InP	600	Si: 1×10^{19}
Emitter	InP	900	Si: 3×10^{17}
Base	$In_{0.53}Ga_{0.47}As$	500	C: 2×10^{19}
Collector	$In_{0.53}Ga_{0.47}As$	4000	Si: 1×10^{16}
Sub-Collector	$In_{0.53}Ga_{0.47}As$	4500	Si: 5×10^{18}
Buffer	InP	5000	/
Substrate			

ATTENTION: The Singapore Copyright Act applies to the use of this document. Nanyang Technological University Library

b)

Layer	Material	Thickness (Å)	Doping Level (cm^{-3})
Cap	$In_{0.53}Ga_{0.47}As$	1400	Si: 1×10^{19}
Cap	InP	600	Si: 1×10^{19}
Emitter	InP	900	Si: 3×10^{17}
Base	$In_{0.53}Ga_{0.47}As$	500	C: 2×10^{19}
Composite Collector	$In_{0.53}Ga_{0.47}As$	100	undoped
	InP	50	Si: 3×10^{18}
	InP	3000	Si: 1×10^{16}
Sub-collector	$In_{0.53}Ga_{0.47}As$	4500	Si: 3×10^{18}
Buffer	InP	5000	/
Substrate			

The HBT devices were fabricated using conventional photolithography and wet chemical etching. For device fabrication, firstly, the cap layers and InP emitter layer were etched to form the emitter mesa. This is followed by etching of the InGaAs base, and collector (or composite collector) layers to form the base mesa. Next, the emitter and collector ohmic contacts were made using Ti/Au (50/250 nm) metallization. The p-type ohmic contact was also made using Ti/Au (50/250 nm) metallization. Both the n-type and p-type ohmic contacts were unannealed. The subcollector layer was etched for isolating the devices. Large emitter area (50 × 50 μm^2) devices were fabricated for DC characterization. Figure 8.3 a), and b) show the schematic of the cross section of InP/InGaAs SHBT and DHBT, respectively.

ATTENTION: The Singapore Copyright Act applies to the use of this document. Nanyang Technological University Library

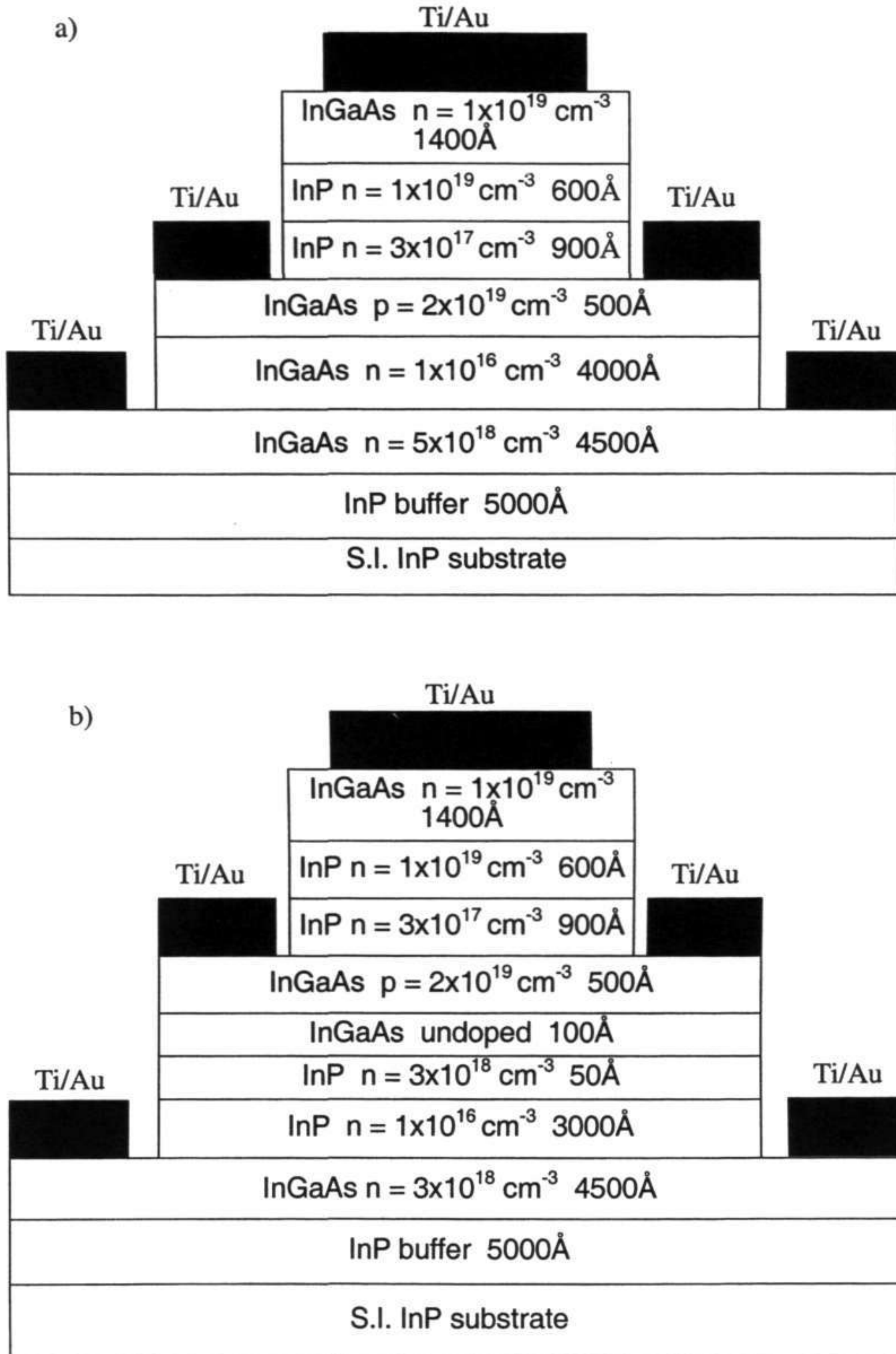

Fig.8.3 Schematic cross section of InP/InGaAs: a) SHBT; b) composite collector DHBT.

ATTENTION: The Singapore Copyright Act applies to the use of this document. Nanyang Technological University Library

8.4 Study of DC characteristics of C-doped InP/InGaAs SHBTs and DHBTs

8.4.1 Energy bandgap analysis of InP/InGaAs composite collector DHBTs

The InP/InGaAs DHBTs with undoped InGaAs layer and n^+-InP layer as composite collector are analyzed from the point of view of energy bandgap. Figure 8.4 a) illustrates the conduction band diagram of the InP/InGaAs DHBT without composite collector. In Fig.8.4 b), an undoped InGaAs layer is inserted between the InGaAs base and InP collector. The intention of the undoped InGaAs layer is to move the potential barrier into the reverse biased collector, where the top of the barrier lies below the corresponding level in Fig.8.4 a) and spatially separated from the base-collector interface. This avoids reflected electrons being trapped in the base. In Fig.8.4 c), an additional n^+-InP layer is inserted. The n^+-InP layer forms an energy spike on the InP side of the base-collector heterojunction. The energy spike does not lower the potential barrier, but because of increased band bending, it effectively narrows the barrier width; thus increasing the tunneling probability of electrons into the collector. This avoids electrons being accumulated in the quantum well formed between the InGaAs and InP collectors even under high current density operation. Without the n^+-InP layer, the I-V characteristics of the composite collector HBTs would suffer from bistable operation.

8.4.2 DC characteristics of C-doped InP/InGaAs SHBTs and DHBTs

The DC characterization of the C-doped InP/InGaAs SHBTs and DHBTs was carried out using a semiconductor parameter analyzer. The temperature dependence of device DC characteristics was measured using a semiconductor parameter analyzer connected to a probe station with a temperature-controlled chuck.

ATTENTION: The Singapore Copyright Act applies to the use of this document. Nanyang Technological University Library

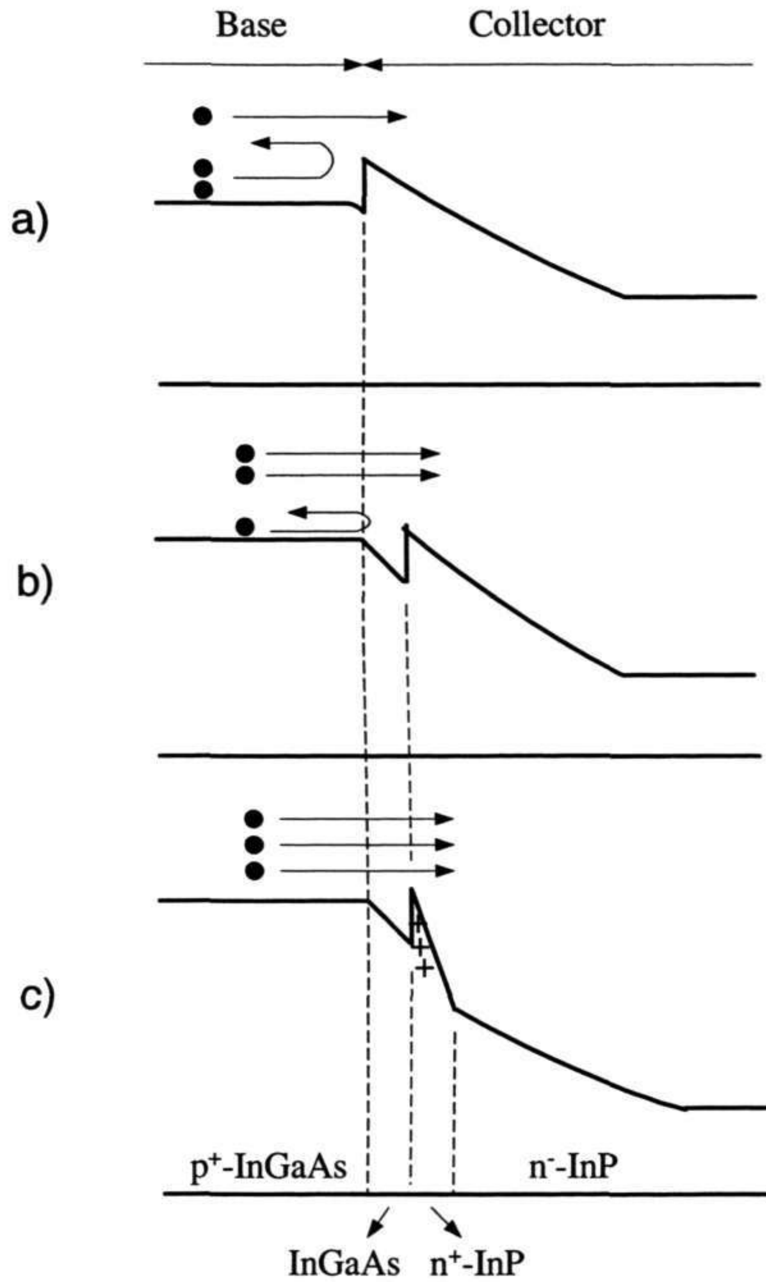

Fig.8.4 Schematic diagram of conduction band at base-collector junction of the InGaAs/InP DHBT: a) without composite collector; b) with undoped InGaAs layer; c) with an additional n^+-InP layer.

ATTENTION: The Singapore Copyright Act applies to the use of this document. Nanyang Technological University Library

Figure 8.5 shows the Gummel plots of the InP/InGaAs SHBT and DHBT. The ideality factors of the base and collector currents for the SHBT were 1.35 and 1.1, respectively. In the DHBT, the ideality factors of the base and collector currents were 1.35 and 1.25, respectively. The values indicate good junction qualities for both types of devices. Figure 8.6 a) and b) shows the common-emitter I-V characteristics of the InP/InGaAs SHBT and composite collector DHBT, respectively. No obvious knee-shape characteristics were observed in the DHBT characteristic, suggesting that the current blocking effect was reduced. The composite collector DHBT exhibits lower output conductance, and higher breakdown voltage of 10 V, compared to 6 V in the InP/InGaAs SHBT. The soft breakdown behavior of InP-based SHBTs is attributed to the weak field dependence of the electron impact ionization coefficient in InGaAs at medium to low electric field [117].

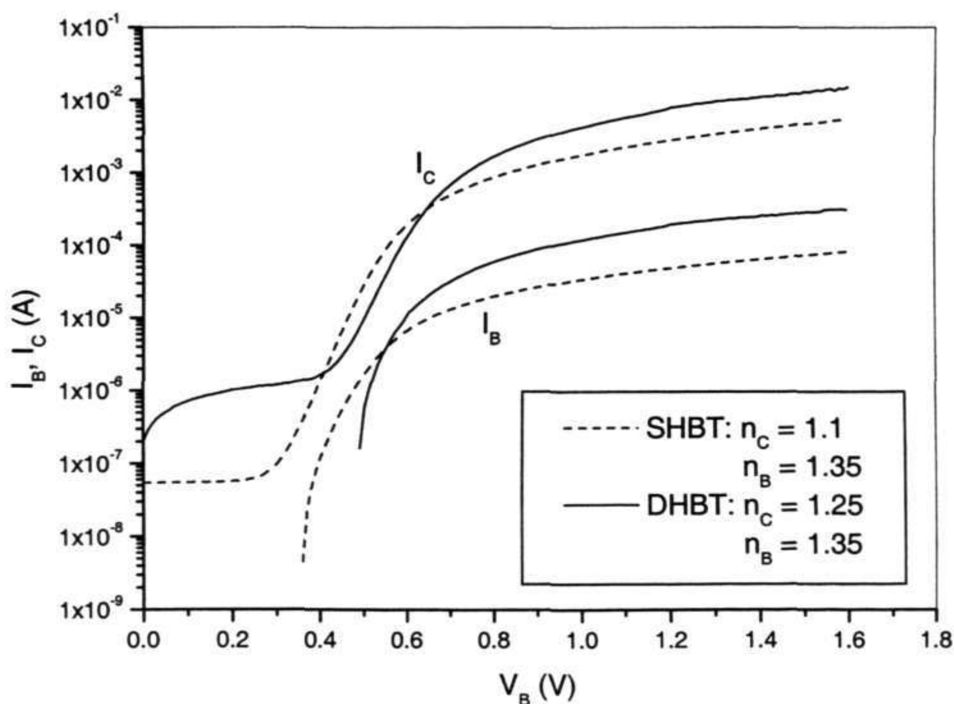

Fig.8.5 Gummel plots of InP/InGaAs SHBT and composite collector DHBT.

ATTENTION: The Singapore Copyright Act applies to the use of this document. Nanyang Technological University Library

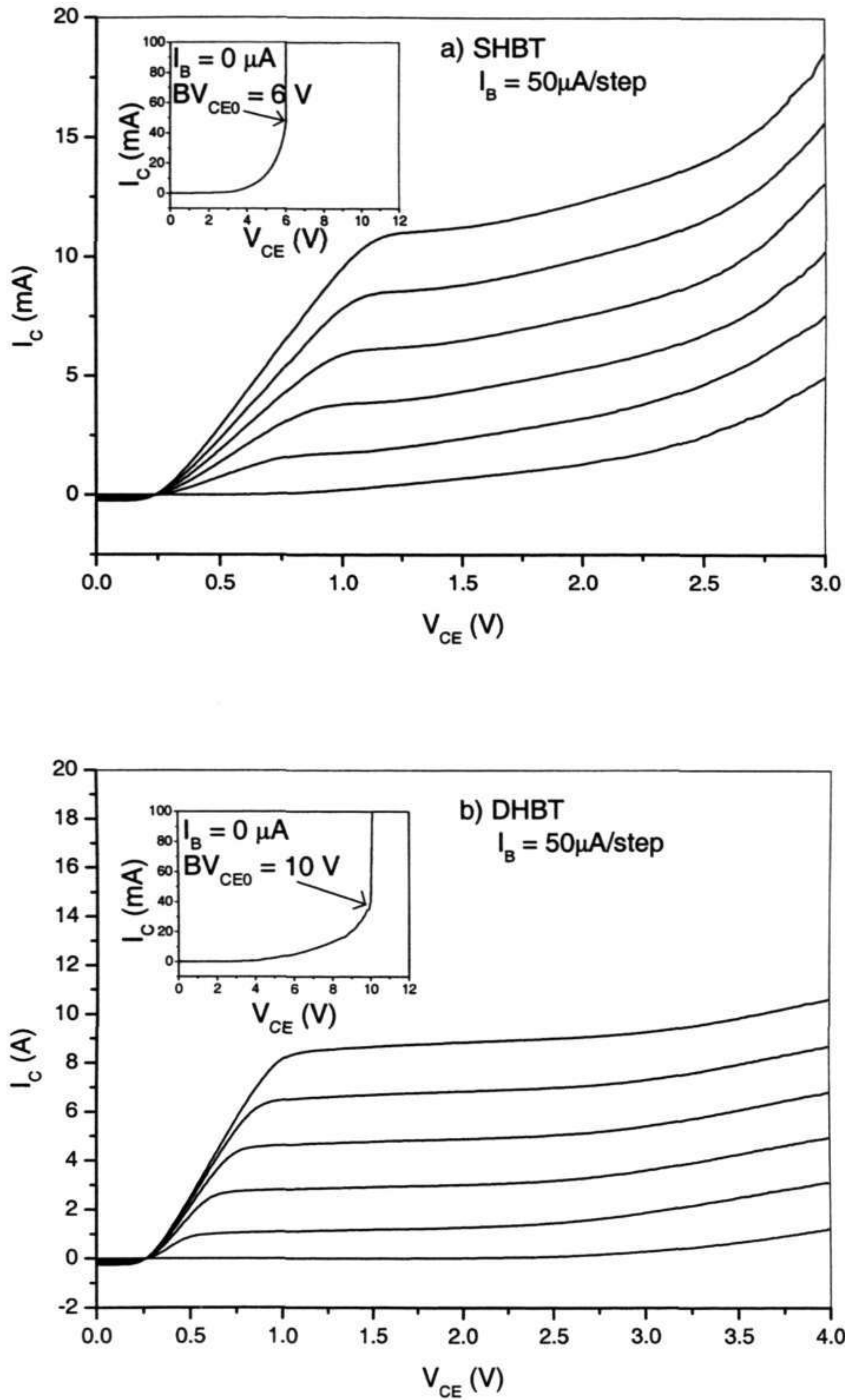

Fig.8.6 Common-emitter I-V characteristics of: a) InP/InGaAs SHBT; b) InP/InGaAs composite collector DHBT.

ATTENTION: The Singapore Copyright Act applies to the use of this document. Nanyang Technological University Library

The common-base I-V characteristics of the composite collector DHBT were measured to further elucidate the effect of the composite collector on the potential spike in the B-C junction. Figure 8.7 reveals no evidence of obvious current blocking or switching effects, which are usually observed in conventional DHBTs. This suggests that the composite collector design effectively suppresses the blocking of electrons by the potential barrier at the base-collector junction.

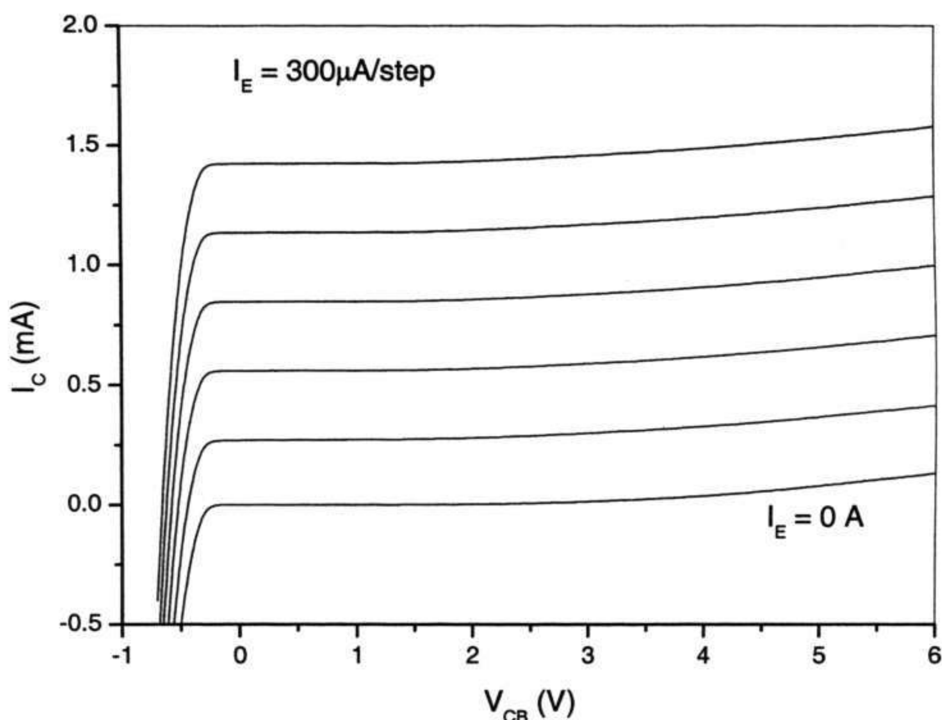

Fig.8.7 Common-base I-V characteristics of InP/InGaAs composite collector DHBT.

Figure 8.8 shows the common-emitter current gain (β) *vs.* collector current (I_C) for the InP/InGaAs SHBT and composite collector DHBT. At I_C of 3×10^{-3} A, β was 45 for the SHBT. For the DHBT, β was 40 at $I_C = 3\times10^{-2}$ A. Although the maximum current gain of the SHBT and DHBT is nearly the same, the current gain at the same

ATTENTION: The Singapore Copyright Act applies to the use of this document. Nanyang Technological University Library

collector current for the DHBT is lower than that of the SHBT. This suggests that the layer thickness of the undoped InGaAs and n^+-InP layer may not be of optimal values. Therefore, further optimization of both the undoped InGaAs and n^+-InP layer thickness in the composite collector structure is necessary to obtain the optimum current gain without compromising the breakdown voltage.

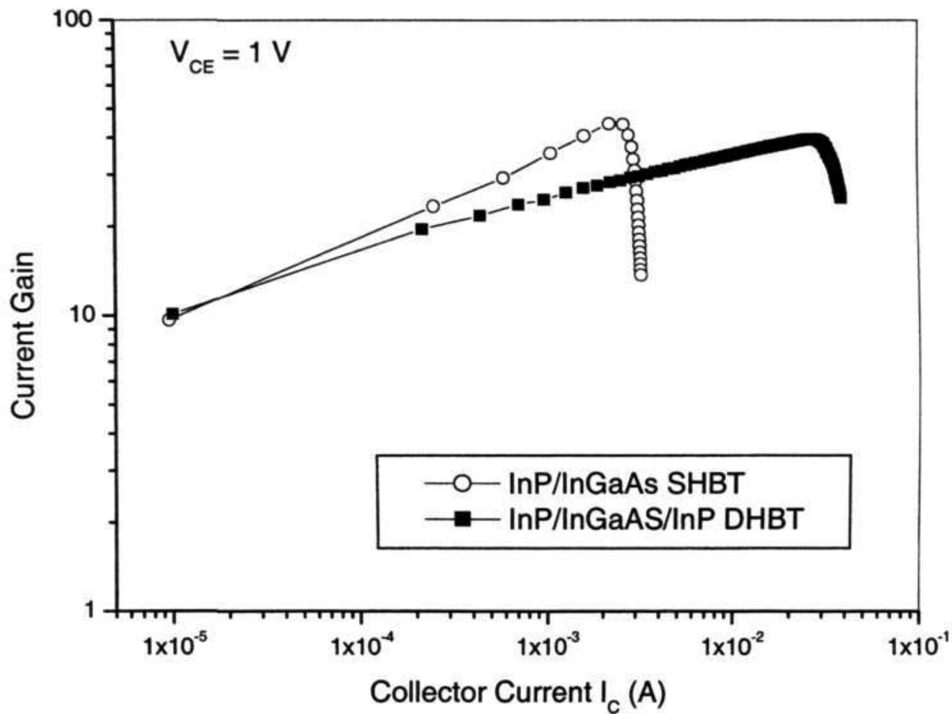

Fig.8.8 Common-emitter current gain *vs.* collector current characteristics of InP/InGaAs SHBT and composite collector DHBT.

ATTENTION: The Singapore Copyright Act applies to the use of this document. Nanyang Technological University Library

8.4.3 Temperature-dependence of breakdown characteristics of InP/InGaAs composite collector DHBT

While the electron impact ionization coefficient in InGaAs has positive temperature dependence [118], the temperature dependence of impact ionization coefficient in InP is negative [119]. In the InGaAs/InP composite collector structure, the dominance of the electron multiplication behavior, and its temperature dependence could depend significantly on the collector design [120]. To investigate the breakdown mechanism in our composite collector DHBTs, the temperature-dependent base-collector currents were measured. Figure 8.9 a) plots the base-collector currents *vs.* bias voltage at various temperatures for the DHBT. The apparent temperature-dependent breakdown behavior in the composite collector structure is affected by the competing temperature dependence mechanism of electron impact ionization coefficients in InGaAs and InP. At low reverse bias (region I), the collector reverse leakage current (I_{C0}) increases with temperature. This is due to the fact that I_{C0} is dominated by thermal generation and impact ionization mechanisms in the InGaAs layer [118]. At high reverse bias (region II), the negative temperature dependence of electron impact ionization coefficient in InP causes a reduction in I_{C0} with increase in temperature ($T \leq 340$ K). However, as the temperature is increased further, the influence of the InGaAs layer in the collector becomes more pronounced, resulting in increase of I_{C0}. The base-collector current *vs.* bias voltage characteristic at different temperature for the SHBT is shown in Fig.8.9 b) for comparison. Unlike that of the DHBT, the reverse leakage current of the base-collector junction for the InP/InGaAs SHBT increases monotonously with temperature at all bias voltages.

ATTENTION: The Singapore Copyright Act applies to the use of this document. Nanyang Technological University Library

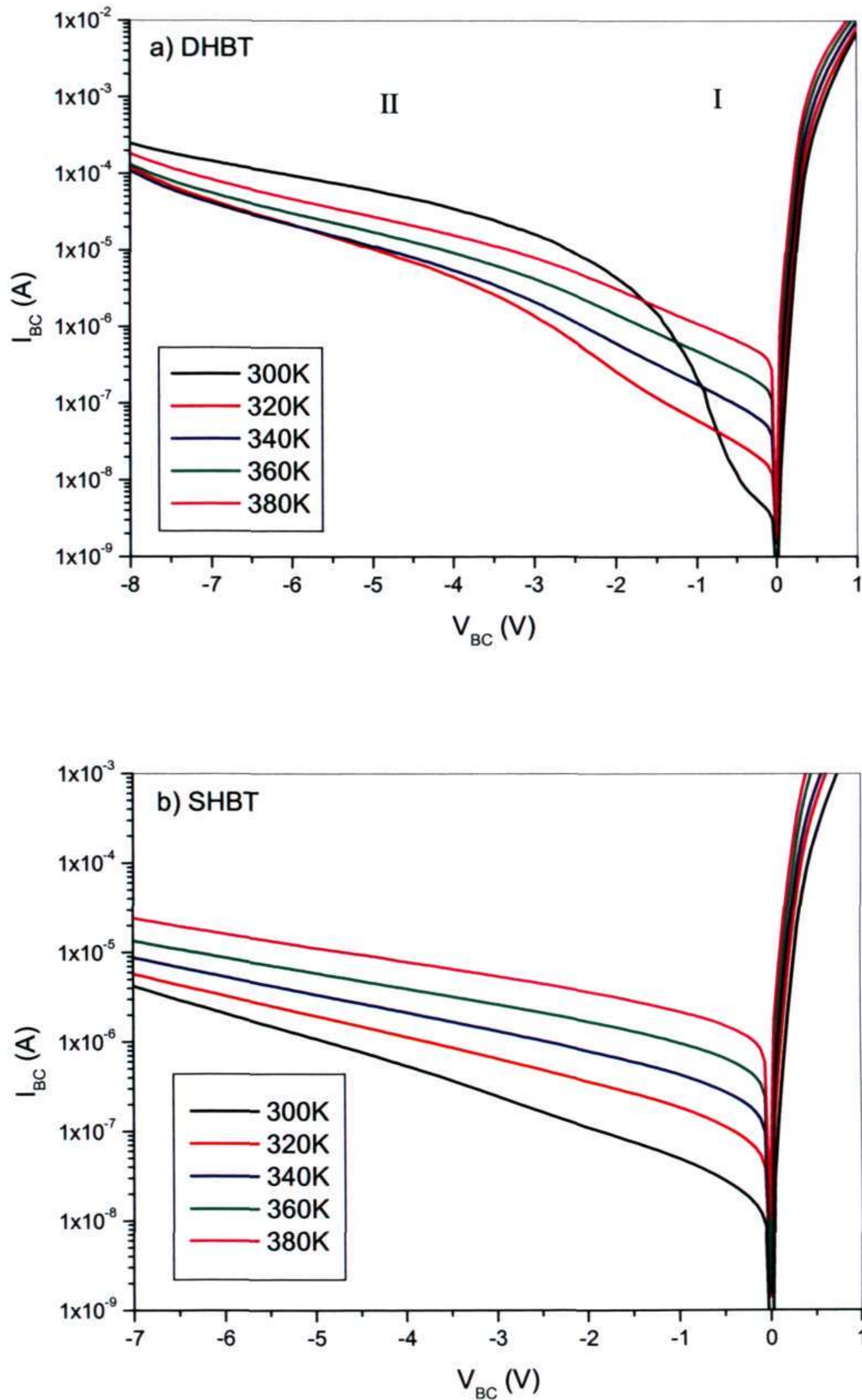

Fig.8.9 Base-collector junction I-V characteristics at different temperatures: a) InP/InGaAs composite collector DHBT; b) InP/InGaAs SHBT.

ATTENTION: The Singapore Copyright Act applies to the use of this document. Nanyang Technological University Library

8.5 Summary

C-doped InP/InGaAs SHBTs and composite collector DHBTs have been grown by SSMBE using CBr_4 as p-type dopant precursor. The hole mobilities in C-doped $In_{0.53}Ga_{0.47}As$ layers grown by our SSMBE system are comparable to those grown by GSMBE, MOCVD and other groups with SSMBE data. The near unity ideality factors of the base and collector currents of both SHBT and DHBT indicate good junction qualities for both device types. The InP/InGaAs composite collector DHBT exhibits lower output conductance and higher breakdown voltage of 10 V, compared to 6 V in the SHBT. The common base characteristics show the current blocking effect was reduced due to the composite collector design. The maximum current gain of the InP/InGaAs composite collector DHBT (current gain: 40) is comparable to that of the SHBT (current gain: 45). The temperature-dependent breakdown characteristic of the base-collector junction demonstrates the complex breakdown mechanisms in the composite collector DHBT.

ATTENTION: The Singapore Copyright Act applies to the use of this document. Nanyang Technological University Library

Chapter 9

Conclusions and future work

9.1 Conclusions

The results described in this work demonstrate the comprehensive characterization of C-doped GaAs and $In_{0.53}Ga_{0.47}As$ materials and C-doped GaAs-based and InP-based HBT devices grown by SSMBE system using CBr_4 as p-type dopant precursor. The characteristics of C-doped GaAs materials, such as the hole concentration, mobility, lattice mismatch, surface morphology, and optical properties, have been comprehensively investigated using various techniques, which help to gain the insight and understanding of the material properties. Especially, the compensation effects of dicarbon defects have been studied. The optimization of the growth conditions has been carried out and discussed, which benefits the development of C-doped GaAs as base layer of GaInP/GaAs HBT devices. Preliminary results of C-doped GaInP/GaAs HBT devices demonstrated poor characteristics due to trap-related recombination. With better control of growth process, improved performances of GaInP/GaAs HBTs have been obtained. Elevated temperature properties revealed good material quality of these devices. C-doped InP/InGaAs SHBTs and composite collector DHBTs have been grown and studied, and the promising device performance demonstrate the potential for commercial wireless communication applications. The complex breakdown characteristics of composite collector DHBTs have been investigated. The conclusion can be summarized as the following:

1) C-doped GaAs materials have been successfully grown by SSMBE using CBr_4 as p-type dopant precursor, and the materials have been comprehensively

ATTENTION: The Singapore Copyright Act applies to the use of this document. Nanyang Technological University Library

characterized. Sustainable and stable CBr_4 flux with variation lower than 2.5% has been obtained. The memory effect has been investigated. For the doping level commonly used for HBTs (~ 5×10^{19} cm^{-3}), the memory effect is negligible. Hole concentration increases following increase in CBr_4 flux and reaches a maximum of 1.86×10^{20} cm^{-3} at CBr_4 flux of 2.6×10^{-7} torr, beyond which, it decreases rather significantly. The SIMS results show that the carbon atoms incorporated into GaAs are nearly fully activated at CBr_4 flux level below 2.6×10^{-7} torr. At room temperature, the C-doped samples showed mobility of 101 to 45 cm^2/Vs at hole concentration of 1.02×10^{19} cm^{-3} to 1.86×10^{20} cm^{-3}, respectively, comparable to samples doped with Be. Low temperature (4K) PL measurements show a reduction in bandgap and broadening of the PL spectrum following increase in the doping concentration. The main PL peak shifts from ~ 1.480 eV at concentration of 1.02×10^{19} cm^{-3} to ~ 1.452 eV at 6.95×10^{19} cm^{-3}. Variable temperature PL measurements show the existence of two peaks, which could arise from conduction band (CB) to heavy hole (HH) valence band and CB to light hole (LH) valence band transitions. Reasonably good C pulsed doping profile has been achieved and verified by SIMS measurement on samples grown without the use of growth interruption.

2) When the CBr_4 flux exceeds 2.6×10^{-7} torr, further increase in the C atomic concentration causes the formation and rapid increase in dicarbon defects. The compensating effects of the dicarbon defects induce the decrease in hole concentration, drop in mobility, and increase in lattice parameter. Unlike the samples grown at CBr_4 flux below 2.6×10^{-7} torr, the lattice mismatch data of the compensated samples, which were grown at high CBr_4 flux exceeding 2.6×10^{-7} torr, deviate from Vegard's Law. The structure of the dicarbon defects formed at high CBr_4 flux needs further investigation. The AFM images of surface morphology show signs of growth

ATTENTION: The Singapore Copyright Act applies to the use of this document. Nanyang Technological University Library

mode transformation from 2D to 3D island formation following increase in CBr_4 flux. The results suggest a possible relationship between increase in surface roughness and formation of dicarbon defects in C-doped GaAs.

3) The effect of substrate temperature, growth rate, and V/III ratio on C-doped GaAs grown by SSMBE was investigated. High substrate temperature can also induce the formation of dicarbon defects in C-doped GaAs, which results in reduction in hole concentration. The surface roughness shows signs of increase at substrate temperature above 590 °C, which indicate possible relationship between the high surface roughness and the dicarbon defects. The presence of the same hole concentration in samples grown at 1:2 growth rate ratio suggests that only half of the carbon atoms reaching the growth surface are incorporated. At low V/III ratio of 10, the surface of C-doped GaAs becomes significantly rougher; the ideality factor of PN junctions became higher at V/III ratio above 25 or below 18. Within the range of experimental conditions in our MBE system, substrate temperature between 560 °C - 590 °C, growth rate of 1 μm/h or 0.5 μm/h and V/III ratio between 18 and 25 are suitable parameters for C-doped GaAs growth for HBT applications.

4) C-doped GaInP/GaAs HBTs have been grown and fabricated successfully. Preliminary devices with base layer thickness of 520 Å showed DC current gain of 30 at collector current density of 3200 A/cm^2. The hole mobility obtained from the base layer sheet resistance is consistent with that of C-doped GaAs bulk layer. The temperature dependence of DC current gain *vs.* collector current showed a slight decrease in current gain at high collector current, and increase in current gain at low collector current. The Gummel plot from 300 K to 380 K suggests that trap-related recombination played a significant role in the poor device DC characteristics. The reverse leakage current of the base-collector junction suggests that the dominant

ATTENTION: The Singapore Copyright Act applies to the use of this document. Nanyang Technological University Library

mechanism could be related to the SRH generation-recombination process. On the other hand, the reverse leakage current of the base-emitter junction could be dominated by carrier tunneling effects.

With better control of the growth process, improved characteristics of GaInP/GaAs HBTs with base doping concentration of 4×10^{19} cm^{-3} have been obtained. The base current and collector current ideality factors at 300 K were 1.12 and 1.01, respectively, which indicates that space charge region recombination current is insignificant in the base current. From the temperature dependent Gummel plot, the activation energies of collector current and base current were obtained. For the collector current, the activation energy is 1.4 eV, which is close to the bandgap of the GaAs base, indicates that the collector current is determined by drift-diffusion process. For the base current, the activation energy is also 1.4 eV, indicating that band-to-band recombination plays a dominant role in determining the base current. No trap-related recombination is observed for the base and collector currents, which further indicates the good base material quality for the HBT structures. Properties of current gain versus collector current at different temperatures were also investigated. At low I_C level of below 1×10^{-2} A, a slight increase in β with the increase of temperature can be seen in the plot. However, at high I_C level of above 1×10^{-2} A, a slight degradation of β is observed. The physical mechanisms involved were analyzed in detail. High-performance C-doped GaInP/GaAs HBTs with base doping concentration of 2×10^{19} cm^{-3} grown by SSMBE using CBr_4 as p-type precursor have also been obtained. Maximum current gain of 138 as well as base current and collector current ideality factors of 1.30 and 1.01, respectively, was achieved. The above results indicate the capability and stability of the C-doping epitaxial growth technique in our group.

ATTENTION: The Singapore Copyright Act applies to the use of this document. Nanyang Technological University Library

5) C-doped InP/InGaAs SHBTs and composite collector DHBTs have been grown by SSMBE using CBr_4 as p-type dopant precursor. The hole mobilities in C-doped $In_{0.53}Ga_{0.47}As$ layers grown by our SSMBE system are comparable to those grown by GSMBE, MOCVD and other groups with SSMBE data. The near unity ideality factors of the base and collector currents of both SHBT and DHBT indicate good junction qualities for both device types. The InP/InGaAs composite collector DHBT exhibits lower output conductance and higher breakdown voltage of 10 V, compared to 6 V in the SHBT. The common base characteristics show the current blocking effect was reduced due to the composite collector design. The maximum current gain of the InP/InGaAs composite collector DHBT (current gain: 40) is comparable to that of the SHBT (current gain: 45). The temperature-dependent breakdown characteristic of the base-collector junction demonstrates the complex breakdown mechanisms in the composite collector DHBT.

9.2 Recommendations for future work

InP/InGaAs composite collector DHBTs

The InP/InGaAs DHBTs with 100 Å undoped InGaAs layer and 50 Å n^+-InP layer as composite collector have shown promising results. However, the structure of the composite collector layers, i.e., the thickness and doping level of the InGaAs layer and the n-InP layer, still needs to be optimized to improve the device DC performance. Simulation work needs to be carried out for the optimization. Further improvement of the DC I-V characteristics without sacrificing the breakdown performance is expected for practical circuit applications after the optimization.

ATTENTION: The Singapore Copyright Act applies to the use of this document. Nanyang Technological University Library

RF characteristics of GaInP/GaAs HBTs and InP/InGaAs HBTs

With the intention of testifying the feasibility of the C-doped epitaxial material using CBr_4 as p-type dopant precursor, and also due to the time limit, all the device results in this thesis were based on the DC characteristics, which were obtained on the large area devices. RF characteristics are also important to evaluate the merit of the HBT devices, which provide important information about both the epitaxial material quality and the device speed performance. Therefore, narrow emitter (down to 1μm) devices are needed to study the RF characteristics so as to give an overall view of the C-doped GaInP/GaAs HBTs and InP/InGaAs HBTs grown by SSMBE.

Reliability characteristics of C-doped GaInP/GaAs HBTs and InP/InGaAs HBTs grown by SSMBE

The work presented in this thesis is motivated mainly by the reliability of the HBTs. It is well known that C-doped HBTs are superior to Be- or Zn-doped HBTs in terms of reliability. However, up to date, the reliability studies of C-doped HBTs are conducted mainly on MOCVD grown HBTs, which may suffer from hydrogen effect. There are few reports on SSMBE grown C-doped HBT reliability issues, such as long term current and temperature stress properties, passivation and degradation properties, as well as mean-time-to-failure (MTTF) measurements. The reliability issue of both the DC and RF (including noise) characteristics of the C-doped GaAs-based and InP-based HBTs grown by SSMBE need further investigation.

ATTENTION: The Singapore Copyright Act applies to the use of this document. Nanyang Technological University Library

Author's publications

Journal papers:

[1] R.Zhang, S.F.Yoon, K.H.Tan, Z.Z.Sun and Q.F.Huang, "Some Properties of Carbon-Doped GaAs Using Carbon Tetrabromide in Solid-Source Molecular Beam Epitaxy", **Journal of Crystal Growth**, vol.243, pp.41-46, 2002.

[2] R.Zhang, S.F.Yoon, K.H.Tan, Z.Z.Sun and Q.F.Huang, J.Jiang, and L.H.Lee, "GaInP/GaAs Heterojunction Bipolar Transistor with Carbon-doped Base Layer Grown by Solid Source Molecular Beam Epitaxy Using Carbon Tetrabromide", **Solid-State Electronics**, vol.47, pp.1339-1343, 2003.

[3] R.Zhang, S.F.Yoon, K.H.Tan, Z.Z.Sun and Q.F.Huang, "Effects of Carbon Tetrabromide Flux, Substrate Temperature and Growth Rate on Carbon-Doped GaAs Grown by Molecular Beam Epitaxy", **Journal of Crystal Growth**, vol.262, pp.113-118, 2004.

[4] R.Zhang, K.L.Lew, S.F.Yoon, K.H.Tan, and Z.Z.Sun, "Study of Direct Current Characteristics of Carbon-Doped GaInP/GaAs Heterojunction Bipolar Transistor Grown by Solid Source Molecular Beam Epitaxy", **Journal of Vacuum Science and Technology B**, vol.22, pp.838-842, 2004.

[5] R.Zhang, S.F.Yoon, K.H.Tan, K.L.Lew, and Z.Z.Sun, "Carbon-doped InP/$In_{0.53}Ga_{0.47}As$ single and double heterojunction bipolar transistors grown by solid-source molecular beam epitaxy", **Journal of Vacuum Science and Technology B**, vol.22, pp.2499-2503, 2004.

[6] K.L.Lew, R.Zhang and S.F.Yoon, "InGaP/GaAs/InGaP Composite Collector DHBT with High Breakdown, Low Offset, and Knee Voltage", **Journal of Vacuum Science and Technology B**, vol.22, pp.579-582, 2004.

ATTENTION: The Singapore Copyright Act applies to the use of this document. Nanyang Technological University Library

[7] K.H.Tan, S.F.Yoon, Q.F.Huang, R.Zhang, and Z.Z.Sun, "Dicarbon defects in carbon-doped GaAs", **Physical Review B**, vol.67, 035208 (1-5), 2003.

[8] Q.F.Huang, S.F.Yoon, K.H.Tan, Z.Z.Sun, R.Zhang, J.Jiang, and L.H.Lee, "Carbon doping in GaAs using carbon tetrabromide in solid source molecular beam epitaxy", **Journal of Crystal Growth**, vol.252, pp.37-43, 2003.

[9] K.H.Tan, S.F.Yoon, R.Zhang, Q.F.Huang, and Z.Z.Sun, "Surface morphology of heavily carbon-doped GaAs grown by solid-source molecular beam epitaxy", **Journal of Crystal Growth**, vol.263, pp.105-113, 2004.

[10] Z.Z.Sun, S.F.Yoon, K.H.Tan, R.Zhang, and J.Jiang, "Incorporation efficiency of carbon in GaAs using carbon tetrabromide in solid source molecular beam epitaxy", **Journal of Vacuum Science and Technology B**, vol.22, pp.1017-1021, 2004.

Conference paper:

[1] R.Zhang, S.F.Yoon, K.H.Tan, Z.Z.Sun and Q.F.Huang, "Elevated Temperature Characteristics of Carbon-Doped GaInP/GaAs Heterojunction Bipolar Transistor Grown By Solid Source Molecular Beam Epitaxy", Material Research Society Meetings, Boston, Fall, 2003.

ATTENTION: The Singapore Copyright Act applies to the use of this document. Nanyang Technological University Library

Bibliography

[1] W. Shockley, "The p-n junctions in semiconductors and p-n junction transistors", U.S. Patent 2,569,347, 1948.

[2] H. Kroemer, Proc. IRE, "Theory of wide-gap emitter for transistors", Vol.45, pp.1535-1537, 1957.

[3] D.L. Miller, and P.M. Asbeck, "Be redistribution during growth of GaAs and AlGaAs by molecular beam epitaxy", J. Appl. Phys., Vol.57, pp.1816-1822, 1985.

[4] F. Ren, T.R. Fullowan, J. Lothian, P.W. Wisk, C.R. Abernathy, R.F. Kopf, A.B. Emerson, S.W.Downey and S.J.Pearton, "Stability of carbon and beryllium-doped base GaAs/AlGaAs heterojunction bipolar transistors", Appl. Phys. Lett., Vol.59, pp.3613-3615, 1991.

[5] M.E. Hafizi, L.M. Pawlowicz, L.T. Tran, D.K. Umemoto, D.C. Streit, A.K. Oki, M.E. Kim, and K.H.Yen, "Reliability analysis of GaAs/AlGaAs HBTs under forward current/temperature stress", Technical Digest of GaAs IC Symposium, pp.329-332, 1990.

[6] Y.C. Pao, T. Hierl, and T. Cooper, "Surface effect-induced fast Be diffusion in heavily doped GaAS grown by molecular-beam epitaxy", J. Appl. Phys., Vol.60, pp.201-204, 1986.

[7] K. Saito, E. Tokumitsu, M. Miyauchi, and K. Takahashi, "Characterization of *p*-type GaAs heavily doped with carbon grown by metalorganic molecular-beam epitaxy", J. Appl. Phys., Vol.64, pp.3975-3979, 1988.

[8] C. Abernathy, S. Pearton, R. Caruso, F. Ren, and J. Kovalchik, "Ultrahigh doping of GaAs by carbon during metalorganic molecular beam epitaxy", Appl. Phys. Lett., Vol.55, pp.1750-1752, 1989.

ATTENTION: The Singapore Copyright Act applies to the use of this document. Nanyang Technological University Library

[9] H. Wang, G.I. Ng, H.Q. Zheng, and P.H. Zhang, "A comprehensive study of AlGaAs/GaAs beryllium- and carbon-doped base heretojunction bipolar transistor structures subjected to rapid thermal processing", J. Appl. Phys., Vol.86, pp.6468-6473, 1999.

[10] F. Alexandre, J.L. Benchimol, P. Launay, J. Dangla and C.Dunbon-Chevallier, "Modern epitaxial techniques for HBT structures", Solid-State Electronics, Vol.38, pp.1667-1674, 1995.

[11] A. Mircea, F. Alexandre, J.Decobert, L. Goldstein, J.C. Harmand, and A. Ougazzaden, "Review and prospects for VPE, MOVPE, MBE and CBE (MOMBE) of InP and related materials", Intern.Conf. on Indium Phosphide and Related Materials, pp.49-52, 1998.

[12] M.R.Leys, "Fundamental growth kinetics in MOMBE/CBE, MBE and MOVPE", J. Crys. Growth, Vol.209, pp.225-231, 2000.

[13] M. Henini, "Molecular beam epitaxy: from research to manufacturing", Thin Solid Films, Vol.306, pp.331-337, 1997.

[14] M.A. Herman and H. Sitter, *Molecular beam epitaxy*, Springer-Verlag Berlin Heidelberg New York, 1989.

[15] K. Zhang, W. Hwang, and D.L. Miller, "Carbon doping of GaAs and (In,Ga)As in solid source molecular beam epitaxy using carbon tetrabromide", Appl. Phys. Lett., vol.63, pp.2399-2401, 1993.

[16] W. Hwang, M. Micovic, D.L. Miller, and M. Geva, "Carbon tetrabromide doping memory effect, incorporation efficiency, and InAlAs/InGaAs heterojunction bipolar transistor application", J. Vac. Sci. Technol. B, vol.14, pp.2301-2304, 1996.

ATTENTION: The Singapore Copyright Act applies to the use of this document. Nanyang Technological University Library

[17] D.I. Lubyshev, M. Micovic, W.Z. Cai, and D.L. Miller, "Molar fraction and substrate orientation effects on carbon doping in InGaAs grown by solid source molecular beam epitaxy using carbon tetrabromide", J. Appl. Phys., vol.84, pp.4281-4284, 1998.

[18] D.L. Miller, M. Micovic, D.I. Lubyshev, W. Cai, W. Hwang, and K. Zhang, "Iodine and carbon tetrabriomide use in the solid source molecular beam epitaxy", J. Vac. Sci. Technol. B, vol.16, pp.1361-1366, 1998.

[19] W.K. Liu, D.I. Lubyshev, P. Specht, R. Zhao, E.R. Weber, J. Gebauer, A.J. SpringThorpe, R.W. Streater, S. Vijarnwannaluk, W. Songprakob, and R. Zallen, "Properties of carbon-doped low-temperature GaAs and InP grown by solid-source molecular-beam epitaxy using CBr_4", J. Vac. Sci. Technol. B, vol.18, pp.1594-1597, 2000.

[20] M. Micovic, C. Nordquist, D. Lubyshev, T.S. Mayer, D.L. Miller, R.W. Streater, and A.J. SpringThorpe, "GaAs/AlGaAs heterojunction bipolar transistors with a base doping 10^{20} cm^{-3} grown by solid-source molecular beam epitaxy using CBr_4", J. Vac. Sci. Technol. B, vol.16, pp.972-976, 1998.

[21] W. Hwang, and D.L. Miller, "Carbon-doped InAlAs/InGaAs heterojunction bipolar transistors in solid-source molecular-beam epitaxy using carbon tetrabromide", J. Vac. Sci. Technol. B, vol.13, pp.667-669, 1995.

[22] H. Kroemer, "Heterostructure bipolar transistors and integrated circuits", Proc. IEEE, Vol.70, pp.13-25, 1982.

[23] W. Liu, *Fundamentals of III-V Devices*, John Wiley & Sons, 1999.

[24] M. Feng, N. Holonyak, Jr., and W. Hafez, "Light-emitting transistor: light emission from InGaP/GaAs heterojunction bipolar transistors", Appl. Phys. Lett., Vol.84, pp.151 -153, 2004.

ATTENTION: The Singapore Copyright Act applies to the use of this document. Nanyang Technological University Library

[25] H. Ito, O. Nakajima, and T. Ishibashi, "Carbon doping for AlGaAs/GaAs heterojunction bipolar transistors by molecular-beam epitaxy", Appl. Phys. Lett., Vol.62, pp.2099-2101, 1993.

[26] C. Giannini, A. Fischer, C. Lange, K. Ploog, L. Tapfer, "Heavy carbon doping of GaAs grown by solid-source molecular-beam epitaxy", Appl. Phys. Lett., Vol.61, pp. 183-185, 1992.

[27] T.J.de Lyon, N.I. Buchan, P.D. Kirchner, J.M. Woodall, G.J. Scilla, and F. Cardone, "High carbon doping efficiency of bromomethanes in gas source molecular beam epitaxial growth of GaAs", Appl. Phys. Lett., Vol.58, pp.517-519, 1991.

[28] C.W. Tu, B.W. Liang, and T.P. Chin, "Heavily carbon-doped p-type GaAs and $In_{0.53}Ga_{0.47}As$ grown by gas-source molecular beam epitaxy using carbon tetrabromide", J. Crys. Growth, Vol.136, pp.191-194, 1994.

[29] K. Ouchi, T. Mishima, K. Mochizuki, T. Oka, and T. Tanoue, "Fully Strained Heavily Carbon-Doped GaAs Grown by Gas-Source Molecular Beam Epitaxy Using Carbontetrabromide and Its Application to InGaP/GaAs Heterojunction Bipolar Transistors", Jpn. J. Appl. Phys., Vol.36, pp.1866-1868, 1997.

[30] M. Seon and M. Holtz, W. M. Duncan and T. S. Kim, "Raman studies of heavily carbon doped GaAs", J. Appl. Phys., Vol.85, pp.7224-7230, 1999.

[31] S. Cho, and E.K. Kim, "Effects of substrate orientation, temperature, and hole concentration on the bandgap energy of carbon-doped GaAs", J. Crys. Growth, Vol.226, pp.240-246, 2001.

[32] C. C. Hsu, Y. F. Yang, H. J. Ou, and E. S. Yang, H. B. Lo, "Carbon-doped GaInP/GaAs heterojunction bipolar transistors grown by metalorganic chemical

ATTENTION: The Singapore Copyright Act applies to the use of this document. Nanyang Technological University Library

vapor deposition using nitrogen as the carrier gas", Appl. Phys. Lett., Vol.71, pp.3248-3250, 1997.

[33] P. Kurpas, E. Richter, M. Sato, F. Brunner, D. Gutsche and M.Weyers, "MOVPE growth of GalnP/GaAs hetero-bipolar-transistors using CBr_4 as carbon dopant source", J. Crys. Growth, Vol.170, pp.442-446, 1997.

[34] Harly. F and Patai. S, *The Chemistry of the Metal-Carbon Bond*, New York: Wiley, pp.53-71, 1982.

[35] H. Ito, and T. Ishibashi, "Carbon incorporation in (AlGa)As, (AlIn)As and (GaIn)As ternary alloys grown by molecular beam epitxay", Jpn. J. Appl. Phys., Vol.30, pp.L944-947, 1991.

[36] D.I. Lubyshev, M. Micovic, W.Z. Cai, and D.L. Miller, "Molar fraction and substrate orientation effects on carbon doping in InGaAs grown by solid source molecular beam epitaxy using carbon tetrabromide", J. Appl. Phys., vol.84, pp.4281-4284, 1998.

[37] K.A. Jackson, *Compound Semiconductor Devices: structures and processing*, Wiley-VCH, pp.49, 1998.

[38] F. Alexandre, J.L. Benchimol, P. Launay, J. Dangla and C. Dunbon-Chevallier, "Modern epitaxial techniques for HBT structures", Solid-State Electronics, Vol.38, pp.1667-1674, 1995.

[39] V.Swaminathan and A.T.Macrander, *Materials Aspects of GaAs and InP Based Structure*, Prentice Hall Advanced Reference Series, New Jersey, 1991.

[40] F. Ali, and A. Gupta, *HEMTs and HBTs: Devices, Fabrication, and Circuits*, 1991.

[41] K.Y. Cheng, Proc. IEEE, Vol.85, pp.1694-1698, 1997.

ATTENTION: The Singapore Copyright Act applies to the use of this document. Nanyang Technological University Library

[42] A. Krost, G. Bauer and J. Woitok, "High resolution X-ray diffraction", in *Optical characterization of epitaxial semiconductor layers*, edited by G. Bauer and W. Richter, Springer-Verlag, 1996.

[43] M. A. G. Halliwell, M. H. Lyons, S. T. Davey, M. Hockly, C. G. Tuppen, C. J. Gibbings, "Estimation of percentage relaxation in Si/Si1-xGex strained-layer superlattices", Semicond. Sci. Technol., Vol.4, pp. 10-15, 1989.

[44] G.D. Gilliland, "Photoluminescence spectroscopy of crystalline semiconductors", Mater. Sci. Eng. R, Vol.18, pp.99-400, 1997.

[45] G. Binning, C. F. Quate and C. Gerber, "Atomic force microscope", Phys. Rev. Lett., Vol.56, pp.930-933, 1986.

[46] H. K. Wichramasinghe, "Scanning probe microscopy: current status and future trends", J. Vacuum Sci. Tech. A, Vol.8, pp. 363-368, 1990.

[47] K. Seeger, *Semiconductor physics: An introduction*, Springer-Verlag, 1997.

[48] A. Benninghoven, F. G. Rüdenauer, and H. W. Werner, *Secondary Ion Mass Spectrometry: Basic Concepts, Instrumental Aspects, Applications, and Trends*, New York: Wiley, 1987.

[49] J. Mimila-Arroyo, A. Lusson, J. Chevallier, M. Barbe, B. Theys, and F. Jomard, S.W. Bland, "Carbon acceptor doping efficiency in GaAs grown by metalorganic chemical vapor deposition", Appl. Phys. Lett., vol.79, pp.3095-3097, 2001.

[50] K.Saito, E.Tokumitsu, T.Akatsuka, M.Miyauchi, T.Yamada, M.Konagai, and K.Takahashi, "Chanracterization of p-type GaAs heavily doped with carbon grown by metalorganic molecular-beam epitaxy", J. Appl. Phys., vol.64, pp.3975-3979, 1988.

ATTENTION: The Singapore Copyright Act applies to the use of this document. Nanyang Technological University Library

[51] T. J. de Lyon, N. I. Buchan, P. D. Kirchner, J. M. Woodall, G. J. Scilla, and F. Cardone, "High carbon doping efficiency of bromomethanes in gas source molecular beam epitaxial growth of GaAs", Appl. Phys. Lett., vol.58, pp.517-519, 1991.

[52] M.C.Hanna, Z.H.Lu, and A.Majerfeld, "Very high carbon incorporation in metalorganic vapor phase epitaxy of heavily doped P-type GaAs", Appl. Phys. Lett., vol.58, pp.164-166, 1991.

[53] T.Usagawa, M.Kobayashi, T.Mishima, P.D.Rabinzohn, A.Ihara, M.Kawata, T. Yamada, E.Tokumitsu, M.Konagai, and K.Takahashi, "Extremely low non-alloyed specific contact resistance $\rho_c(10^{-8}\Omega cm^2)$ to metalorganic molecular beam epitaxy grown super heavily C-doped $(10^{21}cm^{-3})$ p++ GaAs", J. Appl. Phys., vol.69, pp.8227-8232, 1991.

[54] W. E. Hoke, P. J. Lemonias, D. G. Weir, H. T. Hendriks, and G. S. Jackson, "Carbon doping and lattice contraction of GaAs films grown by conventional molecular beam epitaxy", J. Appl. Phys., vol.69, pp.511-513, 1991.

[55] R.PeKa-Sierra, A.Escobosa, and V.M.Sanchez-R., "Carbon doping in GaAs layers grown with trimethylgallium and solid arsenic in a mixture of hydrogen and nitrogen", Appl. Phys. Lett., vol.62, pp.2359-2361, 1993.

[56] K.Zhang, W.Hwang, and D.L.Miller, "Carbon doping of GaAs and (In,Ga)As in solid source molecular beam epitaxy using carbon tetrabromide", Appl. Phys. Lett., vol.63, pp.2399-2401, 1993.

[57] T. B. Joyce, T. J. Bullough, and T. Farrell, "Optical monitoring of the growth of heavily doped GaAs by chemical beam epitaxy and of the in situ etching of GaAs using CBr_4", Appl. Phys. Lett., Vol.65, pp.2193-2195, 1994.

ATTENTION: The Singapore Copyright Act applies to the use of this document. Nanyang Technological University Library

[58] K. Ouchi, T. Mishima, K. Mochizuki, T. Oka, and T. Tanoue, "Fully Strained Heavily Carbon-Doped GaAs Grown by Gas-Source Molecular Beam Epitaxy Using Carbontetrabromide and Its Application to InGaP/GaAs Heterojunction Bipolar Transistors", Jpn. J. Appl. Phys., vol.36, pp.1866-1868, 1997.

[59] G.E. Hofler and K.C. Hsieh, "Observation of interstitial carbon in heavily carbon-doped GaAs", Appl. Phys. Lett., vol.61, pp.327-329, 1992.

[60] S.A. Stockman, G.E. Hofler, J.N. Baillargeon, K.C. Hsieh, K.Y. Cheng, and G.E. Stillman, "Characterization of heavily carbon-doped GaAs grown by metalorganic chemical vapor deposition and metalorganic molecular beam epitaxy", J. Appl. Phys., vol.72, pp.981-987, 1992.

[61] S.A. Stockman, A.W. Hanson, S.L. Jackson, J.E. Baker, and G.E. Stillman, "Effect of post-growth cooling ambient on acceptor passivation in carbon-doped GaAs grown by metalorganic chemical vapor deposition", Appl. Phys. Lett., vol.62, pp.1248-1250, 1993.

[62] T. B. Joyce, T. J. Bullough and S. Westwater, "In-situ monitoring of carbon doped GaAs and of periodic carbon doped GaAs/AlAs structures grown by chemical beam epitaxy", J. Cryst. Growth, vol.146, pp.394-398, 1995.

[63] B. Cheong, and K.J.Chang, "Compensation and diffusion mechanisms of carbon dopants in GaAs", Phys. Rev. B, vol.49, pp.17436-17439, 1994.

[64] J. Wagner, R.C. Newman, B.R. Davidson, S.P. Westwater, T.J. Bullough, T.B. Joyce, C.D. Latham, R. Jones, and S. Oberg, "Di-Carbon Defects in Annealed Highly Carbon Doped GaAs", Phys. Rev. Lett., vol.78, pp.74-77, 1997.

[65] D.I. Lubyshev, M.Micovic, W.Z.Cai, and D.L. Miller, "Molar fraction and substrate orientation effects on carbon doping in InGaAs grown by solid source

ATTENTION: The Singapore Copyright Act applies to the use of this document. Nanyang Technological University Library

molecular beam epitaxy using carbon tetrabromide", J. Appl. Phys., vol.84, pp.4281-4284, 1998.

[66] D. Lubyshev, M. Micovic, N. Gratteau, W.-Z.Cai, D.L. Miller, O. Ray, R.W. Streater, and A.J. SpringThorpe, "A comparative study of carbon incorporation in heavily doped GaAs and $Al_{0.3}Ga_{0.7}As$ grown by solid-source molecular beam epitaxy using carbon tetrabromide", J. Vac. Sci. Technol. B, vol.17, pp.1180-1184, 1999.

[67] K.H. Tan, S.F. Yoon, Q.F. Huang, R. Zhang, Z.Z. Sun, J. Jiang, W. Feng, and L.H.Lee, "Dicarbon defects in carbon-doped GaAs", Phys. Rev. B, vol.67, pp.035208-035212, 2003.

[68] W.E. Hoke, D.G. Weir, P.J. Lemonias, and H.T. Hendriks, "Carbon tetrabromide carbon doping of molecular beam epitaxial (GaAs) films", Appl. Phys. Lett., vol.64, pp.202-204, 1994.

[69] Z.L. Liao, R.L. Aggarwal, P.A. Maki, R.J. Molnar, J.N. Walpole, R.C. Williamson, and I. Melngallis, "Light scattering in high-dislocation-density GaN", Appl. Phys. Lett., vol.69, pp.1665-1667, 1996.

[70] D.W. Schulte, S. Subramanian, and L. Ungier, H.M. Yoo, U. Venkateswaran, J.R. Arthur, "Substrate orientation dependence of carbon doping of GaAs using CBr_4 source in molecular beam epitaxy", J. Vac. Sci. Technol. B, vol.16, pp.1356-1360, 1998.

[71] D. Olego and M. Cardona, "Photoluminescence in heavily doped GaAs. I. Temperature and hole-concentration dependence", Phys. Rev. B, vol.22, pp.886-893, 1980.

[72] M.K. Hudait, P. Modak, S. Hardikar, K.S.R.K. Rao and S.B. Krupanidhi, *Physics of Semiconductor Devices*, vol.312, 1998.

ATTENTION: The Singapore Copyright Act applies to the use of this document. Nanyang Technological University Library

[73] J. Lee, I. Kim, B. Choe, W.G. Jeong, Y.K. Sin and W.S. Min, "Luminescence properties of heavily carbon doped GaAs", J. Appl. Phys., vol.79, pp.9278-9282, 1996.

[74] S. Kim, M. Kim, S. Min, and C. Lee, "Experimental and theoretical photoluminescence study of heavily carbon doped GaAs grown by low-pressure metalorganic chemical vapor deposition", J. Appl. Phys., vol.74, pp.6128-6132, 1993.

[75] P.J. Lemonias, W.E. Hoke, D.G. Weir and H.T. Hendriks, "Carbon p^+ doping of molecular-beam epitaxial GaAs films using carbon tetrabromide", J. Vac. Sci. Technol. B, vol.12, pp.1190-1192, 1994.

[76] A.G. Kuhl, R. Ares, and R.W. Streater, "Effect of growth rate on surface morphology of heavily carbon-doped InGaAs", J. Vac. Sci. Technol. B, vol.19, pp.1550-1553, 2001.

[77] M.J. Mondry, and H. Kroemer, "Heterojunction bipolar transistor using a (Ga,InP) emitter on a GaAs base, grown by molecular beam epitxay", IEEE Electron Device Lett., vol.6, pp.175-177, 1985.

[78] S.L. Delage, F.-P.M. A., H. Blanck, C. Brylinski, E. Chartier, P. Collot, "First microwave characterisation of LP-MOCVD grown GaInP/GaAs self-aligned HBT", Electronics Letters, vol.27, pp.253-254, 1991.

[79] W. Liu, E. Beam, T. Henderson, S. Fan, "Extrinsic base surface passivation in GaInP/GaAs hetero-junction bipolar transistors", IEEE Electron Device Lett., pp.301-303, 1993.

[80] T. Oka, K. Hirata, K. Ouchi, "Advanced Performance of Small-Scaled InGaP/ GaAs HBT's with f_t over 150GHz and f_{max} over 250GHz ", IEEE IEDM Tech. Dig., pp.653-656, 1998.

ATTENTION: The Singapore Copyright Act applies to the use of this document. Nanyang Technological University Library

[81] H. Wang, and G.I. Ng, "Electrical properties and transport mechanisms of InP/ InGaAs HBTs operated at low temperature", IEEE Trans. Electron Devices, vol.48, pp.1492-1497, 2001.

[82] T. Henderson, IEEE IEDM Tech. Dig, pp.811-814, 1995.

[83] R.E. Welser, GaAs-MANTECH Digest, pp.145-148, 2000.

[84] J.J. Liou, *Advanced Semiconductor Device Physics and Modeling*, Norwood, MA:Artech, 1994.

[85] D.D.-L. Tang, and E. Hackbarth, "Junction degradation in bipolar transistors and the reliability imposed constraints to scaling and design", IEEE Trans. Electron Devices, vol.35, pp.2101-2107, 1988.

[86] H.-K. Yow, P.A. Houston, C.-M.S. Ng, C. Button, and J.S. Roberts, "High-temperature DC characteristics of $Al_xGa_{0.52-x}In_{0.48}P$/GaAs heterojunction bipolar transistors grown by metal organic vapor phase epitaxy", IEEE Trans. Electron Devices, vol.43, pp.2-7, 1996.

[87] M.S. Lundstrom, M.E.Klausmeier-Brown, and M.R. Melloch, "Device-related material properties of heavily doped gallium arsenide", Solid-State Electronics, vol.33, pp.693-704, 1990.

[88] M.Takeshima, "Effect of Auger recombination on laser operation in $Ga_{1-x}Al_xAs$", J. Appl. Phys., vol.58, pp.3846-3850, 1985.

[89] W.Bardyszewski, and D.Yevick, "A numerical analysis of Auger processes in *p*-type GaAs", J. Appl. Phys., vol.57, pp.4820-4822, 1985.

[90] Dabing Li, Xun Dong, Jinsong Huang, Xianglin Liu, Zhongying Xu, Xiaohui Wang, Ze Zhang, Zhanguo Wang, "Structural and optical properties of InAlGaN films grown directly on low-temperature buffer layer with (0 0 0 1) sapphire substrate", J. Cryst. Growth, vol.249, pp.72-77, 2003.

ATTENTION: The Singapore Copyright Act applies to the use of this document. Nanyang Technological University Library

[91] M.L. Lovejoy, M.R. Melloch, and M.S. Lundstrom, "Temperature dependence of minority and majority carrier mobilities in degenerately doped GaAs", Appl. Phys. Lett., vol.67, pp.1101-1103, 1995.

[92] K. Beyzavi, K. Lee, D.M. Kim, M.I. Nathan, K. Wrenner, and S.L. Wright, "Temperature dependence of minority-carrier mobility and recombination time in *p*-type GaAs", Appl. Phys. Lett., vol.58, pp.1268-1270, 1991.

[93] H. Wang, and G.I. Ng, "Investigation of the degradation of InGaAs/InP double HBTs under reverse base-collector bias stress", IEEE Trans. Electron Devices, vol.48, pp.2647-2654, 2001.

[94] H. Ito, and K. Kurishima, "Influence of gallium sources on carbon incorporation efficiency into InGaAs grown by metalorganic chemical vapor deposition", J. Cryst. Growth, vol.165, pp.215-221, 1996.

[95] H.C. Kuo, D. Ahmari, B.G. Moser, J. Mu, M. Hattendorf, D. Scott, R. Mayer, M. Feng, and G.E. Stillman, "Growth of carbon doping $Ga_{0.47}In_{0.53}As$ using CBr_4 by gas source molecular beam epitaxy for InP/InGaAs heterojunction bipolar transistor applications", J. Vac. Sci. Technol. B, vol.17, pp.1185-1189, 1999.

[96] R.A. Hamm, S. Chandrasekhar, L. Lunardi, M. Geva, R. Malik, D. Humphrey, and R. Ryan, "Materials and electrical characteristics of carbon-doped $Ga_{0.47}In_{0.53}As$ using carbontetrabromide by MOMBE for HBT device applications", J. Cryst. Growth, vol.164, pp.362-370, 1996.

[97] J. Han, J. Song, S. Park, and D. Woo, "Growth of ultrahigh carbon-doped InGaAs and its application to InP/InGaAs(C) HBTs", IEEE Trans. Electron Devices, vol.49, pp.1-6, 2002.

[98] G.E. Stillman, S.A. Stockman, C.M. Colomb, A.W. Hanson, and M.T. Fresins, Mater. Res. Soc. Symp. Proc., vol.325, pp.197-202, 1994.

ATTENTION: The Singapore Copyright Act applies to the use of this document. Nanyang Technological University Library

[99] S.L. Jackson, J.E. Baker, and G.E. Stillman, "Influence of AsH_3 cracking temperature on the H passivation of C acceptors in $In_{0.53}Ga_{0.47}As$ grown by beam epitaxy techniques", Appl. Phys. Lett., vol.69, pp.1939-1341, 1996.

[100] W.Z. Cai, D.I. Lubyshev, D.L. Miller, R.W. Streater, and A.J. SpringThorpe, "Heavily carbon-doped $In_{0.53}Ga_{0.47}As$ on InP (001) substrate grown by solid source molecular beam epitaxy", J. Vac. Sci. Technol. B, vol.17, pp.1190-1194, 1999.

[101] D. Yu, K. Lee, B. Kim, D. Ontiveros, K. Vargason, J.M. Kuo, and Y.C. Kao, "Ultra high-speed InP-InGaAs SHBTs with f_{max} of 478 GHz", IEEE Electron Device Lett., vol.24, pp.384-386, 2003.

[102] W. Hafez, J.W. Lai, and M. Feng, "InP/InGaAs SHBTs with 75nm collector and f_T>500GHz", Electron. Lett, vol.39, pp.1475-1476, 2003.

[103] W. Hafez, J.W. Lai, and M. Feng, "Record f_T and $f_T + f_{max}$ performance of InP/ InGaAs single heterojunction bipolar transistors", Electron. Lett, vol.39, pp.811-813, 2003.

[104] O.Sugiura, A.G.Dentai, C.H.Joyner, S.Chandrasekhar, and J.C.Campbell, "High-current-gain InGaAs/InP double-heterojunction bipolar transistors grown by metal organic vapor phase epitaxy", IEEE Electron Device Lett., vol.9, pp.253-255, 1988.

[105] A. Feygenson, D. Ritter, R.A. Hamm, P.R. Smith, R.K. Montgomery, R.D. Yadvish, H. Temkin, and M.B. Panish, "InGaAs/InP composite collector heterostructure bipolar transistors", Electron. Lett., vol.28, pp.607-609, 1992.

[106] Y.S. Lin, "Breakdown characteristics of InP/InGaAs composite-collector double heterojunction bipolar transistor", Appl. Phys. Lett., vol.83, pp.5545-5547, 2003.

ATTENTION: The Singapore Copyright Act applies to the use of this document. Nanyang Technological University Library

[107] S.P. McAlister, W.R. McKinnon, R. Driad, and A.P. Renaud, "Use of dipole doping to suppress switching in indium phosphide double heterojunction bipolar transistors", J. Appl. Phys., vol.82, pp.5231-5234, 1997.

[108] M. Ohkubo, A. Iketani, T. Ijichi, and T. Kikuta, "InGaAs/InP double-heterojunction bipolar transistors with step graded InGaAsP between InGaAs base and InP collector grown by metalorganic chemical vapor deposition", Appl. Phys. Lett., vol.59, pp.2697-2699, 1991.

[109] B.T. McDermott, E.R. Gertner, S. Pittman, C.W. Seabury, and M.F. Chang, "Growth and doping of GaAsSb via metalorganic chemical vapor deposition for InP heterojunction bipolar transistors", Appl. Phys. Lett., vol.68, pp.1386-1388, 1996.

[110] M. Ida, K. Kurishima, N. Watanabe, and T. Enoki, "InP/InGaAs DHBTs with 341-GHz f_T at high current density of over 800 kA/cm^2", Proc. IEEE IEDM, pp.35.4.1-35.4.4, 2001.

[111] A. Fujihara, Y. Ikenaga, H. Takahashi, M. Kawanaka, and S. Tanaka, "High-speed InP/InGaAs DHBTs with ballistic collector launcher structure", Proc. IEEE IEDM, pp.35.3.1-35.3.4, 2001.

[112] M. Ida, K. Kurishima, K. Ishii, and N. Watanabe, "High-speed InP/InGaAs DHBTs with a thin pseudomorphic base", GaAs IC Symposium Technical Digest, pp.211-214, 2003.

[113] W. Hwang, D.L. Miller, Y.K. Chen, and D.A. Humphrey, "Carbon doping of InGaAs in solid-source molecular beam epitaxy using carbon tetrabromide", J. Vac. Sci. Technol. B, vol.12, pp.1193-1196, 1994.

ATTENTION: The Singapore Copyright Act applies to the use of this document. Nanyang Technological University Library

[114] E. Kuphal, A. Pocker, and A. Eisenbach, "Relation between photoluminescence wavelength and lattice mismatch in metalorganic vapor-phase epitaxy InGaAs/InP", J. Appl. Phys., vol.73, pp.4599-4604, 1993.

[115] B.P. Yan, J.S. Luo, and Q.L. Zhang, "Study of band-gap narrowing effect and nonradiative recombination centers for heavily C-doped GaAs by photoluminescence spectroscopy", J. Appl. Phys., vol.77, pp.4822-4824, 1995.

[116] D.L. Cui, S.M. Hubbard, D. Pavlidis, A. Einsenbach, and C. Chelli, "Impact of doping and MOCVD conditions on minority carrier lifetime of zinc- and carbon-doped InGaAs and its applications to zinc- and carbon-doped InP/InGaAs heterostructure bipolar transistors", Semiconductor Science and Technology, vol.17, pp.503-509, 2002.

[117] D. Ritter, R.A. Hamm, A. Feygenson, and M.B. Panish, "Anomalous electric field and temperature dependence of collector multiplication in InP/$Ga_{0.47}In_{0.53}As$ heterojunction bipolar transistors", Appl. Phys. Lett., vol.60, pp.3150-3152, 1992.

[118] A. Neviani, G. Meneghesso, E. Zanoni, M. Hafizi, and C. Canali, "Positive temperature dependence of the electron impact ionization coefficient in $In_{0.53}Ga_{0.47}As$/InP HBTs", IEEE Electron Device Lett., vol.18, pp.619-621, 1997.

[119] K. Taguchi, T. Torikai, Y. Sugimoto, K. Makita, and H. Ishihara, "Temperature dependence of impact ionization coefficients in InP", J. Appl. Phys., vol.59, pp.476-481, 1986.

[120] H. Wang, and G. Ng, "Avalanche multiplication in InP/InGaAs double heterojunction bipolar transistors with composite collectors", IEEE Trans. Electron Devices, vol.47, pp.1125-1133, 2000.